The

Geophysical Journal

of the

Royal Astronomical Society

incorporating

the Geophysical Supplement to the Monthly Notices of the R. A. S.

Volume 3 No. 3 September 1960

Published and Sold by the

Royal Astronomical Society

Burlington House, London, W.1, England

Price £1; in U.S.A. $3 Annual Subscription £3; in U.S.A. $9

The Geophysical Journal

of the Royal Astronomical Society

Editors

A. H. Cook, M.A., Ph.D., F.R.A.S., F.G.S. (*Geophysical Secretary*), National Physical Laboratory, Teddington.

T. F. Gaskell, M.A., Ph.D., F.R.A.S. British Petroleum Company, London.

The *Geophysical Journal* is a journal for the publication of research in geophysics and related subjects. In addition to original papers, short notes and letters to the Editors are accepted for publication.

The aims of the Editors are to publish papers of a high standard, to give them a wide international circulation and to assure authors of speedy publication.

Book reviews and reports of geophysical meetings are also published and the Editors are always glad to hear of such meetings and to receive short reports of them.

Notice to Authors

Authors of papers offered for publication need not be Fellows of the Society.

No charges of any kind are made for printing papers or articles accepted. Contributors are entitled to receive 25 reprints free and greater numbers are obtainable at moderate rates, e.g. 300 copies of a 12-page reprint (exc. plates) cost £11 14s. (U.S. $35). Special arrangements can be made for institutions requiring reprints of their contributions with covers, special pagination etc., for issue in their own series of publications.

Attention is drawn to the recommendations to authors printed on the inside of the back cover.

Volume 3 No. 4 December 1960

The following contributions have been accepted for publication in the above issue:

R. J. Donato, Experimental investigation on the properties of Stoneley waves.

T. Hatherton, Microseisms at Scott Base.

B. A. Bolt, The revision of earthquake epicentres, focal depths and origin-times, using a high-speed computer.

E. Irving, Palaeomagnetic directions and pole positions, Part II.

R. W. Willmore & A. M. Bancroft, The time-term approach to refraction seismology.

M. J. P. Musgrave, Reflexion and refraction of plane elastic waves at a plane boundary between aeolotropic media.

J. C. Jaeger & R. F. Thyer, Geophysics in Australia.

The Geophysical Journal

of the

ROYAL ASTRONOMICAL SOCIETY

Vol. 3 No. 3 September 1960

Thickness of the Earth's Crust in Antarctica and the Surrounding Oceans

F. F. Evison, C. E. Ingham, R. H. Orr and J. H. Le Fort

(Received 1960 February 10)

Summary

Love waves and Rayleigh waves from eight earthquakes recorded at Hallett Station, Scott Base and Mirny have been analysed and the dispersion compared with that predicted by theory for simple model crusts. The average thickness of the crust in eastern Antarctica is found to be about 35 km, as is typical of continents, whereas Marie Byrd Land with an average thickness of about 25 km cannot be regarded as truly continental. Love wave dispersion indicates that the thickness of the solid crust in the oceanic regions surrounding Antarctica varies from about 5 km to 10 km, the smaller values being associated with the deeper basins. It is shown that the determination of oceanic crustal thickness from Rayleigh wave dispersion is in general subject to large uncertainties, nor can one usually rely on values of the thickness of unconsolidated bottom sediments obtained by this means.

1. Introduction

The broad structure of the land beneath the Antarctic ice cap can be determined only by indirect means. The ice cap is of continental size but this does not imply a single co-extensive land mass. Geological evidence points to the existence of a continental shield in eastern Antarctica whilst western Antarctica appears to be characterized by young folded belts, but the extent of these two geological provinces is uncertain. Much of the coastline is devoid of exposed rock and little is known of the region between the Weddell Sea and the Ross Sea, separating eastern from western Antarctica. Seismic reflection work in Antarctica has revealed that the rock surface lies below sea-level at many places in the interior, and often at a sufficient depth to remain below sea-level if the ice were to melt, even allowing for consequent isostatic uplift.

The installation of seismograph stations in Antarctica for the International Geophysical Year has provided an opportunity for determining the main features of the Antarctic crust by a study of guided earthquake waves. In a preliminary

The Geophysical Journal

of the Royal Astronomical Society

Editors

A. H. Cook, M.A., Ph.D., F.R.A.S., F.G.S. (*Geophysical Secretary*), National Physical Laboratory, Teddington.

T. F. Gaskell, M.A., Ph.D., F.R.A.S. British Petroleum Company, London.

The *Geophysical Journal* is a journal for the publication of research in geophysics and related subjects. In addition to original papers, short notes and letters to the Editors are accepted for publication.

The aims of the Editors are to publish papers of a high standard, to give them a wide international circulation and to assure authors of speedy publication.

Book reviews and reports of geophysical meetings are also published and the Editors are always glad to hear of such meetings and to receive short reports of them.

Notice to Authors

Authors of papers offered for publication need not be Fellows of the Society.

No charges of any kind are made for printing papers or articles accepted. Contributors are entitled to receive 25 reprints free and greater numbers are obtainable at moderate rates, e.g. 300 copies of a 12-page reprint (exc. plates) cost £11 14s. (U.S. $35). Special arrangements can be made for institutions requiring reprints of their contributions with covers, special pagination etc., for issue in their own series of publications.

Attention is drawn to the recommendations to authors printed on the inside of the back cover.

Volume 3 No. 4 December 1960

The following contributions have been accepted for publication in the above issue:

R. J. Donato, Experimental investigation on the properties of Stoneley waves.

T. Hatherton, Microseisms at Scott Base.

B. A. Bolt, The revision of earthquake epicentres, focal depths and origin-times, using a high-speed computer.

E. Irving, Palaeomagnetic directions and pole positions, Part II.

R. W. Willmore & A. M. Bancroft, The time-term approach to refraction seismology.

M. J. P. Musgrave, Reflexion and refraction of plane elastic waves at a plane boundary between isotropic media.

J. C. Jaeger & R. F. Thyer, Geophysics in Australia.

The Geophysical Journal

of the

ROYAL ASTRONOMICAL SOCIETY

Vol. 3 No. 3 September 1960

Thickness of the Earth's Crust in Antarctica and the Surrounding Oceans

F. F. Evison, C. E. Ingham, R. H. Orr and J. H. Le Fort

(Received 1960 February 10)

Summary

Love waves and Rayleigh waves from eight earthquakes recorded at Hallett Station, Scott Base and Mirny have been analysed and the dispersion compared with that predicted by theory for simple model crusts. The average thickness of the crust in eastern Antarctica is found to be about 35 km, as is typical of continents, whereas Marie Byrd Land with an average thickness of about 25 km cannot be regarded as truly continental. Love wave dispersion indicates that the thickness of the solid crust in the oceanic regions surrounding Antarctica varies from about 5 km to 10 km, the smaller values being associated with the deeper basins. It is shown that the determination of oceanic crustal thickness from Rayleigh wave dispersion is in general subject to large uncertainties, nor can one usually rely on values of the thickness of unconsolidated bottom sediments obtained by this means.

1. Introduction

The broad structure of the land beneath the Antarctic ice cap can be determined only by indirect means. The ice cap is of continental size but this does not imply a single co-extensive land mass. Geological evidence points to the existence of a continental shield in eastern Antarctica whilst western Antarctica appears to be characterized by young folded belts, but the extent of these two geological provinces is uncertain. Much of the coastline is devoid of exposed rock and little is known of the region between the Weddell Sea and the Ross Sea, separating eastern from western Antarctica. Seismic reflection work in Antarctica has revealed that the rock surface lies below sea-level at many places in the interior, and often at a sufficient depth to remain below sea-level if the ice were to melt, even allowing for consequent isostatic uplift.

The installation of seismograph stations in Antarctica for the International Geophysical Year has provided an opportunity for determining the main features of the Antarctic crust by a study of guided earthquake waves. In a preliminary

notice of the work described in this paper it was shown that the eastern Antarctic crust in the region from Victoria Land to Wilkes Land is about 35 km thick (Evison, Ingham & Orr 1959). This finding provided definite geophysical support for the presumption of a land continent in Antarctica, since the continents are characterized by a crustal thickness of about 35 km in contrast to thicknesses of 5–15 km in oceanic regions. Similar studies of the dispersion of Love and Rayleigh waves have also been carried out by Press & Dewart (1959), from seismograms obtained at Wilkes Station, and whilst they confirm the continental thickness of the area mentioned above, they report a much thinner average for paths through other sectors of Antarctica. This latter result is partly explained by the present study.

Hallett Station and Scott Base are well placed for distinguishing between eastern and western Antarctica, and separate determinations have been obtained for the crustal thickness in these two major sectors. Records from Mirny have been used mainly for measuring the dispersion of waves travelling across the South Indian Ocean. It appears that for most of the paths along which Press and Dewart found the average thickness to be less than continental much of the deficiency occurs in western Antarctica. The present results indicate, however, that the crust is continental throughout eastern Antarctica.

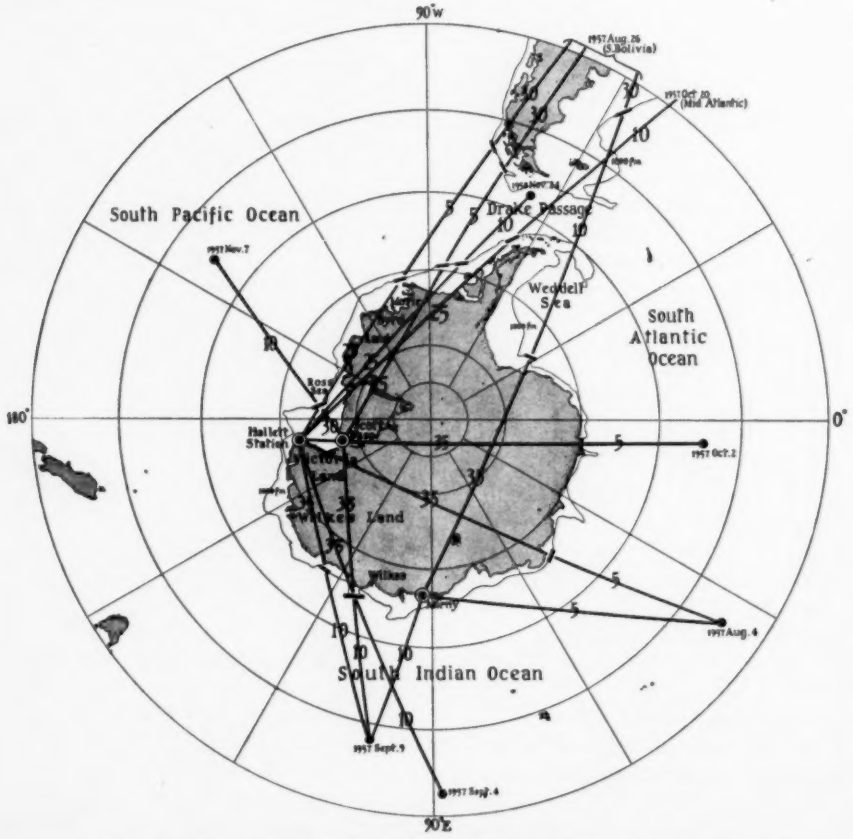

FIG. 1.—Wave paths, showing thickness of crust inferred for each segment.

2. Observations

Details of the eight earthquakes used in this study are listed in Table 1. Epicentres and origin times were taken from the monthly bulletins prepared by BCIS and USCGS. Earthquakes were chosen for which the wave paths would give good coverage of Antarctica, as illustrated in Figure 1. Epicentres close to Antarctica were preferred so that the contribution of the Antarctic segment of the path to the total dispersion would be as large as possible. Details of the seismographs that provided the records used in this study are as follows:

Hallett Station: Columbia seismograph, 3 components
$T_0 = 15$ s, $T_g = 75$ s.

Scott Base: Benioff seismograph, vertical and E–W,
$T_0 = 0{\cdot}6$ s, $T_g = 25$ s.

Mirny: Kirnos seismograph, 3 components,
$T_0 = 12{\cdot}5$ s, $T_g = 1{\cdot}2$ s.

The preference for epicentres close to Antarctica results in shorter paths being used than is usually the case in studies of this kind. Consequently the degree of dispersion on some records was rather limited. A majority of the records studied, however, came from the long period Columbia seismograph at Hallett Station, and a few of these are reproduced in Figure 2.

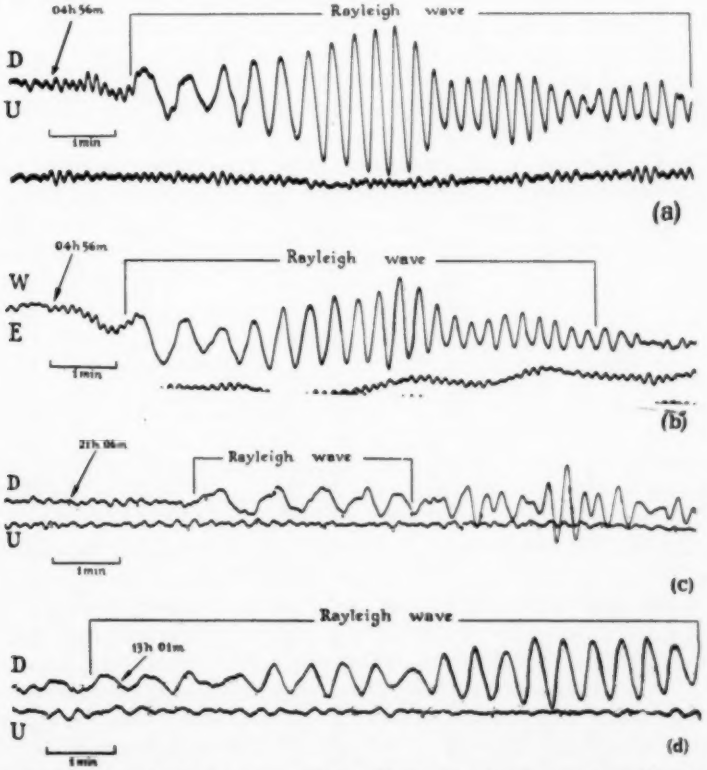

FIG. 2.—Rayleigh waves recorded at Hallett Station for earthquakes of 1957 Sept. 4 (a and b), 1957 Oct. 2 (c), and 1957 Oct. 20 (d).

Table 1

Particulars of Earthquakes

Date	Origin time h	m	s	Epicentre Lat.	Long.	Locality	Recording Station	Distance (km)	Wave	Component	Ocean segments, average water depth (km)	Figure
1957 Aug. 4	21	08	51	45°S	35°E	Prince Edward Is.	Hallett	6510	Love	N–S, E–W	Indian Ocean, 4·50	6
									Rayleigh	Z		8a
							Mirny	4120	Rayleigh	E–W, Z	Indian Ocean, 4·18	8b
Aug. 26	11	28	50	19°S	63°W	S. Bolivia	Scott	8805	Rayleigh	Z	S. Pacific, 4·21	13b
							Hallett	9140	Rayleigh	Z	S. Pacific, 4·45	11b
							Mirny	10315	Rayleigh	N–S, Z	S. Atlantic, 3·80	10b
									Love	N–S		12c
Sept. 4	04	33	52	42½°S	88½°E	Indian Ocean	Hallett	5295	Rayleigh	E–W, Z	Indian Ocean, 3·88	10a
Sept. 9	00	13	31	47¾°S	101°E	S. Indian Ocean	Mirny	2125	Rayleigh	N–S, Z	Indian Ocean, 3·72	9b
							Scott	4290	Rayleigh	E–W, Z	Indian Ocean, 3·80	9a
							Hallett	4350	Rayleigh	E–W, Z	Indian Ocean, 3·80	9a
									Love	N–S		7
Oct. 2	20	42	56	54½°S	5°E	Bouvet Is.	Hallett	5895	Rayleigh	Z	S. Atlantic, 4·35	11a
Oct. 20	12	04	22	11½°N	42°W	Mid Atlantic	Hallett	12915	Rayleigh	N–S, Z	Atlantic, 3·98	13a
											S. Atlantic, 3·81	
Nov. 7	06	21	56	57½°S	143½°W	S. Pacific	Scott	2920	Love	E–W	S. Pacific, 3·71	12a
1958 Nov. 24	06	48	57	57½°S	65½°W	Drake Passage	Hallett	4990	Love	E–W	Drake Passage, 3·80	12b
									Rayleigh	E–W, Z		11c

3. Method of analysis

The virtual absence of seismic activity in Antarctica makes it necessary to rely on waves that have first passed through some neighbouring oceanic region, and perhaps through some other continent as well. The recorded dispersion is therefore composed of two or more separate effects, of which one is of primary interest to us. The usual method of dealing with such composite wave paths is to assume that the dispersion due to an extraneous segment conforms with an empirical curve that has been derived for a known region of normal continent or ocean. When a correction has been made for this segment the remaining dispersion may also be assessed by comparison with the appropriate empirical curve. This is the method used by Press & Dewart (1959) in their analysis of Love and Rayleigh waves across Antarctica. The advantage of the method is that one does not have to postulate a simplified model crust and assume values for the various seismic parameters.

In the present study a different method has been adopted, in which the observations are compared with theoretical rather than empirical results. Theoretical dispersion curves have been computed from equations given by Stoneley (1948) for Love waves, by Lee (1932) for continental Rayleigh waves and by Jardetzky & Press (1953) for oceanic Rayleigh waves. The advantage of this method is that any departure from normal crustal thickness is readily accommodated. One finds that where a well-recorded dispersive wave has traversed a composite path the analysis reveals a value of crustal thickness for each segment, and surprisingly often there is a unique combination of values that will give reasonable agreement between observation and theory. Thus in the present study the results for Antarctica do not depend on assumed values of crustal thickness for the adjacent regions.

The models adopted for the purpose of computing theoretical dispersion curves consist simply of horizontal layers of uniform thickness, overlying a semi-infinite mantle. For the continental case a single crustal layer is postulated, and for the oceanic case a water layer and a single rock layer. The following seismic constants are assumed, incorporating the parameters used in Stoneley's (1948) computations for Love waves:

	Water	Crust	Mantle
Compressional velocity (km/s)	1·52	6·01	7·79
Shear velocity (km/s)		3·47	4·50
	Crust/water	Mantle/crust	
Density ratio	2·65	1·283	

Figure 3 shows the family of theoretical Love wave curves for selected thicknesses of crust. Since Love waves are not affected by a fluid layer the dispersion for any path, whether continental or oceanic, is given by an appropriate curve of this family. Figure 4 shows dispersion curves for continental Rayleigh waves.

In computing the theoretical dispersion of oceanic Rayleigh waves one has to assign a further parameter, namely the ratio of the thickness of the rock layer (H_1) to that of the fluid layer (H_0). Table 2 shows values of U and T/H_0, where U is the group velocity and T the period, computed for $H_1/H_0 = 1$, 2 and 3. Dispersion curves for selected values of H_1 are given in Figure 5.

In a wave path that is made up of a number of segments let m_n be the length of the nth segment, expressed as a fraction of the whole path length, and let U_n be the group velocity of a particular period traversing that segment. Then the group velocity of the period taken over the whole path is $U = 1/\Sigma_n(m_n/U_n)$.

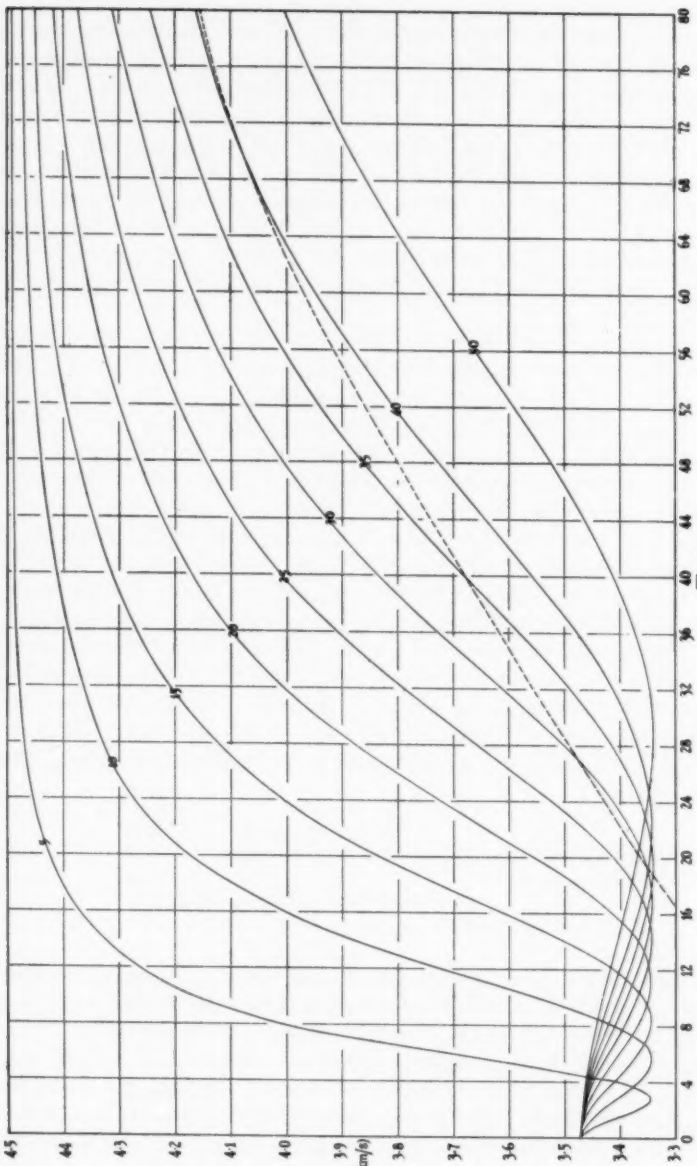

FIG. 3.—Theoretical Love wave dispersion for thicknesses of crust from 5 km to 50 km. Broken line shows empirical curve for North America. (Press & Dewart 1959.)

Thus we may construct theoretical dispersion curves for a composite path by assigning to each segment some curve from Figure 3, 4 or 5, making due allowance in

Table 2

Dispersion of oceanic Rayleigh waves

$H_1/H_0 = 1$		$H_1/H_0 = 2$		$H_1/H_0 = 3$	
U (km/s)	T/H_0 (s/km)	U (km/s)	T/H_0 (s/km)	U (km/s)	T/H_0 (s/km)
1·157	2·595	1·350	2·719	1·584	2·917
1·684	2·723	1·813	2·880	2·123	3·165
2·139	2·856	2·421	3·065	2·642	3·445
3·011	3·138	3·183	3·474	3·244	4·021
3·689	4·195	3·747	5·179	3·776	6·309
3·859	5·239	3·900	6·986	3·905	8·831
4·002	8·210	4·001	11·908	3·998	15·442

each case for the appropriate fractional length m_n. In measuring these lengths we have adopted the usual convention that the boundary between land and ocean is defined by the 1 000 fathom depth contour. In Figure 1 each wave path is shown divided into its segments; the captions to Figures 6–13 give the length of each segment as a percentage of the whole path. For simplicity, in a few cases a short stretch of water shallower than 1 000 fathoms has been included in an oceanic segment.

The recorded dispersion is represented by means of points on a graph; this is achieved by the usual procedure, in which a graph of arrival time against serial number is prepared for a suitable succession of recorded phases. The interpretation of the observed dispersion results for a particular path is then a matter of finding those theoretical curves which, when combined in the manner described above, provide the best fit to the plotted data.

The average depth of water along each oceanic segment has been calculated from bathymetric charts. This depth is useful, as will be seen later, in helping to resolve the indeterminacy that usually arises in interpreting the dispersion of oceanic Rayleigh waves.

4. Choice of parameters

The type of crustal model that one must be content to adopt in this kind of study, if the computations are to be performed in a reasonable time by desk calculator, is undoubtedly very much simpler than any real crust. Consequently it is not to be expected that the seismic parameters appropriate to the model will correspond precisely with particular values that might be determined by other means, for example by a study of body waves from earthquakes or artificial explosions. Such values usually pertain to a limited region of the medium—thus refracted waves are apt to indicate the velocity near the upper surface of the refracting layer—and they cannot well be adopted for theoretical purposes until more complex models can be readily analysed.

Even the simple models adopted here involve seven seismic parameters, apart from the ratio of fluid depth to crustal thickness that is required in the case of oceanic Rayleigh waves. Computations can be found in the literature for a variety

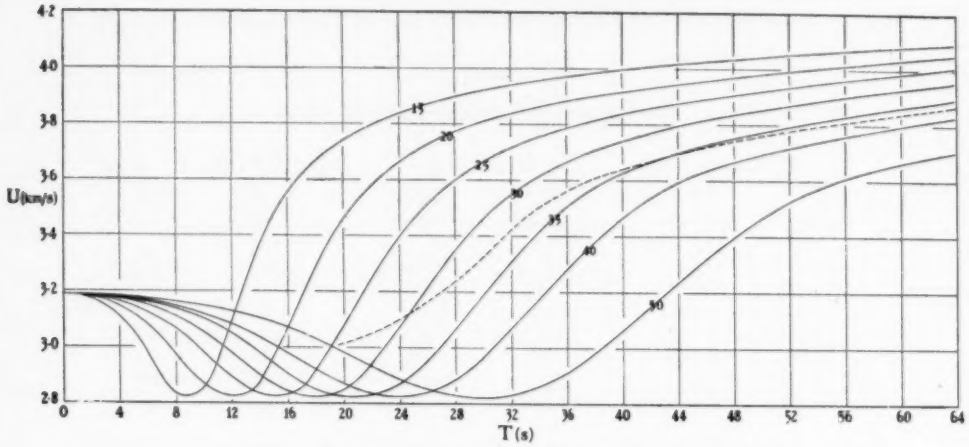

FIG. 4.—Theoretical Rayleigh wave dispersion for land paths, with thicknesses of crust from 15 km to 50 km. Broken line shows empirical curve for North America and Africa (Press & Dewart 1959).

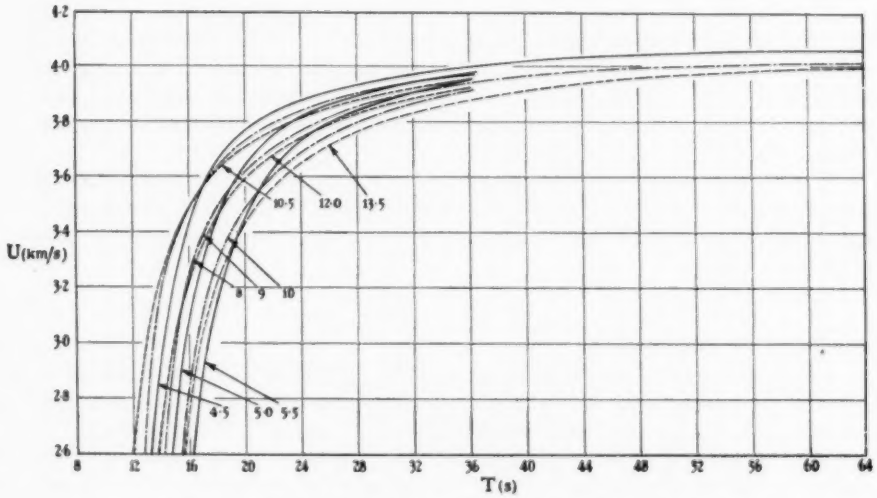

FIG. 5.—Theoretical Rayleigh wave dispersion for oceanic paths.

	Crustal thickness / Fluid depth	Crustal thickness (km)
————	1	4·5, 5·0, 5·5
—·—·—·—	2	8, 9, 10
- - - - - - - - -	3	10·5, 12, 13·5

of parameter values, but a thorough study of the effect of each separate parameter upon the dispersion curve must await a systematic coverage of the problem by electronic computer. In the absence of any compelling reason for a more elaborate choice of parameters it has been thought desirable to use the same values for the continental and oceanic cases, and also for both Love and Rayleigh waves.

The values of compressional velocity (6·01 km/s) and shear velocity (3·47 km/s) chosen for the crust are close to those preferred by Press & Ewing (1955) for the continental case. For the oceanic crust these authors adopt much greater values, especially in their Rayleigh wave computations. According to Hill (1957), however, the evidence of seismic refraction work is that in water depths greater than 4 km the solid crust comprises on an average a layer 1·75 km thick with compressional velocity 4–6 km/s and a layer 4·7 km thick with a velocity 6·71 km/s. Our value of 6·01 km/s may be a little too low, but is not inconsistent with Hill's picture, even though the water depth for some paths is slightly less than 4 km.

The compressional velocity 7·79 km/s chosen for the mantle is at about the lower limit of the range of values that have been measured in various parts of the world by means of refracted waves. This low value, together with the corresponding shear wave velocity (4·50 km/s) gives a better fit in dispersion studies than do values such as 8·1 km/s and 4·7 km/s, which are more commonly indicated by refraction. This is a case where it seems inappropriate to attach more typical measured values of the parameters to our simplified models; conversely, it is not to be thought that a refraction survey would necessarily indicate the same values as those adopted here.

The general validity of the present choice of parameters may be tested by comparing the resulting theoretical dispersion curves with empirical curves that have been obtained for paths of known type. Such empirical curves, as given by Press & Dewart (1959) for continental paths, are included in Figures 3 and 4; it will be seen that they agree quite closely with the theoretical curves for a crustal thickness of 35 km, which is usually regarded as the average thickness for continents.

5. Results

Figures 6–13 show the plots of observed dispersion for each wave path and type of wave, together with the theoretical composite curves that appeared to give the best fit. Two or three such composite curves are presented in each figure so as to give some impression of the sensitivity of the method. In most cases the fit that would be obtained by any other interpretation is distinctly inferior, as may readily be checked by reference to the theoretical curves in Figures, 3, 4 and 5, taking into account the percentage of path contributed by each particular segment.

The most direct evidence that the thickness of the crust in eastern Antarctica averages about 35 km is given by the Love wave analyses in Figures 6 and 7. In both cases a wide range of periods was recorded and the analyses yielded independent determinations of thickness for the oceanic segments. The result was confirmed by analyses of Rayleigh waves from the same two earthquakes, as shown in Figures 8 and 9. Further confirmation from another earthquake is given in Figure 10a. A valuable determination of the same thickness is that of Figure 11a, since the path crosses Antarctica diametrically and the oceanic segment is small. Results for Rayleigh and Love waves recorded at Mirny for an epicentre in south Bolivia are included (Figures 10b and 12c) as offering an interpretation

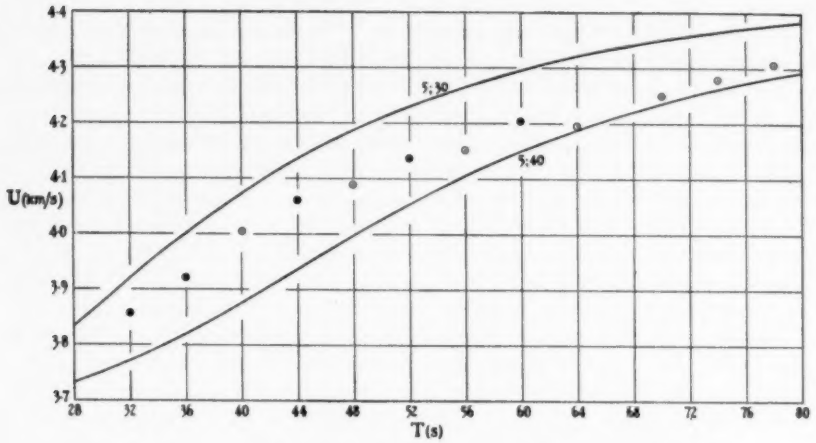

FIG. 6.—Love wave dispersion, Prince Edward Island to Hallett (40 per cent Indian Ocean at 5 km; 60 per cent E. Antarctica at 30–40 km). Components: ⊙ N–S; ● E–W.

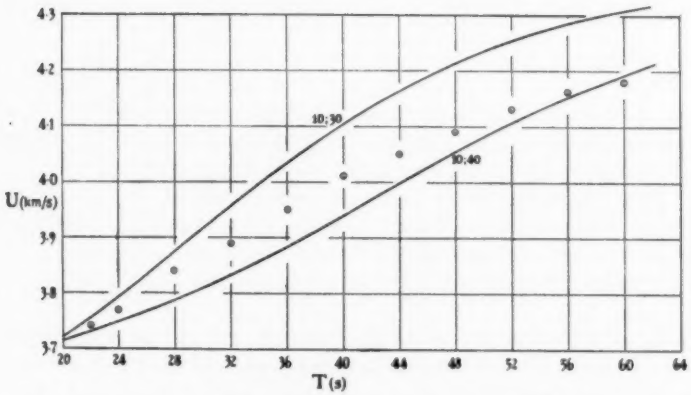

FIG. 7.—Love wave dispersion, S. Indian Ocean to Hallett (50 per cent Indian Ocean at 10 km; 50 per cent E. Antarctica at 30–40 km). Component: ⊙ N–S.

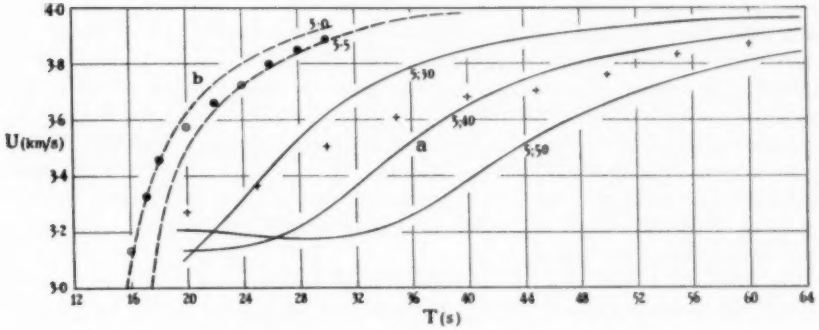

FIG. 8.—Rayleigh wave dispersion, Prince Edward Island to:
(a) Hallett (40 per cent Indian Ocean at 5 km; 60 per cent E. Antarctica at 30–40 km). Component: + Z.
(b) Mirny (100 per cent Indian Ocean at 5·0–5·5 km). Components: ○ E–W; • Z.

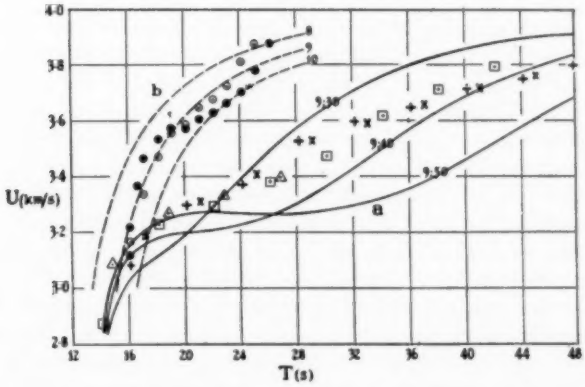

FIG. 9.—Rayleigh wave dispersion, S. Indian Ocean to:
(a) Hallett (50 per cent Indian Ocean at 9 km; 50 per cent E. Antarctica at 30–40 km,). Components: × E–W; + Z.
Scott (50 per cent Indian Ocean at 9 km; 50 per cent E. Antarctica at 30–40 km). Components: △ E–W; ⊡ Z.
(b) Mirny (100 per cent Indian Ocean at 8–10 km). Components: ⊙ N–S; • Z.

consistent with that already put forward, although only a small range of periods was recorded.

A much thinner average crust is indicated for western Antarctica. Four wave paths have been studied, all traversing Marie Byrd Land, and although the observations did not provide so definite a determination as in the case of eastern Antarctica, it appears that the average thickness in this region is about 25 km. The simplest demonstration of this result is given by Figure 12b, which gives the dispersion of a Love wave from an epicentre in Drake Passage, recorded at Hallett Station after traversing some 1 500 km of ocean and 3 500 km in western Antarctica. A glance at the family of theoretical Love wave curves (Figure 3) will serve to show that these observations do not allow of a crustal thickness much greater than 25 km for the Antarctic segment.

The same conclusion arises from the Rayleigh wave analysis of Figure 11b for an epicentre in south Bolivia. This path traversed peninsular South America for 43 per cent of its length, and by allowing a crustal thickness of 30 km for this segment a very satisfactory fit has been obtained. This value seems rather thin for such a region and needs further verification; but if a thicker crust were assumed for the South American segment the western Antarctic crust would have to be taken thinner, and then also the degree of fit in Figure 11b would be inferior. Figure 13a also indicates a thickness of about 25 km for western Antarctica if we assume the normal continental value of 35 km for the Brazilian shield. Further Rayleigh wave data of a more limited kind are presented in Figures 13b and 11c, where they are shown to give a consistent solution for western Antarctica.

The thickness of solid crust beneath the surrounding oceans can be uniquely determined only from Love waves, which are unaffected by the water layer; furthermore, an accurate determination depends on the shorter periods. As we have seen, Figure 6 indicates a thickness of no more than 5 km for the southwest Indian Ocean, and Figure 7 indicates about 10 km for the southeast Indian Ocean. Values close to 10 km have been obtained from Love waves for Drake Passage (Figure 12b) and for the region northeast of the Ross Sea (Figure 12a). The results shown in Figure 12a also involve a short segment of path across the eastern Ross Sea, which appears to have a crust of almost continental thickness, and thus to belong to eastern rather than western Antarctica.

These values of crustal thickness for oceanic regions, obtained from recordings of Love wave dispersion, appear to be related to the depth of the ocean much in the manner that one would expect on the principle of isostatic balance. As Table 1 shows, the water was 4.50 km deep on an average for the path where a 5 km crust was indicated (Figure 6) and about 3·75 km deep for the paths with a crust of about 10 km thick (Figures 7, 12a, 12b). This relation has been used in the interpretation of oceanic Rayleigh waves, which otherwise, as will be discussed further below, do not yield an unambiguous solution. The major uncertainty has been resolved by taking $H_1/H_0 = 2$ for the water depths from 3·71 km to 3·98 km, and $H_1/H_0 = 1$ for depth of 4·18 km to 4·50 km (see Table 1). Thus, although a close fit has been achieved in most cases between the theoretical and observed Rayleigh wave dispersion for oceanic segments, this part of the analysis is essentially dependent upon the Love wave results and the estimates of water depth. The method is capable of further refinement by using fractional values of H_1/H_0, but this is not warranted by the limited quantity of data used in the present study.

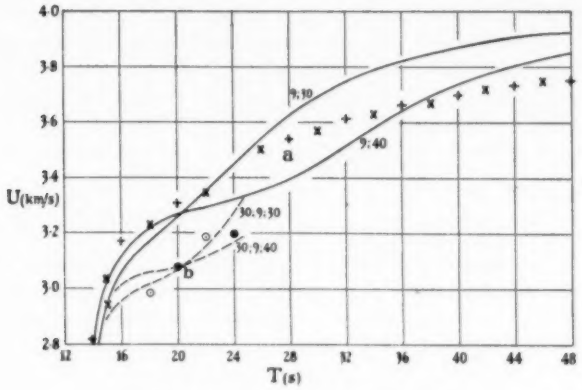

FIG. 10.—Rayleigh wave dispersion:

(a) Indian Ocean to Hallett (60 per cent Indian Ocean at 9 km; 40 per cent E. Antarctica at 30–40 km). Components: × E–W; + Z.
(b) S. Bolivia to Mirny (27 per cent S. America at 30 km; 35 per cent S. Atlantic at 9 km; 38 per cent E. Antarctica at 30–40 km). Components: • N–S; ○ Z.

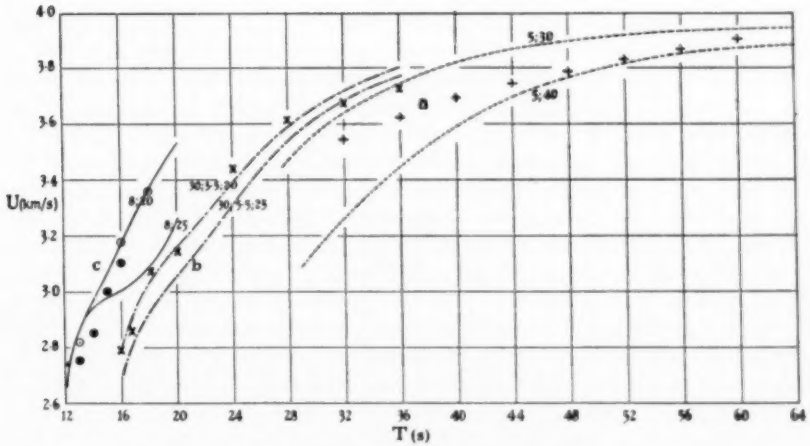

FIG. 11.—Rayleigh wave dispersion:

(a) Bouvet Island to Hallett (28 per cent S. Atlantic at 5 km; 72 per cent E. Antarctica at 30–40 km). Component: + Z.
(b) S. Bolivia to Hallett (43 per cent S. America at 30 km; 26 per cent S. Pacific at 5·5 km; 31 per cent. W Antarctica at 20–25 km). Component: × Z.
(c) Drake Passage to Hallett (30 per cent Drake Passage at 8 km; 70 per cent W. Antarctica at 20–25 km.) Components: • E–W; ○ Z.

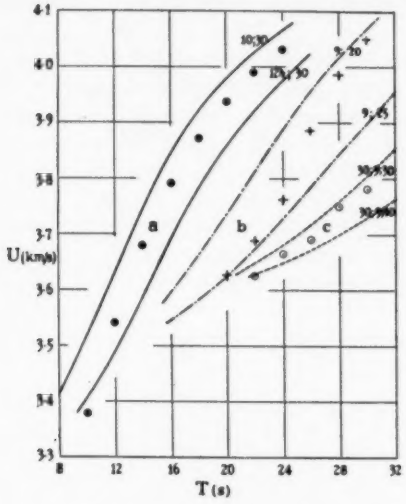

FIG. 12.—Love wave dispersion:

(a) S. Pacific to Scott (80 per cent S. Pacific at 10–12½ km; 20 per cent Ross Sea at 30 km). Component: • E–W.
(b) Drake Passage to Hallett (30 per cent Drake Passage at 9 km; 70 per cent W. Antarctica at 20–25 km). Component: + E–W.
(c) S. Bolivia to Mirny (27 per cent S. America at 30 km; 35 per cent S. Atlantic at 9 km; 38 per cent E. Antarctica at 30–40 km). Component: ⊙ N–S.

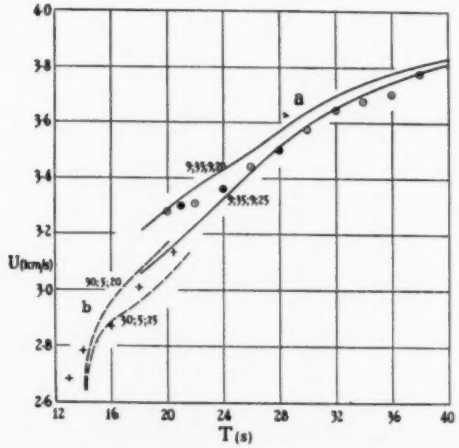

FIG. 13.—Rayleigh wave dispersion:

(a) Mid-Atlantic to Hallett (9 per cent Atlantic at 9 km; 28 per cent S. America at 35 km; 23 per cent S. Atlantic at 9 km; 40 per cent W. Antarctica at 20–25 km). Components: • N–S; ⊙ Z.
(b) S. Bolivia to Scott (47 per cent S. America at 30 km; 19 per cent S. Pacific at 5 km; 34 per cent W. Antarctica at 20–25 km). Component: + Z.

Several wave paths in Figure 1 make rather small angles with the 1000 fathom depth contour. In such cases theory shows that the actual path is deflected from the great circle because of refraction at the boundary. The case where this effect would be expected to be most marked is the path from south Bolivia to Hallett Station. A careful study of this path has shown, however, that the result arrived at in Figure 11b would not be substantially altered by allowing for refraction.

6. Indeterminacy of oceanic Rayleigh wave solutions

The approximate thicknesses of oceanic crust shown in Figure 1 are compatible with the observed dispersion of Rayleigh as well as Love waves, but could not have been ascertained from Rayleigh waves alone, except between rather wide limits. It has been explained that the Love wave results support the idea of an inverse relation between water depth and crustal thickness, as is required by the principle of isostasy. The Rayleigh wave solutions have been obtained with the help of this added condition. In the Rayleigh wave theory, if the thickness of the fluid layer could be taken as equal to the known depth of water, an analysis of Rayleigh wave dispersion would yield a unique value of crustal thickness; the analysis would then consist of finding the value of H_1/H_0 that gave the best fit. It is generally found, however, that better agreement with other lines of evidence can be achieved by assuming a somewhat thicker fluid layer, the additional thickness being ascribed to unconsolidated bottom sediments.

Numerous studies appear in the literature in which estimates of the thickness of the oceanic crust have been based upon Rayleigh wave dispersion. Useful summaries may be found in review articles by Press & Ewing (1955) and Hill (1957). The claim that a thickness of about 5 km is normal for all oceanic areas is largely based on Rayleigh wave data. But these studies do not seem to take account of the fact that very similar dispersion may be produced by widely different crustal thicknesses, as readily follows from the theory if we allow that variations may occur in the ratio of crustal thickness to fluid depth (H_1/H_0).

The point is illustrated in Figure 14, which gives three different interpretations for a Rayleigh wave recorded at Mirny from the earthquake of 1957 August 4, the path being virtually oceanic throughout (Figure 1). The three theoretical curves are computed for the same seismic parameters, but H_1/H_0 is taken as 1, 2 and 3 in turn. To the accuracy that can reasonably be claimed for dispersion studies there is little to choose among the three solutions, yet the crustal thicknesses indicated are respectively $5\frac{1}{4}$ km, $9\frac{1}{2}$ km and 12 km. (The Love wave analysis suggests that the first of these solutions is nearest to the correct one.) Naturally any other value within this range could equally well be deduced by taking the appropriate fractional ratio of the thicknesses. The range of possible solutions might be less in cases where the observations extend over a greater range of velocity; but the later portions of most records bear signs of interference, indicating that energy has been propagated along paths other than the direct one, and hence making the analysis less reliable.

Rayleigh waves have also often been invoked as a means of estimating the thickness of the unconsolidated bottom sediments. Inferred values are usually in the range 0·4–1·2 km; thus the effect of the sediments is a second-order one. But the actual value that is obtained in any particular case is wholly dependent on the assumed ratio of crustal thickness to fluid depth. Thus in Figure 14 the three interpretations give the thickness of the fluid layer as $5\frac{1}{4}$ km, $4\frac{3}{4}$ km or 4 km. The

average water depth for this path as determined from the bathymetric map is 4·18 km. Hence one inferred value of the sediment thickness is 1·07 km, another is 0·57 km, while the third interpretation would imply that not even all the water behaves as a fluid. It is clear that any thickness of sediment could be obtained, at least within the usual range of values, by varying the assumed ratio of crustal thickness to fluid depth.

Most authors have assumed, for purposes of computation, that the thicknesses of crust and fluid layer are equal. Curve fitting has then consisted of selecting the most favourable value of this thickness. The assumption is at variance both with

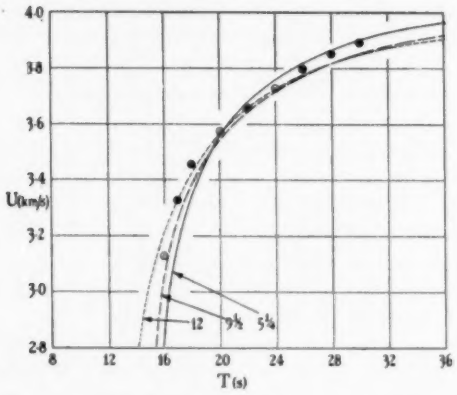

FIG. 14.—An example of the indeterminacy of Rayleigh wave solutions for oceanic paths. Dispersion from Prince Edward Island to Mirny (cf. Figure 8b), with three different interpretations.

Crustal thickness / Fluid depth	Crustal thickness (km)
1	5¼
2	9½
3	12

the principle of isostasy (which seems to hold good in oceanic regions except for local anomalies), and with the evidence of seismic refraction results as summarized by Hill (1957). The case of a crust twice as thick as the fluid layer has occasionally been considered (see Press & Ewing 1955), but at the same time the very low value 5·5 km/s has been adopted for the compressional velocity in the crust, in place of the usual 6·9 km/s. This has obscured the effect of varying H_1/H_0. The refraction results actually show that the average compressional velocity in the oceanic crust is very nearly the same for a thickness of 10 km as for 5 km.

We thus see that Rayleigh wave dispersion does not, by itself, provide a reliable measure of crustal thickness in oceanic regions, much less of the thickness of fluid sediments on the ocean floor. The high degree of uniformity that has been attributed to the oceans may be illusory in as much as it depends largely on Rayleigh wave evidence. Indeed the growing amount of data from seismic refraction work at sea, and also the evidence of Love waves, suggests that thicknesses of 10 km or more are not uncommon. We have found that this is the case in the oceanic regions adjacent to Antarctica. A contrary view of the major oceans regards the Pacific as having an essentially different crustal structure from the other oceans.

Since the Pacific is appreciably the deepest ocean we must expect it to have the least average thickness of crust, but the difference is not such as would suggest any uniqueness of structure.

7. Structure of Antarctica

It is concluded that eastern Antarctica as a whole is continental, for the present study has given a good coverage of this large area, and a crustal thickness of about 35 km has been consistently obtained. By contrast, Marie Byrd Land has an average crustal thickness of about 25 km and cannot be regarded as truly continental in structure. The data do not extend to the remainder of western Antarctica, nor has it been possible to study the important transition zone which runs from the Ross Sea to the Weddell Sea.

These findings are evidently related to the known geological contrast between eastern and western Antarctica. The result for the western sector, however, requires further elaboration, for the average crustal thickness of 25 km could be made up in a variety of ways. Beneath the high mountain ranges of Marie Byrd Land one would expect to find crustal roots giving locally a total thickness of at least 40 km. If this is so there must be other zones where the crust is much thinner than 25 km, implying that the rock surface lies well below sea-level. The offshore depth contour at 1 000 fathoms generally lies much further from the coastline in western than in eastern Antarctica; this would account for some small fraction of the difference in average crustal thickness.

The picture of Marie Byrd Land as an archipelago made up of mountainous island chains finds support in recent seismic and gravity observations. A detailed survey of ice thickness has revealed extensive regions where the rock surface would undoubtedly be below sea-level if the ice were to melt. For example, along a traverse running close to latitude 77° S, between longitudes 87° W and 113° W, the rock surface was located consistently at between 1 km and 2 km below sea-level for a distance of some 400 km (Bentley & Ostenso 1959).

The conclusion that eastern Antarctica as a whole is continental and that the smaller average thickness of crust is confined to western Antarctica differs substantially from the conclusion of Press & Dewart (1959). For paths in all directions from Wilkes Station except to the southeast these authors obtained an average crustal thickness about as small as that indicated for Marie Byrd Land in the present study, and concluded that "at most only three-fourths of the Antarctic ice sheet is underlain by continent, the remaining area being oceanic in structure". The two exceptional paths, which passed close to Hallett Station, indicated a fully continental thickness. Six paths included approximately equal distances across eastern and western Antarctica, and traversed the Ross Sea–Weddell Sea zone. If it happens that this zone includes a wide belt of very thin crust, the average thickness obtained by Press and Dewart may prove to be consistent with the present results. Three further paths crossed eastern but not western Antarctica, and for these it is not easy to find agreement unless there is a large region of oceanic crust south-west of Wilkes Station, which seems unlikely since Wilkes itself is situated on rock and the value of gravity there is close to normal.

8. Acknowledgments

This work has been made possible by the efforts of the New Zealand International Geophysical Year Antarctic party under the supervision of Dr T.

Hatherton, Chief Scientist. The authors wish to acknowledge the courtesy of the Institute of Physics of the Earth, Moscow, in providing copies of records from Mirny.

Department of Scientific and Industrial Research,
Wellington, New Zealand:
1959 *December.*

References

Bentley, C. R. & Ostenso, N. A., 1959. IGY Glaciological Report Series No. 2, Amer. Geograph. Soc., Group II.

Evison, F. F., Ingham, C. E. & Orr, R. H., 1959. *Nature*, **183**, 306–308.

Hill, M. N., 1957. *Physics and Chemistry of the Earth, 2* (ed. Ahrens, Press, Rankama & Runcorn), 129–163.

Jardetzky, W. S. & Press, F., 1953. *Bull. Seismol. Soc. Amer.*, **43**, 137–144.

Lee, A. W., 1932. *Mon. Not. R. Astr. Soc. Geophys. Suppl.*, **3**, 83–116.

Press, F. & Dewart, G., 1959. *Science*, **129**, 462–463.

Press, F. & Ewing, M., 1955. *Geol. Soc. Amer. Spec. Paper 62* (ed. Poldervaart), 51–60.

Stoneley, R., 1948. *Bull. Seismol. Soc. Amer.*, **38**, 263–274.

Focal Mechanisms of some Earthquakes of the year 1950

A. R. Ritsema

(Received 1960 March 3)

1. Data and Methods

The data used in this study are compressions and dilatations of *P* and *PKP* waves to be found in the International Seismological Summary of the year 1950, supplemented with some initial motion directions of these waves asked for and contributed by seismic stations situated in the zones relevant to the determination (Table 1).

Table 1

Additional data not reported in ISS

Earthquake No. (see Table 2)	Data
1	de Bilt *C*; Honolulu *C*; Hyderabad *D*.
2	de Bilt *D*; La Paz (*C'*); New Delhi *D*; Scoresby Sund *D*.
3	de Bilt *D*; Djakarta *C*; Honolulu *C*; La Paz *C*; New Delhi *D*.
4	de Bilt *D*; La Paz *D*; La Plata *D*; San Juan *C*.
5	La Paz *C*;
6	de Bilt *D*; Djakarta *D*; Honolulu *D*; New Delhi *D*; Ottawa *C*.
7	de Bilt *C*;
8	College *D*; Resolute Bay *C*; Sverdlovsk *D*.
9	Christchurch *C*; de Bilt *D'*; Djakarta *D*; Honolulu *C*; Wellington *C*.
10	de Bilt *D*; Djakarta *C'*; Honolulu *C*.
11	College *C*; de Bilt *C*; La Plata (*C*); San Juan *D*; Scoresby Sund *C*.
12	de Bilt *C'*; Djakarta *C*; La Paz (*C*); Wellington *C*.
13	Bogota *D*; de Bilt *C*; Guadalayara *D*; Honolulu (*D*); La Paz *D*; Scorseby Sund *D*.
14	Bogota *C*; de Bilt *D*; Honolulu *C*; Scoresby Sund *C*.
15	Christchurch *D*; de Bilt *D'*; Honolulu *C*; Hyderabad *D*; Riverview *D*; Sendai *D*; Wellington *D*.

Remarks: *C* : compressional *P* wave
D : dilatational *P* wave
C': compressional *PKP* wave
D': dilatational *PKP* wave
( ): inconsistent with the solution reached.

The amplitude of the longitudinal wave radiated as a result of a sudden motion along a flat fault plane in the focus of an earthquake is proportional to

$$\sin 2\theta \,.\, \sin \phi,$$

where θ and ϕ are spherical coordinates measured relative to the direction of the fault motion and the position of the fault plane respectively (Hodgson 1957). There are thus two quadrants with compressional onsets of the longitudinal wave interchanging with two quadrants with dilatational onsets. In the fault plane ($\phi = 0$) and in the plane perpendicular to the direction of fault motion ($\theta = 90°$) the amplitude of P is reduced to zero; these are the so-called nodal planes for longitudinal waves.

Assuming now that the initial character of the longitudinal wave remains unchanged on the pathway from the focus to the recording station, it is possible to determine the position of the two nodal planes in the focus with the help of the compression or dilatation data of many seismic stations all over the world. The problem is reduced to the determination of the angle i_r with the downward vertical in which the wave left the focus to emerge in the recording station at the known epicentral distance Δ. This (i_r, Δ)-function has been determined with the help of the travel-time tables of Jeffreys and Bullen ((t, Δ)-function) and the velocity distribution of longitudinal waves in the upper mantle derived by Jeffreys ((v_r, r)-function), by means of

$$\sin i_r = \frac{R}{r} \cdot v_r \cdot \frac{dt}{d\Delta}$$

where R is the Earth's radius, r is the radial distance from the focus to the centre of the Earth, v_r is the velocity of longitudinal waves at the depth of focus, and $d\Delta/dt$ is the velocity of the P wave front along the Earth's surface (Ritsema, 1958).

The compression and dilatation data are now plotted in a stereographic diagram. The tangential co-ordinate in the diagram is the azimuth of the recording station as seen from the epicentre, and the radial coordinate is taken in

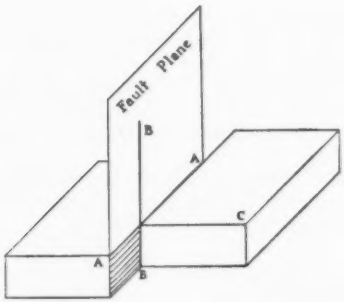

FIG. 1.

proportion to the value of tan $\frac{1}{2}i$. The compressions and dilatations are separated by two nodal lines that both follow the course of a meridional line in Wulff 's stereographic net and that in addition stand perpendicular to each other. The position of the nodal planes in the focus represented by these lines can directly be

read in the stereographic net. One of these nodal planes is the fault plane and the motion direction in the plane is given by the pole of the auxiliary plane.

2. Presentation of the results

The solutions, presented in Table 2, are given in the form of the positions, (azimuth and plunge) of the *A*-, *B*- and *C*-axes and of the earthquake type.

The fault motion direction is called the *A*-axis, the line in the fault plane perpendicular to the *A*-axis is called the *B*-axis, and the normal to the fault plane the *C*-axis (Figure 1). The *B*-axis is determined solely by the longitudinal wave data, it is the line of intersection of the two nodal planes. The positions of the *A*- and *C*-axes—the poles of the two nodal planes—are also determined in this way. These two axes, however, cannot be distinguished mutually without an investigation of the initial motions of the transverse waves in many directions around the focus. Since *S* waves have not been considered, the solutions in Table 2 are ambiguous with respect to the *A*- and *C*-axes. For each earthquake both possible solutions are given (*a* and *b* respectively).

The earthquake type is given in the form of a combination of the symbols *P* and *T* with *R* and *L* according to the accompanying scheme (Figure 2). The first of the two symbols noted gives the dominating characteristic of the earthquake.

Earthquakes of mainly *P* and mainly *T* type are characterized by a *B*-axis plunging at a smaller angle than 45°. The *B*-axis is the direction in which the second greatest stress component (σ_2) is acting. That means that the so-called plane of action, formed by the *A*- and *C*-axes, in which plane also the two principal stresses (σ_1 and σ_3) are situated, dips steeper than 45°. Assuming that the angle with the principal stresses in which the fault motion takes place is approximately 45°, type *P* is defined in such a way that the maximal stress component (σ_1) is more nearly horizontal than the minimal stress component (σ_3). In type *T* the minimal stress component (σ_3) plunges at a smaller angle than the maximal stress component (σ_1). Motions that are characterized by *P* and *T* type stress configurations are along reverse and normal faults respectively.

In the case that the *B*-axis plunges steeper than 45°, the principal stress components (σ_1 and σ_3) are situated in a plane dipping at a smaller angle than 45°. Transcurrent fault motions are characterized by such a stress configuration. The earthquake type is given as *R* or *L* respectively according to the dextral or sinistral character of the resulting fault motion.

Pure normal, pure reverse and pure transcurrent fault motions only rarely occur. Mostly there is a smaller or greater transcurrent component in mainly normal and mainly reverse fault motions; and also a smaller or greater normal or reverse component in the mainly transcurrent fault motions. The characterization of this minor component is given as a second symbol in the earthquake type.

3. Conclusions

The predominance of transcurrent fault motions in earthquake foci over reverse and normal fault motions is a confirmation of older results (Hodgson 1957). That the *A*- and *C*-axes show a preference for directions that are about perpendicular to and parallel with the seismic zones in which the earthquakes take place also is in accordance with known facts.

Table 2

The solutions reached

No.	Date 1950	Time h m s	Epicentre Lat. deg.	Epicentre Long. deg.	Depth		A-axis Azimuth	A-axis plunge	B-axis Azimuth	B-axis plunge	C-axis Azimuth	C-axis plunge	Type	Remarks
1	Feb. 28	10 20 55	46·0 N	143·8 E	0·04 R	a	N 87° E	20°	N 219° E	61°	N 350° E	20°	RP	Only a slight difference from Ishikawa's (1955) solution. We have consistent Honolulu and Hyderabad data, that in Ishikawa's solution are inconsistent.
						b	350	20	idem		87	20	LP	
2	April 26	07 04 55	33·7 N	135·8 E	0·00 R	a	N 70 E	70	N 313 E	10	N 220 E	18	TR	
						b	220	18	idem		70	70	TL	
3	May 17	11 46 48	39·4 N	130·3 E	0·08 R	a	N 258 E	43	N 52 E	46	N 155 E	13	RP	See also Keylis-Borok (1957). Our solution is well documented with 62 consistent against 3 inconsistent *P* data.
						b	155	13	idem		258	43	LP	
4	June 7	16 52 34	4·5 S	77·0 W	0·01 R	a	N 65 E	18	N 312 E	50	N 167 E	34	RT	The only difference between the two solutions is a dilatational *pP* wave of de Bilt that is consistent in cases *a* and *b*, inconsistent in *a'* and *b'*.
						b	167	34	idem		65	18	LT	
						a'	N 235 E	32	N 357 E	40	N 120 E	33	LT	
						b'	120	33	idem		235	32	RT	
5	July 9	02 35 29	7·9 N	72·6 W	shallow	a	N 90 E	5	N 347 E	70	N 182 E	20	LP	Solution fair, but small number of data. For macroseismic data see Ramirez (1953).
						b	182	20	idem		90	5	RP	
6	July 13	04 03 59	28·0 N	139·6 E	0·08 R	a	N 234 E	10	N 110 E	73	N 326 E	14	RT	The solution given by Kogan and Keylis-Borok (1957) is not in accordance with a large number of Japanese and North American compression data, that are consistent in our solution.
						b	326	14	idem		234	10	LT	
7	Sept. 10	03 21 22	35·5 N	140·4 E	shallow	a	N 182 E	25	N 294 E	40	N 69 E	40	PR	A small variation (5–10°) in the position of *A*-, *B*- and *C*-axis is possible.
						b	69	40	idem		182	25	PL	
8	Sept. 16	21 58 17	52·0 N	177·1 E	0·01 R	a	N 186 E	30	N 41 E	54	N 286 E	17	RT	A small variation (5–10°) in the position of *A*-, *B*- and *C*-axis is possible.
						b	286	17	idem		186	30	LT	

9	Sept.	22	23 53 32	17·6 S	177·1 W	0·06 R	a	N 139 E	6	N 33 E	68	N 231 E	21	LP	
							b	231	21	idem		139	6	RP	
10	Sept.	29	06 32 13	18·9 N	107·0 W	shallow	a	N 44 E	0	N 314 E	88	N 134 E	2	L	
							b	134	2	idem		44	0	R	
11	Oct.	5	16 09 42	10·4 N	85·7 W	0·015 R	a	N 180 E	68	N 28 E	20	N 295 E	10	PL	Tentative solution. With only a small decrease of consistent data also other solutions are possible. The reverse fault type is definite.
							b	295	10	idem		180	68	PR	
12	Oct.	21	04 12 59	18·5 S	173·5 W	0·005 R	a	N 170 E	5	N 274 E	70	N 78 E	20	LT	Fair solution, but small number of data.
							b	78	20	idem		170	5	RT	
13	Oct.	21	09 42 58	17·8 N	105·5 W	shallow	a	N 312 E	16	N 75 E	62	N 215 E	22	RP	
							b	215	22	idem		312	16	LP	
14	Nov.	17	19 28 16	16·8 N	100·7 W	shallow	a	N 185 E	30	from N 75 E to N 303 E	30 40	from N 310 E to N 70 E	45 36	P	Large variation possible in one of the nodal planes. The reverse fault type is definite.
							b	from N 310 E to N 70 E	45 36	idem		N 185 E	30	P	
15	Dec.	14	01 52 53	19·7 S	175·9 W	0·03 R	a	N 240 E	8	N 336 E	39	N 140 E	50	TL	A small variation (5–10°) in the position of *A*-, *B*- and *C*-axis is possible.
							b	140	50	idem		240	8	TR	

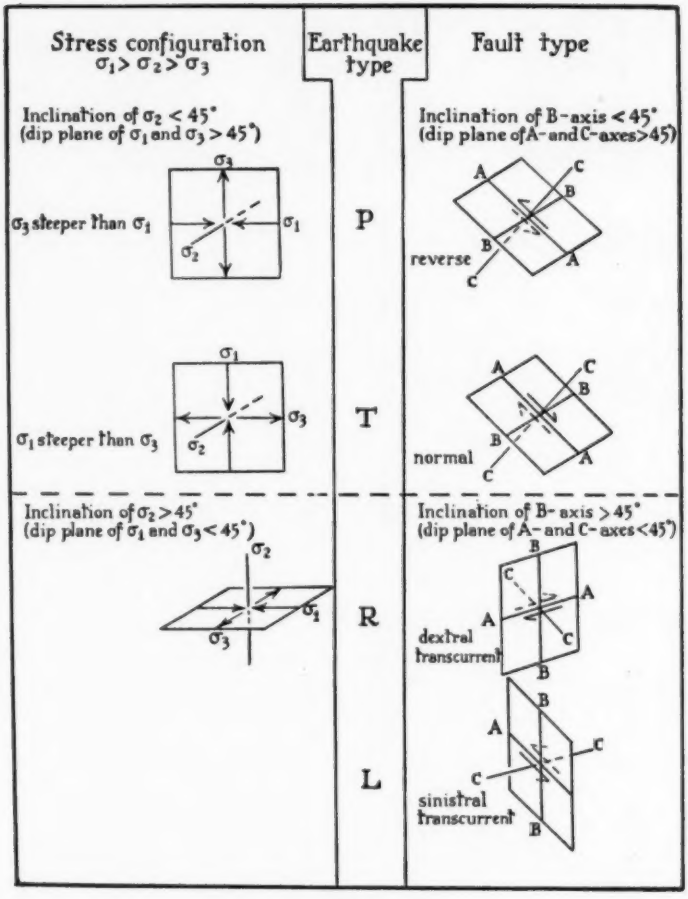

FIG. 2

The principal stresses are denoted by σ_1, σ_2, and σ_3, where $\sigma_1 > \sigma_2 > \sigma_3$. The *A*-axis is the fault motion direction, the *B*-axis is the line in the fault plane perpendicular to the *A*-axis, and the *C*-axis is the normal to the fault plane.

The *B*-axis is parallel to σ_2.

The plane of *A*- and *C*-axes is identical with the plane of σ_1 and σ_3.

The fault types are given as an illustration of the different stress configurations rather than as an equivalent definition for the earthquake types.

Acknowledgments

The readiness with which the Directors of the seismic stations replied to our questionnaires is gratefully acknowledged.

Royal Netherlands Meteorological Institute,
de Bilt,
Holland:
1960 May

References

Hodgson, J. H. (Ed.), 1957. Symposium on the Mechanics of Faulting, *Publ. Dominion Obs., Ottawa*, **20**, No. 2.

Ishikawa, M., 1955. *Quart. J. Seismol. Japan.* **20**, no. 4.

Keylis-Borok, V. I., 1957. *Trudy Geof. Inst. Akad. Nauk. SSSR*, **40**, 166.

Ramirez, S. J., J. E., 1953. *Inst. Geof. de los Andes Colomb. Bogotà*, Ser. A, Boll. 10.

Ritsema, A. R., 1958. (i, Δ)-curves for bodily seismic waves of any focal depth. *Verhand. no. 54, Lembaga Meteor. and Geofisik, Djakarta.*

A Theory of Polar Geomagnetic Storms

J. H. Piddington

(Received 1960 April 20)

Summary

This is the third of a series of papers outlining a hydromagnetic theory of geomagnetic storms. The first two dealt with the storm-time variations *Dst* in terms of isotropically propagating hydromagnetic compression (first phase) and rarefaction (main phase) of the geomagnetic field and its plasma.

The three phases of the longitude-dependent disturbance *Ds*, the first phase or *Sc*, the main phase and the preliminary reverse are all accounted for in terms of hydromagnetic waves whose Poynting fluxes are directed along the magnetic lines of force. These disturbances originate from "electromagnetic friction" between the solar wind and geomagnetic lines of force near 06 and 18h local time. These lines of force are bent out of their meridian planes and cause two pairs of "twist" waves to reach the Earth, being focused into relatively confined regions at high latitudes. These twists are stable or force-free and result in space-charge accumulations in the lower ionosphere where the resultant Hall current accounts for the observed disturbances.

During the main phase the twists are maintained by a deformation of the geomagnetic field which was described in the first two papers (the geomagnetic "tail"). Thus the tail theory accounts for both *Dst* and *Ds* main phase. It is difficult to see how any ring-current theory or other theory dependent on trapped corpuscular radiation could account for the asymmetric features of a storm.

The mechanism also provides the beginning of a theory of aurorae.

1. Introduction

It is generally agreed that geomagnetic storms and associated effects result from the passage past the Earth of neutral, ionized gas ejected from the Sun. Chapman & Ferraro (1931) showed that a cloud of such gas approaching the Earth would have electric currents induced in its surface layers and they explained the world-wide sudden increase in the horizontal component of the geomagnetic field as a direct result of these currents.

The discovery that the outer geomagnetic field encloses a highly conducting plasma has necessitated some modification of this theory. The currents at the surface of the cloud cannot affect the field directly (that is according to the Biot–Savart law) at the Earth. They can, and do, initiate a hydromagnetic disturbance comprising a general movement and distortion of the field and of the plasma into which the field is "frozen". This disturbance travels into the vicinity of the

Earth with a speed of $\sim 10^7$–$10^8\,\mathrm{cm\,s^{-1}}$ until it envelopes the lower ionosphere. The geomagnetic disturbance then diffuses through the ionospheric E-region as through a solid conductor according to ordinary "skin-effect" theory (Piddington 1959, called P.1).

Apart from this transmission theory the important difference between the Chapman–Ferraro theory and the hydromagnetic theory is that solar gas cannot flow freely into the geomagnetic field along lines of force which cut the Earth at high latitudes (P.1). These "horns" of gas are rigorously excluded by violent self-inductance effects and all the lines of force are bent (P.1, Figure 2), rather than cut (Chapman & Ferraro, Figure 4).

A second difference between the two theories follows from this: if the solar gas may only *diffuse* into the geomagnetic field then the initiation of the mass motion* required by a large-scale ring current seems improbable. Chapman & Ferraro's (1933) theory of the main phase of the *Dst* disturbance and Martyn's (1951) auroral zone theory encounter this difficulty; also it is likely that the fast westward drift at $\sim 10^8\,\mathrm{cm\,s^{-1}}$ required by this theory would have been noted during satellite experiments. An alternative mechanism involving a geomagnetic "tail" on the dark side of the Earth has been proposed (Piddington 1960, called P.2).

These theories have all dealt with the world-wide storm-time variations *Dst*, averaged in longitude and comprising an increase in the horizontal component of the geomagnetic field during the initial phase (*SC*) and a decrease during the main phase. When the *Dst* variations have been eliminated the remaining disturbance (*Ds*) is found to consist of three separate phases, each highly dependent on longitude as well as latitude and each concentrated towards the polar regions. It is with these complex systems of disturbances, which may be referred to broadly as "polar magnetic storms", that the present paper is concerned.

2. Polar magnetic storms

The total geomagnetic disturbance during a sudden commencement storm is represented by a function D of the longitude λ_S referred to the direction of the Sun and the time *tst* reckoned from the beginning of the storm. Thus, as Obayashi & Jacobs (1957) have written:

$$D(\lambda_S;\, tst) = Dst(tst) + Ds(\lambda_S;\, tst).$$

The longitude dependent part of the storm *Ds* takes three distinct forms during three phases of the storm as follows:

(*a*) During the initial phase or sudden-commencement (*SC*) phase the field has a form referred to here as *Ds*(*SC*).

(*b*) During the main phase disturbance field changes to *Ds*(*MP*).

(*c*) Sometimes, prior to *SC*, there is a preliminary reverse disturbance (*SC**) starting a minute or so before *SC*. This is referred to here as *Ds*(*PR*).

The longitude dependent part of magnetic storms which have no sudden commencement generally have a form similar to *Ds*(*MP*) and the theory of their origin is similar to that given below.

* This motion is not merely the differential drift which constitutes the ring current. In addition the whole mass of plasma within the current zone must spin around the Earth with a speed of order $10^8\,\mathrm{cm\,s^{-1}}$. This mass motion and the centrifugal force resulting from it is the basic requirement of the main phase of a storm; without it the current itself would rapidly die away.

The averaged atmospheric current systems which could account for these disturbances are complex; examples calculated and plotted by Obayashi & Jacobs (1957) are reproduced in Figure 1. These diagrams indicate that in polar regions the horizontal intensity could either increase or decrease during any of the periods, depending on λ_S and on the latitude. The whole of each of the three equivalent current systems is needed for a satisfactory description of the storm phenomenon, although it may be that *Ds*(*PR*) and even *Ds*(*SC*) are absent from particular storms.

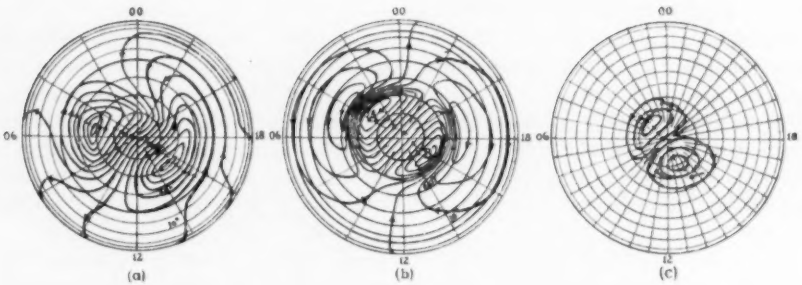

FIG. 1.—Atmospheric current systems which could account for the three phases of the *Ds* geomagnetic disturbance field (after Obayashi & Jacobs). (*a*) The *SC* phase, (*b*) the main phase, and (*c*) the preliminary reverse phase.

An examination of Figure 1 suggests that the main features of the *Ds* variations are as follows:

(*a*) The disturbances comprise sets of clockwise and anticlockwise current loops situated mainly in and above the auroral zones with one system of loops in the morning and one in the evening hemispheres.

(*b*) The disturbance vector changes rapidly both with longitude and latitude, within distances less than 1 000 km. This is remarkably small scale considering the likely dimensions of the original disturbance (~ 30 000 km).

(*c*) The *Ds*(*MP*) currents are generally similar to the *Ds*(*SC*) currents except for greater concentration in the auroral zone and also for two weak lower-latitude current loops.

(*d*) The *Ds*(*PR*) currents are almost perfectly reversed and weakened *Ds*(*SC*) currents (see Figures 1a and 1c).

(*e*) The *Ds*(*PR*) appears to be the initial part of the same disturbance which causes *Ds*(*SC*); when *Ds*(*PR*) is present then *Ds*(*SC*) is delayed for the duration of the reverse impulse (Gerard 1959).

(*f*) The centre of the morning disturbance occurs at about 05 hours local time or earlier; that of the evening disturbance at 17 hours or earlier.

(*g*) The intensity of the disturbance is about four times that of the *Dst* field.

3. The location and immediate cause of the *Ds* current systems

The equivalent (atmospheric) current systems of Figure 1 are not necessarily the systems actually responsible for the *Ds* field—they are merely a handy way of displaying this disturbance. The location of the actual *Ds* currents is the first

step in formulating a theory of their origin, but first it is instructive to review the corresponding problem for the *Dst* field.

There can be little doubt that the first phase of *Dst* results from a compression of the plasma and its frozen-in geomagnetic field. The compression wave travels towards the Earth causing a general increase in the horizontal component of the geomagnetic field. On reaching the ionosphere the wave sets up currents which account for the *initiation* of the observed geomagnetic disturbance. However, because of the low integrated conductivity of the ionosphere the electromagnetic wave front soon penetrates this region and establishes itself as a current sheet in the body of the Earth. Thus the *Dst* field, while *originating* in ionospheric current, is *maintained* by two other current systems*, one in the Earth and one adjacent to the solar wind (P.2).

Similar considerations apply to the main phase of *Dst* when the horizontal component of the field decreases everywhere due to an inward propagating rarefaction wave. The important point is that in either case ionospheric currents are driven by an induction electric field which only lasts while the requisite magnetic flux is entering or leaving the ionospheric "shell" and then ceases.

The *Ds* current system is much more complex but, as before, no currents above about 1 000 km may affect the field at the Earth's surface directly (according to the Biot–Savart law). This result is consistent with the tentative conclusions of Chapman & Bartels (1940, Chapter 22) based on harmonic analysis of the surface field. More distant current systems may, however, initiate hydromagnetic motions which result in currents in the ionosphere or Earth or both. The alternative, that ionospheric currents are due to winds there, appears most unlikely from the discussion in the appendix.

Let us then consider a possible origin of *Ds* in terms of a hydromagnetic disturbance incident on the lower ionosphere from above. The equivalent current systems indicate that its form must be quite different from that of the *Dst* compression and rarefaction waves. To determine its form consider an elementary ionospheric current loop as shown in Figure 2, corresponding to one current loop around region *A* of Figure 1b. An explanation of this elementary loop could be extended to cover all the main features of all three phases of the *Ds* field.

The clue to the origin of the current loop is the nature of the electric field required to drive the current. If the medium concerned were isotropically conducting, this would be necessarily an induction field $\mathbf{E}_i$ in the direction of the current and given by

$$\operatorname{curl} \mathbf{E}_i = -\frac{d\mathbf{H}}{dt}, \quad \operatorname{div} \mathbf{E}_i = 0, \tag{1}$$

where $\mathbf{H}$ is the magnetic vector. The hydromagnetic disturbance which could cause such a field comprises the expansion of a cylindrically shaped bundle of magnetic lines of force. It is shown in the appendix that such disturbances could not account for the main *Ds* features and that the actual current system must flow in the ionosphere rather than the Earth.

In the ionosphere the conductivity is anisotropic, having components σ_0 along the magnetic field, and σ_1 (Pedersen) and σ_2 (Hall) perpendicular to the field. In

* The statement in P.1 (Summary) that "the currents responsible for all geomagnetic disturbances must flow at levels below about 1 000 km" should be corrected to "the currents *directly* responsible ...". The Earth is certainly shielded from the direct effects of the current sheet at the surface of the solar wind. However, as already stated, the latter initiates the train of events leading to the observed disturbances and it is also needed to maintain any quasi-stable *Dst* field.

polar regions (and in Figure 2), the currents flow nearly perpendicular to the field, so that we are concerned with σ_1 and σ_2 and, when Hall current is prevented by the development of space-charge, an "effective" conductivity $\sigma_3 \equiv \sigma_1 + (\sigma_2^2/\sigma_1)$ (Baker & Martyn 1953). An electric field without divergence (equation (i)) would cause the observed current loop* but as seen in the appendix such a field may not be invoked because it may only be applied for brief periods (corresponding to the passage of a hydromagnetic disturbance).

A second type of electric field may also explain the current loop in Figure 2, provided this flows in an anisotropically conducting medium. This is a potential field $\mathbf{E}_p$ radially outwards and due to an accumulation of positive space-charge near O, having density q (e.m.u.). Then

$$\text{curl } \mathbf{E}_p = 0, \quad \text{div } \mathbf{E}_p = 4\pi q c^2, \tag{2}$$

and since $\sigma_2 > \sigma_1$, the current is mainly Hall current. Since it flows in closed loops the maximum effective conductivity σ_3 is not developed. As well as Hall

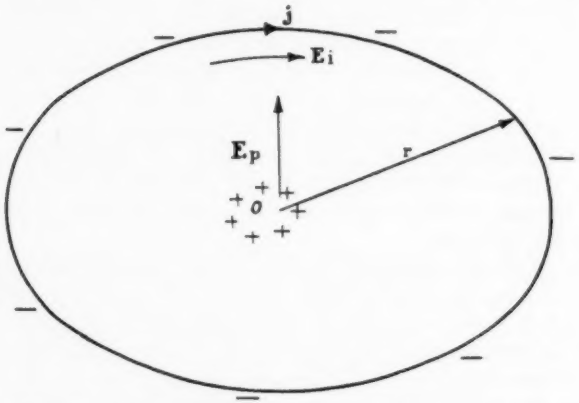

FIG. 2.—Two possible ionospheric electric field systems which could explain the *Ds* equivalent current loops.

current, Pedersen current $\sigma_1 \mathbf{E}_p$ must flow radially. This in turn requires a current to flow downwards into the ionosphere in the interior of the loop (and in region A of Figure 1b) and upwards out of the ionosphere near the boundaries of the loops.

The nature of the hydromagnetic disturbance needed to drive the *Ds* current system is now evident. It comprises a twist in the bundle of magnetic lines of force passing through the region between A and the outermost current loop of this particular (clockwise) system. This twist is identified with the downward flowing current $\mathbf{j}$ by the equation curl $\mathbf{H} = 4\pi\mathbf{j}$. This disturbance differs in two important ways from the *Dst* disturbances. First it is substantially force-free because the current follows the lines of force; this means that the phenomenon is magneto-hydrostatic and stable. Second, the downward current cannot flow below the ionosphere so that the disturbance remains anchored there instead of descending into the Earth.

In the following section it is shown that there are two distinct types of hydromagnetic wave which may propagate above the ionosphere. One of these is

* The appropriate conductivity would be σ_3 because the Hall current $\sigma_2 \mathbf{H} \wedge (\mathbf{E}_i/H)$ tends to flow radially and so is prevented by the development of a space-charge field.

responsible for the *Dst* disturbances and the second for the *Ds* disturbances. The latter has the distinction that it may only propagate along magnetic lines of force so that it tends to concentrate its effects near the poles, as observed for the *Ds* field.

4. The two types of wave responsible for the transport of the *Dst* and the *Ds* disturbances

There are two types of weak hydromagnetic wave*, having quite different properties. The differences are revealed by the equation for the mechanical force exerted by the distorted magnetic field on the plasma:

$$\begin{aligned} \mathbf{F} = \mathbf{j} \wedge \mathbf{H} &= \frac{1}{4\pi}(\operatorname{curl} \mathbf{H}) \wedge \mathbf{H} \\ &= -\operatorname{grad}\left(\frac{\mathbf{H}^2}{8\pi}\right) + \frac{1}{4\pi}(\mathbf{H} \cdot \nabla)\mathbf{H}. \end{aligned} \tag{3}$$

Of the two stress terms the first represents a gradient in the magnetic pressure and permits propagation as for a sound wave; the second denotes "magnetic stiffness" and permits propagation as for a transverse wave along a stretched string.

One type of hydromagnetic wave has the perturbation magnetic field **h** and and the gas velocity **v** in the plane containing **H** and the wave normal **n**. This wave uses either or both of the above stresses and always propagates with velocity $V = H(4\pi\rho)^{-\frac{1}{2}}$, where ρ is the plasma mass density. The energy flow (direction of the Poynting vector) is along **n**.

The second type of wave has **h** and **v** perpendicular to the **H**–**n** plane and this removes the stress term grad($\mathbf{H}^2/8\pi$) so that the wave is purely transverse and propagates with velocity $V\cos\psi$ where ψ is the angle between **H** and **n**. The Poynting flux is along **H** so that the energy flow is directed along the main field rather than along the wave normal.

The velocities of these two wave types, called *E*† or "isotropic" and *O* or "twist" waves respectively are shown in Figure 3 (reproduced from Piddington 1955). The most important difference between them, as far as geomagnetic disturbances are concerned, is the direction of energy flow.

In the geomagnetic meridian plane containing the Sun, the solar wind must distort the field always so that **h** also lies in this plane. A disturbance moving towards the Earth has **n** in the same plane and is therefore an isotropic wave. The result is a more or less uniform change in magnetic energy around the Earth, an increase during the initial phase and a decrease during the main phase. This is the proposed extension and modification (P.1, P.2) of the Chapman & Ferraro theory to account for the *Dst* field.

In meridian planes within a few hours of sunrise and sunset the solar wind moves mainly at right angles to the planes containing the magnetic field lines. There is a tendency here, as noted by Chapman & Ferraro and Martyn (1951), for the solar wind to blow *through* the outermost regions of the field. This is permitted by the setting up of an electric space-charge field which opposed the induction field $\mathbf{v} \wedge \mathbf{H}$ caused by the passage of the plasma through the geomagnetic

* A third wave which may be regarded as a modified sound wave is probably not important in the exosphere because of the low gas pressure.

† The symbols *E* and *O* stand for extraordinary and ordinary; at high frequencies these waves become the two well-known radio waves in a magneto-ionic medium.

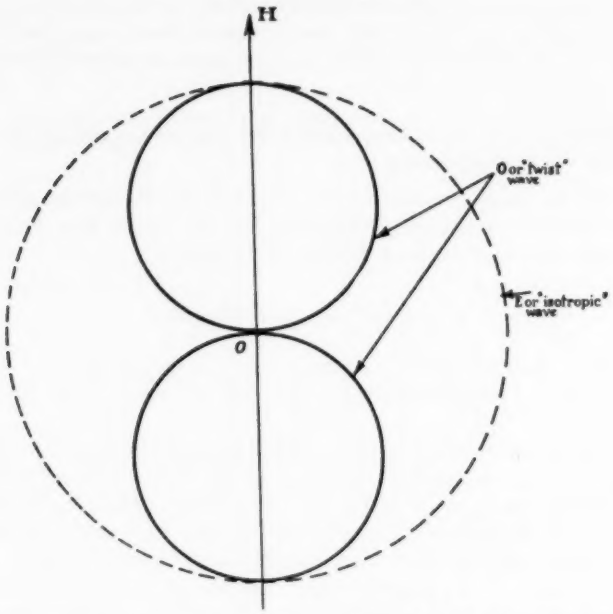

FIG. 3.—Wave fronts of the *E* or isotropic and *O* or twist hydromagnetic waves originating in the region near *O*.

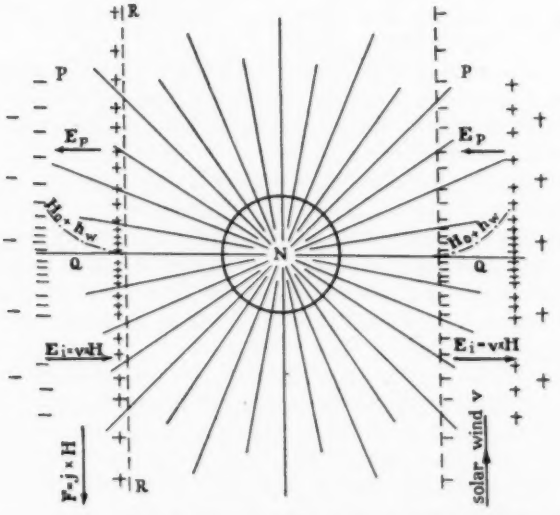

FIG. 4.—A schematic diagram of the Earth's magnetic dipole field viewed from a great distance above the north geomagnetic pole. Near the geomagnetic equatorial plane the solar wind of velocity v flows in the regions beyond the dashed lines (one marked *RR*). Electric space-charge fields E_p are set up and the magnetic lines of force bent as shown by the dot-dash lines.

field. In the morning hemisphere solar protons are forced inwards towards the Earth and electrons outwards, thus creating an outwardly directed space-charge field; an inward field develops in the evening hemisphere.

The situation is shown schematically in Figure 4 where the Earth is viewed from a long way above the north geomagnetic pole. The magnetic lines of force are all in meridian planes passing through the point of observation and so appear as straight lines, longer ones cutting the Earth at higher latitudes as shown. The inner boundaries of the solar wind, in regions not far from the equatorial plane, are represented by dashed lines on which electric space-charge is shown. Space-charge of opposite sign accumulates beyond the boundaries of the solar wind so that the potential electric fields shown as $\mathbf{E}_p$ are set up according to equation (2). The Lorentz forces responsible for setting up $\mathbf{E}_p$ are very powerful but as $\mathbf{E}_p$ tends to neutralize $\mathbf{E}_t = \mathbf{v} \wedge \mathbf{H}$, they are balanced and the situation tends to be stable without further flow of current or dissipation of energy of the solar wind. Situations where the dissipation is zero have been examined by Chapman & Ferraro (1931) for an infinite slab and by Ferraro (1937) for the non-uniform rotation of a magnetic star (the case of isorotation).

In the present situation the electrically polarized slabs of gas are not infinite in extent and substantial space-charge must leak away all around their boundaries. The current density in the slab ($\mathbf{j}$) required to replace this loss flows in the direction of $\mathbf{E}_t$ and exerts a force on the solar wind given by equation (3) and opposite to $\mathbf{v}$. Thus the current leakage results in a frictional drag on the solar wind. Additional drag may result from the formation of small space-charge clouds in the region of interaction (P.2) and by hydromagnetic instability (Parker 1959).

For the purpose of the present discussion the important result of the drag on the solar wind is that it causes a large-scale distortion of the geomagnetic field which propagates along the magnetic lines of force until it reaches the Earth as a twist hydromagnetic wave. This is discussed in the following section.

5. The electromagnetic field components of the *Ds* disturbance

The electric current systems in and around the electrically polarized slabs of solar wind are complex, particularly near the outer limits of the field (as at *P*, Figure 4). Nearer the centres of the slabs however (*Q*) the current should be predominantly in the direction $\mathbf{v} \wedge \mathbf{H}$ of the Lorentz force, even though this is opposed by a weaker space-charge electric field*. This current system, which for weak perturbation is everywhere nearly perpendicular to $\mathbf{H}_0$ and to the vector $\mathbf{v}$, initiates the sequence of events leading to *Ds*.

In Figure 5 the geomagnetic field is shown schematically, as seen from a direction a few degrees north of the Sun†. Two undisturbed lines of force are shown (full lines) and this field is referred to as $\mathbf{H}_0$. The solar wind passes through the outer parts of this field and the wind current system $\mathbf{j}_w$ is represented by the full lines at the left of the figure. The perturbation magnetic field due to $\mathbf{j}_w$ is $\mathbf{h}_w$, having the form of loops with $\mathbf{h}_w$ clockwise when looking towards the Earth. One such loop is shown, seen by an observer who has moved from his original position

* The question of Hall current does not arise because the electrons and positive ions do not spiral. If the opposed fields were equal, then the ions would follow straight paths. To replace boundary leakages the positive ions drift to the right across the lines of force in the direction $\mathbf{v} \wedge \mathbf{H}$. A possible secondary effect of Hall current is discussed in Section 9 below.

† So that the distorted lines of force may be shown in perspective.

towards the left-hand side of the diagram. This current system has no direct effect near the Earth because of shielding.

Near the geomagnetic equatorial plane the field $\mathbf{h}_w$ opposes $\mathbf{H}_0$ in front of the plane of the paper and reinforces it behind that plane and so constitutes a movement of lines of force away from the Sun. In the (meridian) plane of Figure 5 and north of the equatorial plane $\mathbf{h}_w$ is towards the Sun, south it is away from the Sun. Clearly the combined field $\mathbf{H} = \mathbf{H}_0 + \mathbf{h}_w$ is as shown by the dot-dash lines in Figure 4, the lines of force being on surfaces formed by bending the outer parts of meridian planes away from the Sun. Such a bend in the lines of force must propagate as a hydromagnetic disturbance by virtue of the force term $(\mathbf{H} \cdot \nabla)\mathbf{H}$ of equation (3). At the bend the perturbation field is perpendicular to

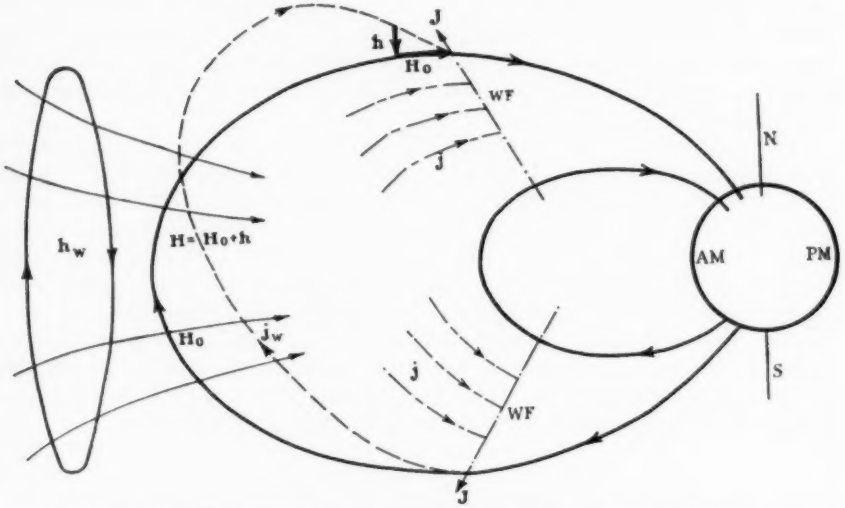

FIG. 5.—A hydromagnetic twist caused by the solar wind dragging on the geomagnetic field. To provide perspective the Earth is viewed from a point north of the Sun.

the meridian plane which contains the main field $\mathbf{H}_0$. Any wave which is to reach the vicinity of the Earth and cause observable geomagnetic effects must have its normal in that plane and so must propagate as an *O* wave with its Poynting flux along $\mathbf{H}_0$ (Section 4 above). This explains why the observed *Ds* disturbance is mainly polar.

Now let us consider the hydromagnetic *O* wave when its front has advanced to the position *WF* shown by dot-dashed lines in Figure 5. It must have separated into two parts, one following the lines of force to the northern and one to the southern hemisphere. Just as for the *Dst* wave front, the passage of the *Ds* wave front must cause changes in the geomagnetic field and its plasma as it passes through a particular region. These changes will remain after its passage so that before examining conditions inside *WF* it is desirable to consider those between *WF* and the solar wind.

Consider the line *RR* of Figure 4 representing the inner boundary of the solar wind. Outside this boundary the current $\mathbf{j}_w$ is mainly across the magnetic lines of force. Inside the boundary, however, the plasma is at rest and the current $\mathbf{j}$ consti-

tutes a leakage of space charge from the wind region. Because of the much higher conductivity along the magnetic field the current flows mainly in that direction as shown in Figure 5. This current system not only accounts for leakage from *RR* and hence the wind current system itself but also, as shown below, is a necessary adjunct to the wave front itself. The magnetic field $\mathbf{h}$ caused by $\mathbf{j}$ is similar to $\mathbf{h}_w$ but it combines with $\mathbf{H}_0$ in a very different manner causing the lines of force to assume spiral forms. In other words $\mathbf{j}$ introduces a *twist* into the bundle of lines of force in which it flows. In the northern hemisphere and looking along $\mathbf{H}_0$ it is a right-handed twist.

The electromagnetic field within the wave front itself is examined in the following sections. It is evident, however, that as *WF* defines the lower boundary of the twist, current must flow down the magnetic lines of force into its central region and then out across the lines of force and in the plane *WF*. Some must escape into interplanetary space as shown by the vector $\mathbf{J}$; some must flow in other directions and so into the geomagnetic field. Variations in plasma conductivity and extent of the current paths make it likely that the $\mathbf{J}$ current will vary around the wave front so that the twist is asymmetric.

The three current systems discussed above and their magnetic fields and mechanical forces may be described in a more quantitative manner by use of the equations:

$$\text{curl } \mathbf{h}_w = 4\pi\mathbf{j}_w, \qquad \text{curl } \mathbf{h} = 4\pi\mathbf{j}. \tag{4}$$

Consider a right-hand system of axes with Ox tangential to $\mathbf{H}_0$ at the origin and Oy in the direction $\mathbf{v}$; the directions of Ox and Oz change as O moves about in the geomagnetic field. In the region penetrated by the solar wind we have $\mathbf{j}_w \sim 0, 0, -j_{wz}$, so that

$$\frac{\partial h_{wz}}{\partial y} - \frac{\partial h_{wy}}{\partial z} = 4\pi j_{wz}, \tag{5}$$

which indicates that the lines of force are bent like the dashed line in Figure 5. There is a retarding force of density $\mathbf{f}_y = -j_{wz}\mathbf{H}_0$ on the wind and an opposite stress on the magnetic field. Near the equatorial plane the important perturbation is h_{wx} so that

$$\mathbf{f}_y \sim \frac{\mathbf{H}_0}{4\pi}\frac{\partial h_{wx}}{\partial y}. \tag{6}$$

Integrating in the Oy direction, the total force per cm^2 opposing the solar stream is $\mathbf{H}_0 h_{wx}/4\pi$. Far from the Earth the dipole field is too weak to oppose the solar stream and h_{wx} must be small. It should increase to a maximum in the region where the perturbation field is approximately equal to the dipole field, that is where the lines of force are substantially bent. Here the $h_{wx} \sim \mathbf{H}_0 \sim \mathbf{h}_m$ and the total force $\mathbf{h}_m^2/4\pi$ must be equated to the rate of loss of momentum of the solar stream:

$$h_m^2 = 8\pi\beta NMu^2. \tag{7}$$

Here N, M and u are the ion density, mass and velocity and β (< 1) the proportion of the total momentum lost. It is shown below that the relative intensities of *Ds* and *Dst* suggest a value of $\beta \lesssim 0{\cdot}4$.

Between the solar wind and *WF* the important current is along the field, so that

$$\frac{\partial h_z}{\partial y} - \frac{\partial h_y}{\partial z} = 4\pi j_x, \tag{8}$$

which describes a twisted bundle of lines. The force on the plasma is $\mathbf{j} \wedge \mathbf{H} = 0$ so that the field is force-free. Since there are no electromagnetic forces on the plasma (which would need to be balanced by inertial forces or pressure gradients) the situation should be stable. Conditions inside *WF* are discussed in the following section.

6. The propagation of a hydromagnetic twist

The *Ds* twists are probably asymmetrical but their important features should be revealed by analysing a circularly symmetrical twist shown schematically in Figure 6, which is now described.

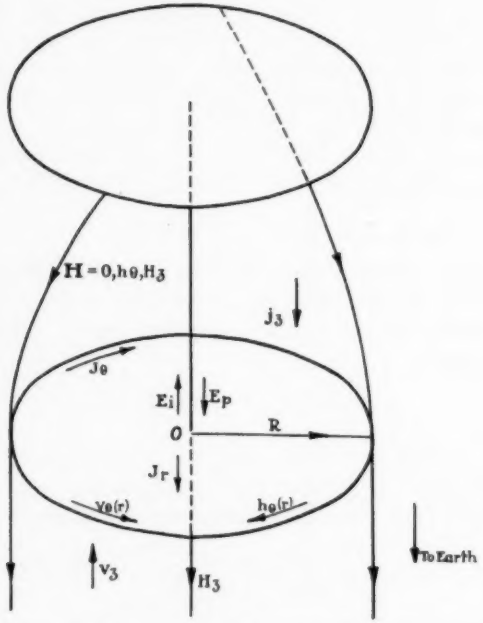

FIG. 6.—A simplified (cylindrical) hydromagnetic twist propagating down the magnetic field H_3.

In a right-handed system of cylindrical co-ordinates (r, θ, z) assume a uniform magnetic field and ion plasma contained within a cylinder $r = R$. The field is parallel to Oz and may be assumed substantially frozen into the plasma which, in turn, is contained within an insulating cylinder. A twist is now introduced into part of the bundle of lines of force and the propagation of the disturbance is examined.

Assume that in the region $z < 0$ there is a perturbation magnetic field $\mathbf{h} = 0, h_\theta(r), 0$ which is associated with a current of density $\mathbf{j} = 0, 0, j_z(r)$. Maxwell's equation relating these parameters is then

$$\frac{1}{r}\frac{\partial}{\partial r}(rh_\theta) = 4\pi j_z. \tag{9}$$

There must be a second current system $J_r(r)$, being the *total* radial current density

in the surface of discontinuity $z = 0$. The equation $\operatorname{div} \mathbf{j} = 0$ must be satisfied to a very high degree of approximation and integrating through the region of discontinuity we have

$$\frac{1}{r}\frac{\partial}{\partial r}(rJ_r) - j_z = 0. \tag{10}$$

Combining these equations we find

$$h_\theta = 4\pi J_r. \tag{11}$$

The propagation of the boundary of this twist may be studied by transforming to axes in which the magnetic field does not change with time, so that the wave front is at rest and the plasma enters it with velocity $-v_z$ and leaves with velocity $(0, -v_\theta, -v_z)$, as shown in Figure 6. The force-momentum equation in the θ direction is then

$$\rho v_z v_\theta = J_r H_z, \tag{12}$$

where ρ is the mass density of the plasma. Also, if the gas is constrained to move along the magnetic lines of force, then

$$v_\theta = v_z \frac{h_\theta}{H_z}. \tag{13}$$

Combining equations (11), (12) and (13),

$$v_z = H_z(4\pi\rho)^{-\frac{1}{2}}, \tag{14}$$

so that the front of the twist advances through the plasma with the usual Alfvén velocity.

This result shows that twist waves have velocities which are independent of their wavelength and strength (provided they remain weak). The medium is non-dispersive and the disturbance advances as a single front with conditions changing more or less abruptly from one side to the other. The propagation of an asymmetric wave, that is a wave in which h_θ varies with θ, should be similar to that analysed above although its effects on arriving in the ionosphere will be different.

7. Electric fields and "slipping"

In the previous section propagation of the twist was discussed in terms of the momentum change of the plasma and the consequent electric current and magnetic field gradient. It is also necessary to consider the electric field responsible for J_r. If the plasma were isotropically conducting this would simply be the induction field caused by the flow of plasma across the perturbation field h_θ in the transition region (Figure 6):

$$\mathbf{E}_i = \mathbf{v} \wedge \mathbf{H} = (v_z h_\theta, 0, 0). \tag{15}$$

This field drives current out of the twist cylinder where, to ensure its further progress (to complete the current loop), positive space charge will accumulate, giving rise to a potential field $\mathbf{E}_p$.

This secondary field has several interesting effects: in the first place it performs the function for which it was created, namely of driving current up the

lines of force surrounding the twist thus limiting the extent of the twist and allowing its current to escape. Within the wave front $\mathbf{E}_p$ is radially inwards, thus opposing $\mathbf{E}_t$. The difference between the two is related to the total current J_r integrated through the front, by Ohm's law:

$$J_r = \Sigma\,(v_z h_\theta - \mathbf{E}_p), \quad \text{where } \Sigma = \int \sigma\, dz, \tag{16}$$

σ being the ordinary conductivity and Σ the conductivity integrated through the slip region.

If the external circuit has high resistance then $\mathbf{E}_p$ will largely cancel $\mathbf{E}_t$ as in a homopolar generator with little or no load. The transition region then tends to be extensive in order that Σ may be large enough to provide the required current J_r with a much reduced net electric field. Since it is the front of the disturbance region which travels at the velocity given by equation (14), the main part of the twist tends to be delayed behind this front. This delay and the prior arrival of a space-charge electric field is shown to be the cause of the preliminary reverse impulse *Ds*(*PR*).

Now consider a plasma which is not only anisotropically conducting but in which the ion collision distance and gyro-radius may exceed the dimensions of the disturbance. The concept of conductivity may no longer be applied; rather must the paths of individual ions be studied.

In axes in which the disturbance is at rest the plasma flows with velocity $-v_z$ into the twist. The electrons may be regarded as firmly attached to the magnetic lines of force. The heavy ions, having a velocity component $v_z h_\theta / H_z$ perpendicular to the lines of force are deflected outwards and if space-charge could be neglected they would be deflected inwards again and would spiral down the lines of force. Thus the whole mass of the gas would be deflected along the lines of force as required.

However, as the ions start to move out from the plasma* they create space charge. If they moved out one gyro-radius $v_z h_\theta M / H_z^2 e$, where e and M are their charge and mass, then space charge per cm^2 area of cylinder wall would be

$$Q = \frac{NMv_z h_\theta}{H_z^2} = \frac{v_z h_\theta}{4\pi V^2}. \tag{17}$$

The corresponding radial electric field is found by integrating equation (2):

$$\begin{aligned} \mathbf{E}_p &= (E_{pr}(r),\, 0,\, 0) = -4\pi q c^2 \\ &= \frac{-c^2}{V^2} \cdot v_z h_\theta. \end{aligned} \tag{18}$$

The induction field $v_z h_\theta$ is responsible for the creation of the reverse (space-charge) field. The latter may approach the former in magnitude but cannot exceed it; yet if the ions were allowed to spiral freely then $\mathbf{E}_p$, as given by equation (18), would exceed $v_z h_\theta$ by the very large factor c^2/V^2. This means that the plasma must continue to move nearly parallel to the axis of the cylinder; in other words the space-charge provides slip between the field and plasma as in the case of the isotropically conducting fluid. Since the space-charge field must cause external currents to flow there will also be some twist as well as the slip.

* The enclosing insulating cylinder might here be assumed to be replaced by plasma at a pressure sufficient to contain the magnetic field.

Now consider the situation when the disturbance collides with a rigid semi-conducting sheet behind which is an insulating medium. The sheet is meant to represent the ionosphere which, as far as the propagation of geomagnetic disturbances is concerned, may be considered a rigid sheet (P.1).

8. The principal ionospheric current system

Although the preliminary reverse impulse, when it occurs, precedes the *Ds*(*SC*) and *Ds*(*MP*) disturbances, its discussion will be delayed to the following section.

Consider the situation when the twist has been established right down to the lower ionosphere. There is no longer any slip, the current j_z flows into the ionosphere and the geomagnetic field lines are twisted (h_θ) down to the same level. The situation is magneto-hydrostatic, being stable because the current flows very nearly along the field so that the force on the plasma, $\mathbf{j} \wedge \mathbf{H}$, is nearly zero, even though $\mathbf{j}$ is finite. This is the important difference between the *Ds* current system and the *Dst* system; the latter flows at a large angle to $\mathbf{H}$ and so moves the plasma in such a way as to transfer the current down through the ionosphere and into the Earth.

The downward current system j_z cannot continue past the ionosphere but must flow radially outwards from the cylinder and back up the magnetic lines of force which surround the cylinder. Thus a quasi-stable current is established in and above the ionosphere. However, as this current flows in a closed system of sheets* its magnetic field at the surface of the Earth is likely to be small. A more important feature of the radial ionospheric current is that a space-charge electric field must be established to drive it. The current flowing down from above causes positive space-charge to accumulate in the cylinder, giving a radial outward electric field. This field will drive a Hall current in a clockwise direction (viewed from above). Since the height-integrated ionospheric Hall conductivity is about twice the Pedersen conductivity (Baker & Martyn 1953, p. 291) the Hall current J_θ is about double J_r. The magnetic effects of J_θ at the Earth are likely to be more than double those of J_r.

It is this clockwise current system which is proposed as the cause of the first phase of a sudden-commencement geomagnetic storm in the morning hemisphere. A corresponding anticlockwise system, caused by an oppositely directed twist, would then account for the afternoon disturbance.

In Figure 5 the outer line of force is shown as deflected out of its meridian plane away from the observer. If it is gripped firmly enough by the solar wind it will become frozen into the wind and be carried away to contribute to a geomagnetic "tail". This tail may explain the *Dst* main phase (P.1 and P.2) since it causes a general decrease in magnetic energy and magnetic pressure throughout the remaining geomagnetic field. It may also explain that part of the *Ds* field which continues after the solar gas cloud has passed the Earth. The magnetic lines of force will remain bent in much the same way as shown in Figure 5 except that the outermost part will be carried away entirely.

In P.2 certain advantages of the magnetic tail theory of *Dst* over ring-current theories were discussed. However, the total main-phase disturbance comprises $Dst+Ds$, their separation being quite arbitrary; any satisfactory theory must

* Comprising pairs of co-axial cylinders with current flowing down the inner cylinder and up the outer cylinder and connected via the ionosphere.

explain the *total* disturbance. Any ring current theory or other theory involving ions trapped within the geomagnetic field could only cause a *circularly symmetrical* disturbance such as *Dst*. Some separate mechanism, in which the direction of the wind vector **v** retained its significance *after the wind ceased to blow*, is needed to explain *Ds*. The magnetic tail theory explains the whole phenomenon.

The equations of Section 5 may now be used to find the electric current for a given amount of twist of the magnetic field. For simplicity assume the pitch of the magnetic spiral to be independent of r so that

$$h_\theta(r) = rh_0, \tag{19}$$

where h_0 is independent of r. Then from equation (9)

$$j_z = \frac{h_0}{2\pi}, \tag{20}$$

so that j_z is also independent of r. The ionospheric current is then found from equation (10)

$$J_r = \frac{rh_0}{4\pi}. \tag{21}$$

During a moderate magnetic storm a total Hall current of $\sim 2\times 10^5$ A flows in a loop of radius ~ 1000 km so that the current per cm strip $J_\theta \sim 2\times 10^{-3}$ A or 2×10^{-4} e.m.u. If the integrated Hall conductivity is $1{\cdot}4\times 10^{-8}$ (Baker & Martyn 1953) then the electric field required is $1{\cdot}4\times 10^4$ e.m.u. or $1{\cdot}4\times 10^{-4}$ V cm^{-1}. The total potential difference across the current system is $1{\cdot}4\times 10^4$ V, a value large enough to be significant in auroral theory.

The Pedersen current J_r flowing during a moderate stor will be about half J_θ or 10^{-4} e.m.u. per cm strip. The total current flowing out of the cylinder is $2\pi RJ_r$ or $6{\cdot}3\times 10^4$ e.m.u.; this is also the total current flowing down the cylinder. In the case of the geomagnetic field the radius R of the bundle of lines of force varies with the distance from the Earth but the product $2\pi RJ_r$ is constant so that equation (21) gives

$$h_0 = 1{\cdot}3\times 10^4 R^{-2}. \tag{22}$$

The angle through which a line of force rotates in a distance dz is

$$d\theta = \frac{h_0}{H_z}dz = \frac{1{\cdot}3\times 10^4}{R^2H_z}dz. \tag{23}$$

The magnetic flux in the bundle is πR^2H_z and must be a constant so that equation (23) may be integrated to give

$$\theta = \frac{1{\cdot}3\times 10^4 z}{R^2H_z}. \tag{24}$$

The value of R^2H_z at the Earth is about 5×10^{15} and if z is taken as say 6 earth radii then $\theta \sim 0{\cdot}1$ radian which provides a rough estimate of the total twist. If this is related to the form of distortion depicted in Figure 5, then the outermost lines of force will twist through $\sim 0{\cdot}2$ radian and those much closer to the Earth through zero angle. The twist relative to an intermediate region is then $\sim 0{\cdot}1$ radian.

A twist of $0{\cdot}2$ radian originating in the region where $h_m \sim H_0 \sim 10^{-3}$ gauss, is easily accounted for by a modest solar wind provided β in Equation (7) is not

too small. For example, if $\beta = 0{\cdot}2$ and $u = 10^8\,\mathrm{cm\,s^{-1}}$ then the number density required is $N \sim 50\,\mathrm{cm^{-3}}$ and the particle flux Nu is about 5×10^9 protons $\mathrm{cm^{-2}\,s^{-1}}$. This is about 20 times less than some estimates of the peak value.

The greatest uncertainty in the above estimate of the solar wind flux is the value of the "frictional" term β. An order-of-magnitude estimate of β may be made by comparing the magnitudes of observed *Dst* and *Ds*. The former results from an isotropically propagating wave, the latter is focused by converging lines of force and so should increase in strength by a factor $(H_e/h_m)^{\frac{1}{2}}$, where H_e is the strength of the main field near the Earth ($\sim 0{\cdot}4$ gauss). Putting $h_m = 10^{-3}$ gauss as above the gain factor is 20 whereas the observed difference in intensity is about 4. This suggests that β might have a value of $0{\cdot}4$. There is another factor which may increase the transmission efficiency of the *Ds* wave, however, that is the fact that the observed disturbance is due to Hall current and stronger than the original current by a factor $\int \sigma_2 ds \div \int \sigma_1 ds \sim 2$ (Baker & Martyn 1953). This would reduce β to the value $0{\cdot}2$.

9. Some secondary storm effects (including *SC**)

Of the various features of a *Ds* disturbance listed in Section 2 above, three remain to be explained, perhaps the most notable being the preliminary reverse impulse.

9.1. *The preliminary reverse impulse Ds (PR or SC*).*—In Section 7 it was shown that if the current J_r at the leading edge of the twist in a bundle of lines of force could not escape freely, then its reverse space-charge field would cause slipping. This effect is simply relative rotation of plasma and field as in an unloaded homopolar generator. The leading edge of the slip region moves with the Alfvén velocity but the arrival of the full twist and its radical current system J_r is delayed. The arrival of the reverse electric field is not delayed however; in fact it might even precede the wave front because of the flow of space charge *down* the lines of force.

In the example given above and in Figure 6, negative space-charge develops inside the cylinder of lines of force and positive charge on its surface. The electric field is directed inwards and the ionospheric Hall current flows in an anticlockwise direction, opposite to that during the subsequent phases. In this way the two features of *Ds*(*PR*) are explained: first it is almost an exactly reversed (and weakened) *Ds*(*SC*). Second, the presence of *Ds*(*PR*) implies a delay in the onset of *Ds*(*SC*) (Gerard 1959).

9.2. *Asymmetry about the noon meridian.*—From the above theory, as developed to this point, perfect symmetry of the *Ds* field about the noon meridian would be anticipated. However, instead of the centres of the equivalent current systems (*A* and *B* of Figure 1b) being at 06 hours and 18 hours local time they are an hour or so earlier. This time difference varies from storm to storm and by smaller amounts during a particular storm.

The obvious asymmetrical feature in the interaction of the solar wind and geomagnetic field is that the heavier protons are deflected to the right and the lighter electrons to the left. This feature might account for the positions of the *Ds* current loops in the following manner. In Section 5 it was stated that within the region of interaction of the geomagnetic field and the solar wind Hall current was

not of primary importance because the electric fields $\mathbf{v} \wedge \mathbf{H}$ and $\mathbf{E}_p$ nearly balanced and so the ions followed nearly straight lines. However, they will not follow perfectly straight lines and any residual deflecting force will affect the electrons much more than the ions.

If the electrons suffer appreciable deflection they will lag behind the ions, thus creating an electric current in the direction $\mathbf{v}$ of the solar wind. This current is simply Hall current and flows in both layers of gas outside the dashed lines (*RR*) of Figure 4. Since this current flows only in the gas passing through the geomagnetic field, it is not continuous and causes positive space charge to accumulate in the dark hemisphere (at *PP*) and negative charge in the light hemisphere. These accumulations shift the "centres of gravity" of the space charge on the boundaries *RR* in a clockwise direction both in the *AM* and *PM* hemispheres. This movement in turn moves the centres of the hydromagnetic twists and so the ionospheric current loops to positions of earlier local time.

9.3. *The low-latitude current loops of Ds(MP).*—The remaining feature of *Ds* requiring explanation is the pair of weak current loops of Figure 1b centred at latitude $\sim 58°$. These loops and the squeezing of the main loop systems *A* and *B* up into the region in and above the auroral zone are the main differences between the *Ds(SC)* and *Ds(MP)* phases.

These differences should be accounted for in terms of the different origins of *Ds(SC)* and *Ds(MP)* described above. The former is caused by the solar gas impinging on the solar side of the geomagnetic field and bending the lines of force out of their meridian planes. This bending away from the Sun causes a clockwise ionospheric current loop in the *AM* hemisphere. As the main phase develops, lines of force from all longitudes are swept away to form a geomagnetic tail. Only lines of force which cut the Earth at high latitudes contribute to this tail and after the solar gas cloud has passed the main twists and ionospheric current loops are associated only with these lines. Hence the current loops should be concentrated at high latitudes as observed.

Apart from the tail section, the geomagnetic field is now free from forces in the Sun–Earth direction. It will, however, experience forces from the opposite direction due to expansion of the bundle of lines of force forming the tail. For the present discussion this bundle may be regarded as consisting of three parts. The first is a central part whose lines of force cut the Earth at longitudes a few hours from local midnight. The pressure of this bundle in tending to expand has much the same effect as the pressure of the solar wind near the midday meridian. It causes a small increase in the horizontal component which partially neutralizes the general decrease (*Dst* main phase) resulting from the formation of the whole tail (P.2).

The two outer parts of the geomagnetic field comprise lines of force which have been pulled away from the sunlit hemisphere. In tending to expand they push those remaining parts of the geomagnetic field lying near the 06 and 18 hour meridians in the direction of the Sun. This pressure should have the reverse effect of that of the solar wind blowing past these same lines of force (*Ds(SC)*) and so should lead to reverse current loops at latitudes below the auroral zones.

10. Discussion

In Section 3 and Appendix it was shown probable that the equivalent current systems of all three phases of a polar geomagnetic storm are real current systems

flowing in the ionosphere and that the main observed effects are due to Hall currents. These quasi-steady currents may only be maintained by electric currents flowing into and out of the ionosphere from the region of interaction of the solar wind and the geomagnetic field.

The origin and propagation of those external disturbances have been studied quantitatively and found to fit the observational results. Essentially they are due to a type of hydromagnetic disturbance which may only travel along the magnetic lines of force. The important effect during the main phase of a storm is the formation of a geomagnetic "tail" directed away from the Sun.

Although the discussion has centred on sudden commencement storms because these comprise such a variety of features, it applies equally well to the storms which start slowly, last for 3–4 days or more and have a 27-day recurrence period. The explanation of these storms is similar to the *Ds*(*SC*) or *Ds*(*MP*) above.

It is important to notice that although storm effects have been arbitrarily divided into longitude independent (*Dst*) and longitude dependent (*Ds*) parts any satisfactory theory of the main phase must explain both parts. It would seem that any ring-current theory or any theory depending on trapped (van Allen) radiation could only account for circularly symmetrical effects (*Dst*) while the magnetic tail theory introduces the important element of asymmetry.

Appendix

There is now fairly conclusive evidence that the various geomagnetic storm effects result, indirectly, from temporary increases in the flow of solar ions past the geomagnetic field. If the direct cause of the storms (or of their polar parts) is a system of ionospheric winds then the latter must be caused by the solar wind. This could only be effected by hydromagnetic action and if this occurs we already have a source of magnetic disturbance without postulating violent ionospheric wind systems. To be more specific it has been shown that geomagnetic disturbances in general pass through the ionosphere as through a solid semi-conductor (P.1). This is because neutral atoms collide so infrequently with ions that it takes a number of hours (~ 6) to start ionospheric winds by means of electromagnetic forces. It is concluded that a storm theory based mainly on changes in ionospheric winds is untenable.

Another form of atmospheric dynamo theory is that of Obayashi & Jacobs (1957) in which the wind system remains that of geomagnetically quiet days but the electrical conductivity (and hence the current density) increases. This theory and the earlier version (or their combination) has been criticized by Maeda (1959) on the grounds that the winds or conductivity changes needed would be unreasonably large. The quiet day ionospheric current system driven by the wind dynamo flows in low as well as high latitudes and it is known that no substantial increase in the conductivity at these low latitudes occurs at the time of a storm. An examination of the whole dynamo current system suggests that even if the conductivity near the poles became infinite the current around the whole dynamo circuit would show no great increase (D. F. Martyn, private communication). Added to these difficulties is that of the *Ds*(*PR*) which shows a completely reversed system of currents and so could hardly be accounted for in terms of changing conductivity.

It is concluded that ionospheric winds play no important part in driving the currents responsible for *Ds*.

There is another way in which the electric field $\mathbf{E}_t$ of Figure 2 could be induced, apart from ionospheric winds flowing radially inwards towards *O*. That is, by an outward movement of magnetic lines of force and hence a decrease in **H** (equation (1)). Such movement would require a radially outward stress on the bundle of lines of force above the current loop. In view of the results of P.1 on hydromagnetic transmission in this region it seems most unlikely that the plasma there could continue to exert such a mechanical force for the many hours of *Ds*(*SC*) and *Ds*(*MP*). However, even if it could, it is easily shown that the low conductivity of the ionosphere would allow such a large value of $-\partial\mathbf{H}/\partial t$ that the vertical component would decrease much more than observed. This would mean that the inductive current loop opposing the decrease in **H** (which is mainly vertical component) would transfer to the Earth itself. Here the conductivity is sufficient but the components of the perturbation field other than the vertical component are quite different from those inferred from Figure 1(b).

Thus the electric field driving the *Ds* current system cannot be an induction field (irrespective of where the currents flow) and the current system cannot flow in the Earth, where only an induction field would be effective.

C.S.I.R.O.,
Radiophysics Division,
Sydney,
Australia:
1960 *April*.

References

Baker, W. G. & Martyn, D. F., 1953. *Phil. Trans. Roy. Soc.*, *A* **246**, 281.
Chapman, S. & Bartels, J., 1940. *Geomagnetism*, Vol. 11 (Clarendon Press Oxford).
Chapman, S. & Ferraro, V. C. A., 1931. *Terr. Mag.*, **36**, 171.
Chapman, S. & Ferraro, V. C. A., 1933. *Terr. Mag.*, **38**, 79.
Ferraro, V. C. A., 1937. *Mon. Not. R. Astr. Soc.*, **97**, 458.
Gerard, V. B., 1959. *J. Geophys. Res.*, **64**, 593.
Maeda, H., 1959. *J. Geomag. Geoelec.*, **10**, 66.
Martyn, D. F., 1951. *Nature* (London), **167**, 92.
Obayashi, T. & Jacobs, J. A., 1957. *J. Geophys. Res.*, **62**, 589.
Parker, E. N., 1959. *Phys. Fluids*, **1**, 171.
Piddington, J. H., 1955. *Mon. Not. R. Astr. Soc.*, **115**, 671.
Piddington, J. H., 1959. *Geophys. J.*, **2**, 173.
Piddington, J. H., 1960. *J. Geophys. Res.*, **65**, 93.

World-Wide Characteristics of Geomagnetic Micropulsations

J. A. Jacobs and K. Sinno*

(Received 1960 May 19)

Summary

A detailed investigation is carried out on geomagnetic micropulsations recorded by rapid-run magnetograms during the International Geophysical Year from 17 observatories as widely distributed geographically as possible. A number of well-defined cases (14 *Pt*'s and 3 *Pc*'s) are investigated in detail. Diurnal and world-wide characteristics are derived and the equivalent overhead current systems which may give rise to the micropulsations are constructed.

Many of the examples of *Pt*'s can be divided into two groups: *viz.* Pt^- which is a *Pt* associated with a negative bay in the auroral zone and Pt^+ which is a *Pt* either associated with a positive bay or one which appears with no bay in the auroral zone. Although both groups of *Pt*'s, with their associated bays, have different characteristics, there are many points of similarity. Both classes have more or less coherent, synchronous wave forms over a wide area, i.e. they have the same period at different stations, where they are either nearly in or out of phase.

It is found that *Pc*'s consist of two different wave bands, both occurring during the daylight hours. The first band contains shorter period *Pc*'s (15–30s) with maximum amplitudes of a few gammas in moderate latitudes. They are not synchronous over wide areas. The second band contains longer period *Pc*'s (30–90s) with maximum amplitudes in the polar regions, amounting, on occasions, to as much as a few tens of gammas. They are well synchronized round the world.

Attention is drawn to the occurrence of long period, continuous, pulsations (called *LPc*'s) which have a longer period than *Pc*'s and usually appear simultaneously with *Pc*'s in polar regions.

The characteristics of micropulsations found in this investigation may throw some light on their origin. In this regard, a tentative discussion is given of hydromagnetic oscillations in the outer atmosphere which are excited by solar corpuscular streams.

1. Introduction

Geomagnetic micropulsations are fluctuations of the Earth's magnetic field whose amplitudes range from a fraction of a gamma to, on rare occasions, as much as a few tens of gammas. Periods range from about 0·1 s to 10 min. Most work

* On leave of absence from the Radio Research Laboratories, Kokubunji, Tokyo, Japan.

has been done in the lower frequency end of this range, very little being known at the higher frequencies from 0·1 to 10 c/s. In recent years, mainly as a result of the greatly increased number of continuous observations that are being made, certain definite types of micropulsations have been recognized and some systematic classification has been attempted. Ironically enough the great increase in the amount of data obtained during the International Geophysical Year has only served to show in some cases that the earlier classification was too simple and that in reality there exist many more different types or variations of the earlier, broader classification. This classification divided micropulsations into three categories, *Pc*'s, *Pt*'s and *Pg*'s, which are defined below.

Pc's (pulsations continues)

A series of pulsations lasting for many hours with periods usually in the range of from 10 to 60 s and amplitudes of the order of 0·1 γ. The maximum occurrence frequency is during the morning hours. Well-defined oscillations with periods less than 10 s have been observed by Troitskaya (1959a), Benioff (1960) and other workers. There is no doubt that they form a distinct class from *Pc*'s, but they are not investigated in this report.

Pt's (trains de pulsations)

These appear as several series of oscillations, each series usually lasting from 10 to 20 min the whole phenomenon lasting for periods of not more than about 1 h. They are well damped with longer period than *Pc*'s (from 40 s to a few min) and usually of greater amplitude, i.e. of the order 0·5 γ. The maximum occurrence frequency is before midnight.

Pg's (giant pulsations)

A series of pulsations of large amplitude (up to a few tens of gammas) appearing only in or near the auroral zones. The period is longer than that of *Pc*'s (up to several minutes), and the duration is of the order of an hour or more.

The results of several Soviet investigators were presented at a recent symposium on rapid variations in the Earth's field held under the auspices of the International Association of Geomagnetism and Aeronomy at Utrecht, 1959 September. Mainly as a result of their work in the Arctic and the Antarctic, Troitskaya (1959b) recommended that *Pc*'s be subdivided into three groups, with periods in the range 5–15 s, 20–40 s and 50–90 s. Of particular interest is the sharp fall in the number of hours that recorded *Pc*'s (in the 20–30 s range period) during the middle months of the long polar night. There are also differences in the characteristics of *Pt*'s in polar regions and middle latitudes. Troitskaya stressed the importance of shorter period pulsations, which fall into two classes—*Pc*'s with periods from 5–15 s, characteristic mainly of the polar regions and whose diurnal distribution is quite different from that of *Pc*'s of longer period (20–30 s), and beating pulsations (pearls) with periods from 1–4 s.

Kalashnikov (1959) maintained that the present classification *Pc* and *Pt* is too subjective and that definitions of pulsations should be based on more objective elements, period, amplitude and duration of the oscillations. Series of oscillations of different amplitude and period are often superimposed and may be caused by different sources and different excitation processes. Kalashnikov stated that at the Soviet stations there were often periods when the field of rapid variations became non-homogeneous and noticeable differences of the order of tenths of a

gamma existed at a distance of 1 km both in latitudinal and longitudinal directions.

It was to investigate further some of these problems that a detailed analysis was carried out of a number of well defined cases of *Pc*'s and *Pt*'s, using data from stations as widely distributed as possible. This enabled the equivalent overhead current systems, which may give rise to these micro-pulsations, to be constructed.

2. Source of data

In order to investigate the morphology of micropulsations, it is desirable not only to obtain information on their average characteristics, but also some knowledge of their world-wide behaviour. Unfortunately, magnetic stations, operating rapid-run magnetograms, are not well distributed geographically. The only reasonable coverage is in North America and the Pacific, the stations being mainly operated by the United States Coast and Geodetic Survey. The observatories whose data are used in the present study are given in Table 1.

Table 1

Stations supplying data used in this report

		Geographic		Geomagnetic	
Station	Abbreviation	Lat.	Long.	Lat.	Long.
Point Barrow	PB	71° 18′N	156° 46′W	68°·6N	241°·0E
College	Co	64° 51′N	147° 50′W	64°·7N	256°·5E
Big Delta	BD	64° 09′N	145° 51′W	64°·4N	259°·0E
Healy	Hy	63° 51′N	149° 00′W	63°·6N	256°·5E
Sitka	Si	57° 03′N	135° 20′W	60°·0N	275°·4E
Lovo	Lo	59° 21′N	17° 50′E	58°·2N	105°·8E
Fredericksburg	Fr	38° 12′N	77° 22′W	49°·6N	349°·9E
Tucson	Tu	32° 14′N	110° 57′W	40°·4N	312°·1E
Kakioka	Ka	36° 14′N	140° 11′E	26°·0N	206°·0E
Honolulu	Ho	21° 18′N	158° 08′W	21°·0N	266°·4E
Guam	Gu	13° 27′N	144° 45′E	3°·9N	212°·8E
Koror	Kr	07° 16′N	134° 32′E	3°·3S	203°·5E
Apia	Ap	13° 48′S	171° 46′W	16°·0S	260°·2E
Hermanus	Hr	34° 24′S	19° 13′E	33°·3S	80°·3E
Byrd Station	By	79° 59′S	120° 01′W	70°·6S	336°·0E
Little America	LA	78° 18′S	162° 10′W	74°·0S	312°·0E
Wilkes	Wk	66° 15′S	110° 31′E	77°·8S	179°·0E

The data from these 17 observatories were recorded photographically, not only on rapid-run magnetograms with a recording speed of 20 mm per 5 min, but also on standard speed magnetograms with a recording speed of 20 mm/h. Additional data were obtained from the publications of the International Association of Geomagnetism and Aeronomy (supplied by Dr J. Veldkamp, Kon. Nederlansch. Meteorologisch Instituut, De Bilt, Holland).

A number of well-defined micropulsations, which occurred mainly in American regions (3 cases of *Pc*'s, 14 cases of *Pt*'s and 5 cases unclassified) are considered. After reading and comparing the data, diurnal and world-wide characteristics are

derived, and the equivalent overhead current systems drawn for some typical cases. Table 2 gives the times and dates of the examples of micropulsations which are analysed in this paper. The table also contains information on the newly defined pulsation, *LPc*, which appears mainly in polar regions, with long-period (3–7 m) continuous oscillations, lasting several hours.

3. Characteristics of *Pc*'s

(*a*) *Amplitude distribution.*—*Pc*'s are defined as continuous pulsations usually appearing on the daylight side of the Earth, lasting for many hours with periods in the range from 10 to 60 s, and amplitudes of the order of a few tenths of a gamma in middle latitudes. However, if the evidence of all investigators over a wide area is considered, it becomes apparent that *Pc*'s do not correspond to a single wave band but to two wave bands, the first a shorter period *Pc* (about 15–30 s) and the second a longer period *Pc* (about 30–90 s). Figure 1 shows the spectrum of *Pc*'s which have been investigated by several workers from stations all over the world, and clearly illustrates the division into these two different wave bands.

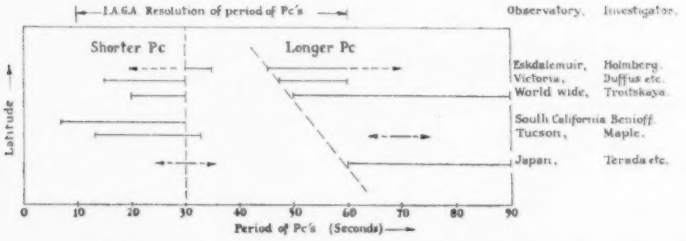

FIG. 1.—Latitudinal distribution of spectrum of *Pc*'s with periods greater than 10 s as reported by different investigators from data shown on the right-hand side.

In a previous investigation (Jacobs & Sinno 1959, 1960), latitudinal and longitudinal characteristics were obtained of the diurnal occurrence frequency of *Pc*'s during the International Geophysical Year. It was found that the occurrence of *Pc*'s increased from the equator towards higher latitudes regardless of period. The present investigation shows that for one type of *Pc* (the longer-period *Pc*), the amplitude also increases from the equator towards the poles. This is shown in the examples observed on 1958 February 12 (Figures 2 and 3) and 1958 April 2 (Figure 2), which have periods of 33 s and 45 s, respectively. These examples of *Pc*'s have coherent, synchronous wave forms over a wide area. As can be seen from these figures, *Pc*'s of this type often have amplitudes up to ten gammas or more in polar regions.

A pulsation appeared on 1958 May 7 (Figures 2 and 4), with a period of about 20 s and with maximum amplitude at about latitude 50°. Many similar examples (such as those which occurred on 1958 February 8 and May 28) have been found: they all have in common comparatively short periods (from about 15 to 30 s). These shorter-period *Pc*'s show different periods at different latitudes although it is not possible to be definite on this point since the speed of the rapid run recordings is too slow for any fine resolution. Although wave bands below 15 s period have been defined by several investigators (Troitskaya, Maple, Benioff, Duffus,

etc.) they have not been included in the present report because the records were obtained at too slow a speed to identify them.

According to Maple (1959), oscillations with a period of about 20 s occur more often than those of longer period (70 s) at Tucson (geomagnetic latitude 40° 4′ N). On the other hand, 70 s oscillations predominate at Eskdalemuir (geomagnetic latitude 58° 4′ N). This frequency dependence ties in with the results of the present investigation, where short-period *Pc*'s were found to have their maximum amplitude at comparatively low latitudes. The latitudinal distribution of amplitude for the short-period *Pc*'s is quite different from that of the longer-period *Pc*'s which have maximum amplitudes in the polar regions, the amplitudes decreasing at lower

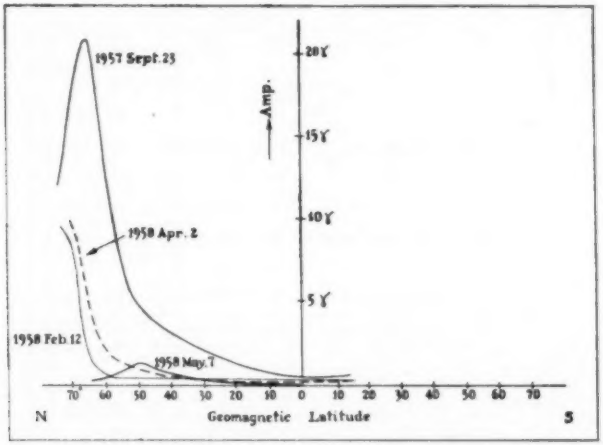

FIG. 2.—Amplitude distributions for various *Pc*'s which occurred on 1957 September 23, 1958 February 12, April 2 and May 7.

latitudes. This tendency is also shown in Figure 1 where the period at the lower boundary of the longer *Pc* wave band increases with decreasing latitude. Moreover, of the two examples of longer-period *Pc*'s, that with the shorter period has a greater range of amplitude variation as is shown in Figure 3. Combining the results of previous investigations with the latitudinal distribution of the amplitude of *Pc*'s which has been derived in the present analysis, equi-amplitude contours can be drawn as shown in Figure 5.

Other micropulsations, which could not be rigorously classified or analysed, were observed. Thus a pulsation appeared on 1957 September 23, with a very enhanced amplitude—up to several tens of gammas in the auroral zone (see Figure 2). However, this pulsation may not belong to the category of *Pc*'s, because of its irregular wave form and different period at distant observatories. It may form part of a series of irregular variations during a severe magnetic storm. It is worth noting, however, that the diurnal (longitudinal) characteristics of all types of *Pc* show a more or less daytime maximum as shown in Figure 6.

Finally, attention is called to beating *Pc*'s which have been reported by Kato & Watanabe (1957, 1958). These are of longer period than the "pearls" of Troitskaya (1953, 1959a) and Benioff (1960). Beating *Pc*'s usually show a pulsation whose amplitude varies with a period of several minutes. Sometimes the modulating period is identical with that of *LPc*'s which often appear in polar regions.

(*b*) *Equivalent overhead current system.*—As shown in Figure 3, cases can be found where *Pc*'s occur simultaneously over a wide area. Strictly speaking, the recording paper speed of the rapid-run magnetogram is too slow to resolve the phase difference between distant stations. However, it is possible to determine

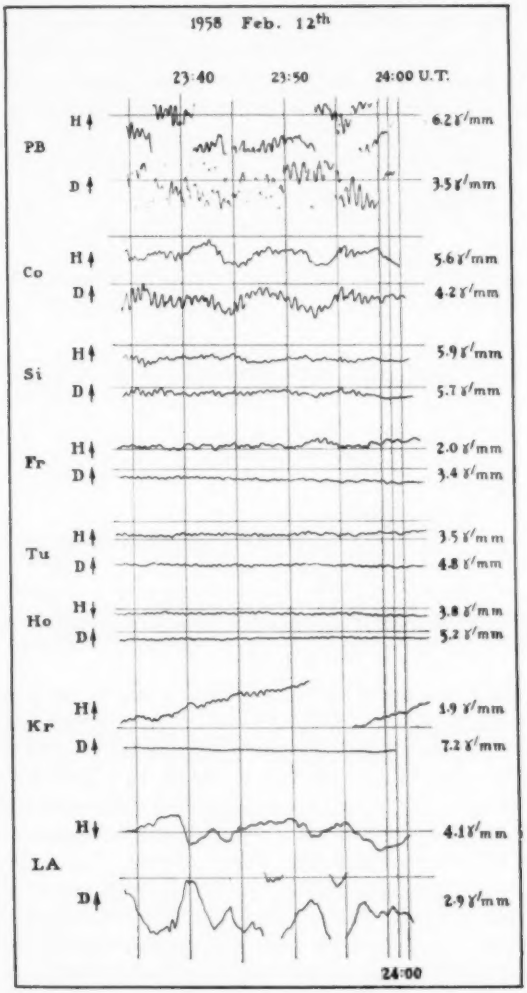

FIG. 3.—Traces from rapid-run magnetograms of longer-period *Pc*'s at various stations on 1958 February 12.

whether the records are nearly in or out of phase. With this proviso, the ideal overhead current system which would induce the observed *Pc*, can be drawn as shown in Figure 7. The centre of the current vortex is located at about 50 degrees latitude and at about the sub-solar point. The concentrated current lines over the polar regions do not close in one sheet; these open-ended current contours may be extended to three-dimensional space.

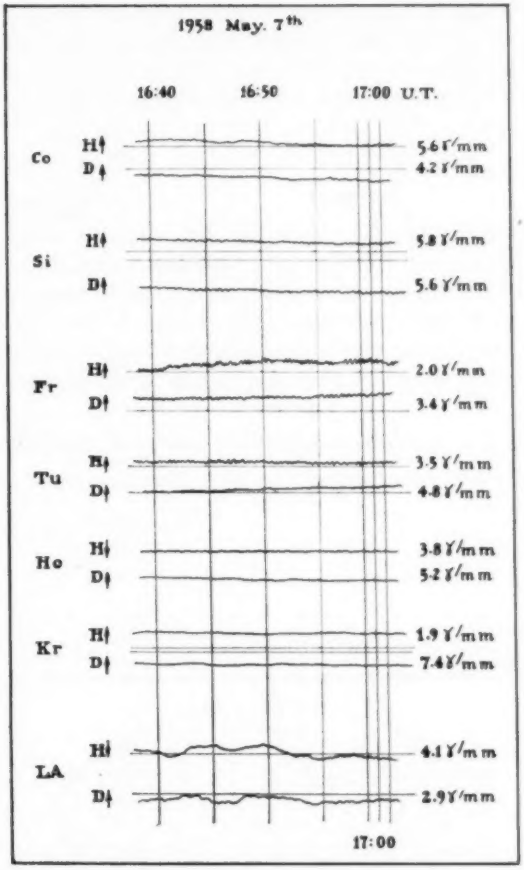

FIG. 4.—Traces from rapid-run magnetograms of shorter-period *Pc*'s at various stations on 1958 May 7.

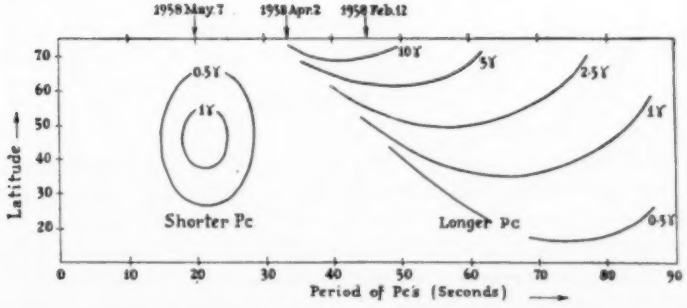

FIG. 5.—Equi-amplitude contours of *Pc*'s, derived from Figure 1.

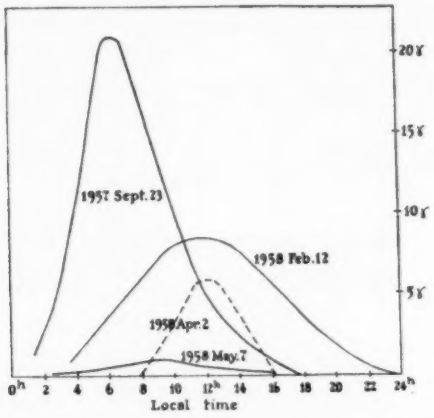

FIG. 6.—Local time (longitudinal) variation of various *Pc*'s.

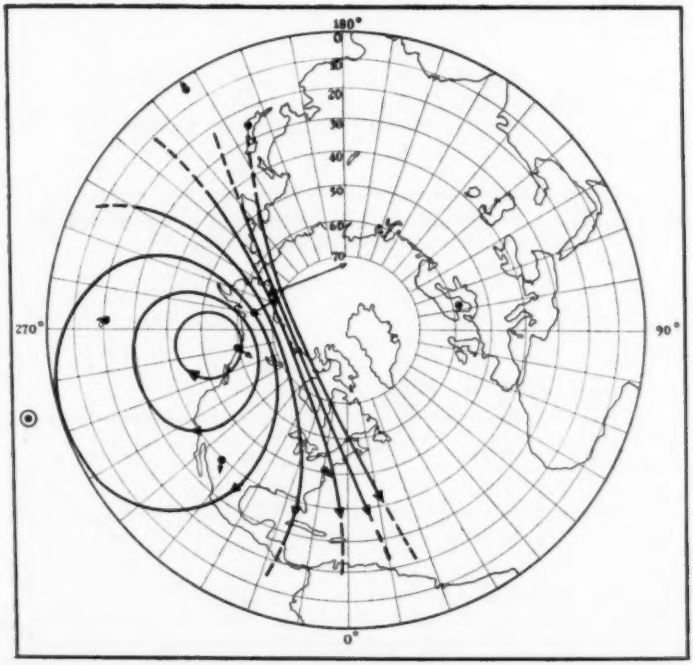

FIG. 7.—Equivalent overhead current system for *Pc* at 2220–2225 U.T. 1958 April 2. Electric current between successive lines is 5×10^3 A.

The equivalent overhead current system cannot be drawn for the shorter-period *Pc*'s because they are not synchronous at different stations. These shorter-period *Pc*'s may be caused by hydromagnetic waves in the lower atmosphere or ionosphere where local inhomogeneities, not present in the outer atmosphere, may develop.

4. Characteristics of *Pt*'s

(*a*) *Amplitude distribution.*—*Pt*'s are defined as well-damped transient oscillations with periods longer than *Pc*'s. Generally *Pt*'s occur during the night time and often accompany a geomagnetic bay. In the present investigation the latitudinal dependence of the amplitude of several well-defined *Pt*'s is obtained. Fourteen examples of *Pt*'s with large amplitudes (see Table 2) were selected from data obtained from United States geomagnetic stations.

Table 2

Times of the occurrence of micropulsations analysed in this report

Date	Commencement (U.T.)	Duration	Type	Association
1957 Sept. 15	0402	6 m	*Pt*	
1957 Sept. 16–17	0800	4·5 h	*LPc**	*Pc*
1957 Sept. 23	0700	13 h	unclassified	
1957 Sept. 24	0440	5 m	*Pt*	
1957 Sept. 24	0456	>30 m	*Pt*	
1957 Nov. 24–25	1555	6 h	*LPc**	*Pc*
1957 Dec. 5	0332	10 m	*Pt*	
1957 Dec. 21	0448	6 m	*Pt*	
1957 Dec. 25	0704	9 m	*Pt*	
1957 Dec. 26	0936	10 m	*Pt*	severe bay
1958 Jan. 2	0849	6 m	*Pt*	severe bay
1958 Feb. 9	0051	5 m	*Pt*	
1958 Feb. 10	0455	5 m	*Pt*	
1958 Feb. 12–13	2100	4 h	*LPc**	*Pc*
1958 Feb. 12–13	2250	6 h	*Pc*	*LPc**
1958 Feb. 23–24	1730	6·5 h	*LPc**	
1958 April 2–3	1800	7 h	*Pc*	*LPc**
1958 May 7–8	1400	8 h	*Pc*	
1958 May 15	0505	8 m	*Pt*	severe bay
1958 May 28	2339	6 m	*Pt*	
1958 June 28	0340	30 m	*Pt*	
1958 July 30	0640	35 m	*Pt*	

* Defined in this report.

It was found that the latitudinal distribution of the amplitudes of *Pt*'s is different between that group of *Pt*'s associated with severe negative bays in the auroral zone and that group of *Pt*'s associated with positive bays or without any accompanying bay. These two groups of *Pt*'s are distinguished, as Pt^- and Pt^+, respectively. The latitudinal amplitude distributions derived from two examples are shown in Figures 8 and 9. The main features of these graphs are confirmed in many other cases.

Pt⁻'s show a very sharp maximum in the auroral zones where the peak value reaches about ten gammas or more. On the other hand *Pt*⁺'s show a comparatively flat distribution with a maximum amplitude in the sub-auroral zone and subsidiary peaks in the polar and equatorial regions. These latitude trends of the amplitudes of *Pt*⁻'s and *Pt*⁺'s are the same as those of their associated bays, and lead to the

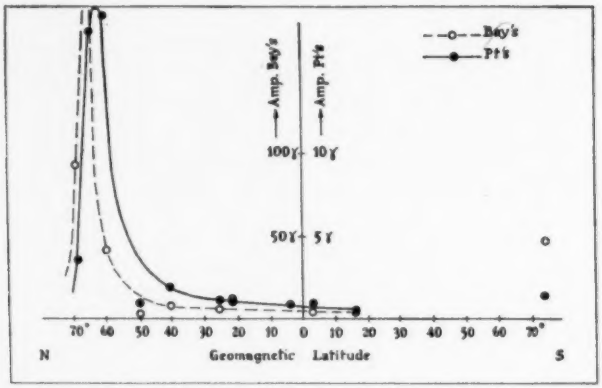

FIG. 8.—Amplitude distribution of *Pt*⁻ and its associated bay, commencing 0936 U.T. 1957 December 26.

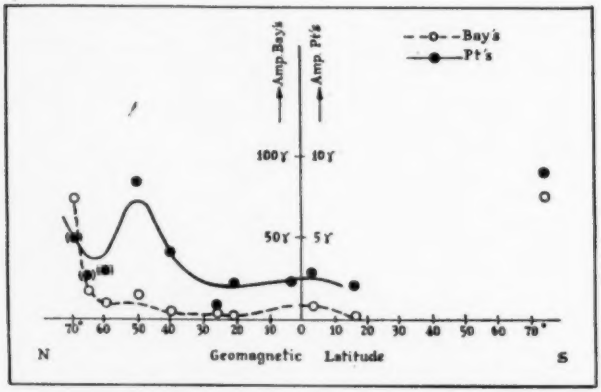

FIG. 9.—Amplitude distribution of *Pt*⁺ and its associated bay commencing 0051 U.T. 1958 February 9.

conclusion that *Pt*'s are fundamentally very closely related with bays. Thus the causal mechanism of these two phenomena may well be identical.

(*b*) *Equivalent overhead current system.*—The equivalent overhead current systems for an example of *Pt*⁻ and *Pt*⁺ are shown in Figures 10 and 11 respectively. Although both types of *Pt*'s have synchronous wave forms at different stations, it is not easy to draw the contours in the case of *Pt*⁻ on account of the complexity of the wave form, especially near the auroral zones. For simplicity,

the direction of the current contours and magnetic arrows are shown for the maximum amplitude of the oscillation which fluctuates with the period of the *Pt*'s. This procedure was also adopted in drawing the overhead current systems for *Pc*'s.

Both the contours for Pt^- and Pt^+ resemble the well-known bay current systems which have been drawn by Silsbee & Vestine (1942), although *Pt*'s have only one intense current vortex centre, on the night side. The current vortex centres are located at about 50–60 degrees latitude which is in the sub-auroral zone.

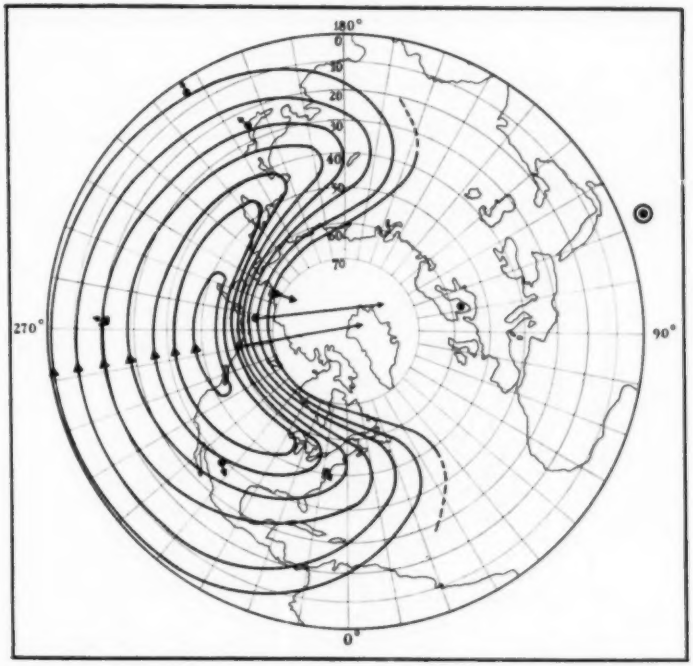

FIG. 10.—Equivalent overhead current system for Pt^- at 0936 U.T. 1957 December 26. Electric current between successive lines is 5×10^3 A.

5. Long-period continuous pulsations (*LPc*) in polar regions

(*a*) *Amplitude distribution.*—Figure 12 shows part of the traces of standard magnetograms, speed 20 mm/h, from College, Alaska, and Fredericksburg, Virginia, on 1958 February 12–13. Between 2300–2400 U.T. on February 12 a series of very intense longer-period *Pc*'s were observed. They continued for about one hour and appear as thick traces on the magnetograms because of the slow paper speed. The same series of *Pc*'s were shown in Figure 3 recorded on rapid-run magnetograms. Of special interest are the pre- and post-oscillations of this particular *Pc*. Figure 12 shows clearly the intense pulsation of about six minutes period which prevailed during the previous two hours and after the *Pc*. Usually this type of pulsation is observed in polar regions and is frequently associated with *Pc*'s; it has been called a long-period continuous pulsation (*LPc*) in this paper.

An example of an *LPc* on rapid-run magnetograms (which is also seen in Figure 3 as a pre-*Pc* pulsation), is shown in Figure 13. The oscillations, of about six minutes period, are nearly synchronous over a very wide area, from the Arctic to the Antarctic and in equatorial regions. Moreover, the polarization is nearly linear at each station. Sometimes, however, elliptically polarized *LPc*'s are observed as shown in Figure 14. The latitudinal dependence of the amplitude distributions for both *Pc*'s and *LPc*'s are very similar, as is shown in Figure 15. Usually the amplitudes of *LPc*'s are about ten times greater than *Pc*'s in polar regions.

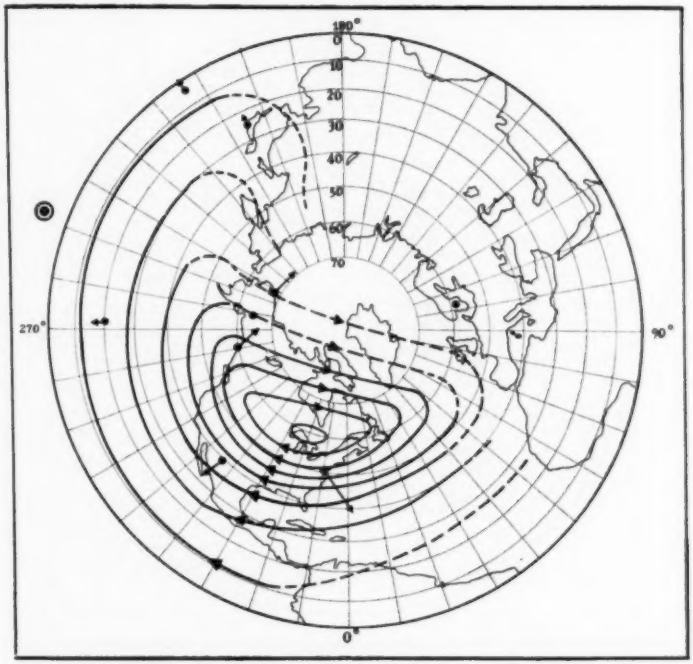

FIG. 11.—Equivalent overhead current system for Pt^{+} at 0051 U.T. 1958 February 9. Electric current between successive lines is 5×10^{3} A.

(*b*) *Equivalent overhead current system.*—Although the polarity of the horizontal component is not always exactly linear, small phase differences have been neglected for simplicity. The polarization when non-linear appears as a counter-clockwise, flat-shaped ellipse (see Figure 14). The equivalent overhead current system for *LPc*'s (Figure 16) is very similar to that for *Pc*'s except over the polar cap where *LPc*'s are not so well defined, as is shown, for example, in the traces at Point Barrow (see Figure 13).

(*c*) *Relation between long-period Pc's and LPc's.*—Figure 13 shows the remarkable time association of *Pc*'s and *LPc*'s, although *LPc*'s do not usually occur in middle latitudes. This is further illustrated in Figure 17 which shows the occurrence of *Pc*'s and *LPc*'s at Point Barrow, Alaska, during 1958 February. The diurnal occurrence of *LPc*'s, like that of *Pc*'s, has a daytime maximum a few hours

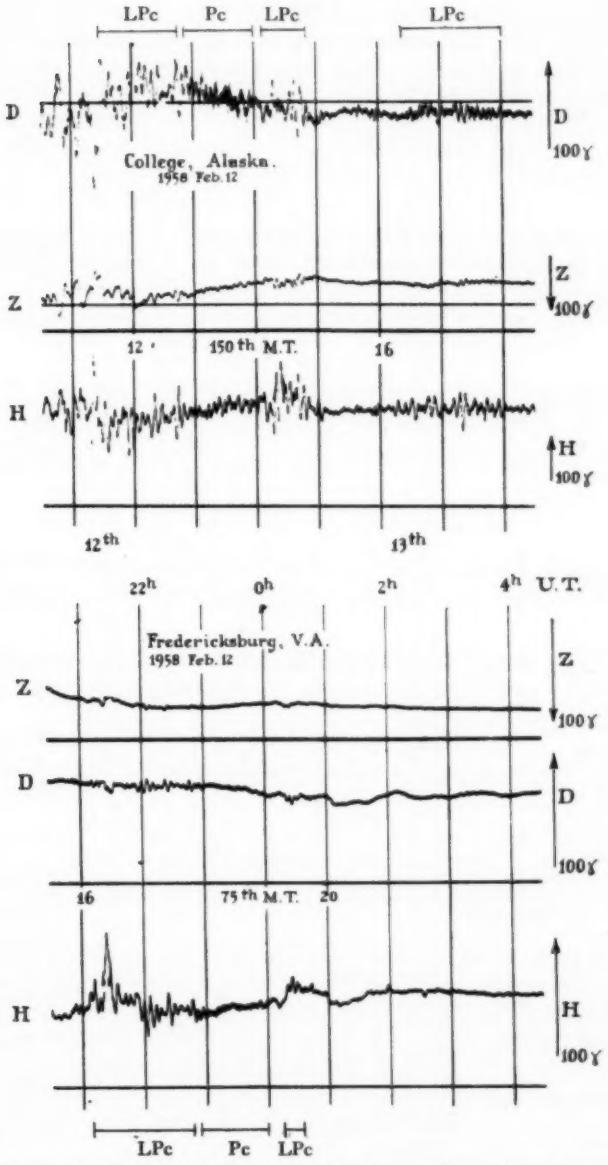

FIG. 12.—Examples of *Pc* and *LPc*. Traces are from ordinary magnetograms at College and Fredericksburg on 1958 February 12–13.

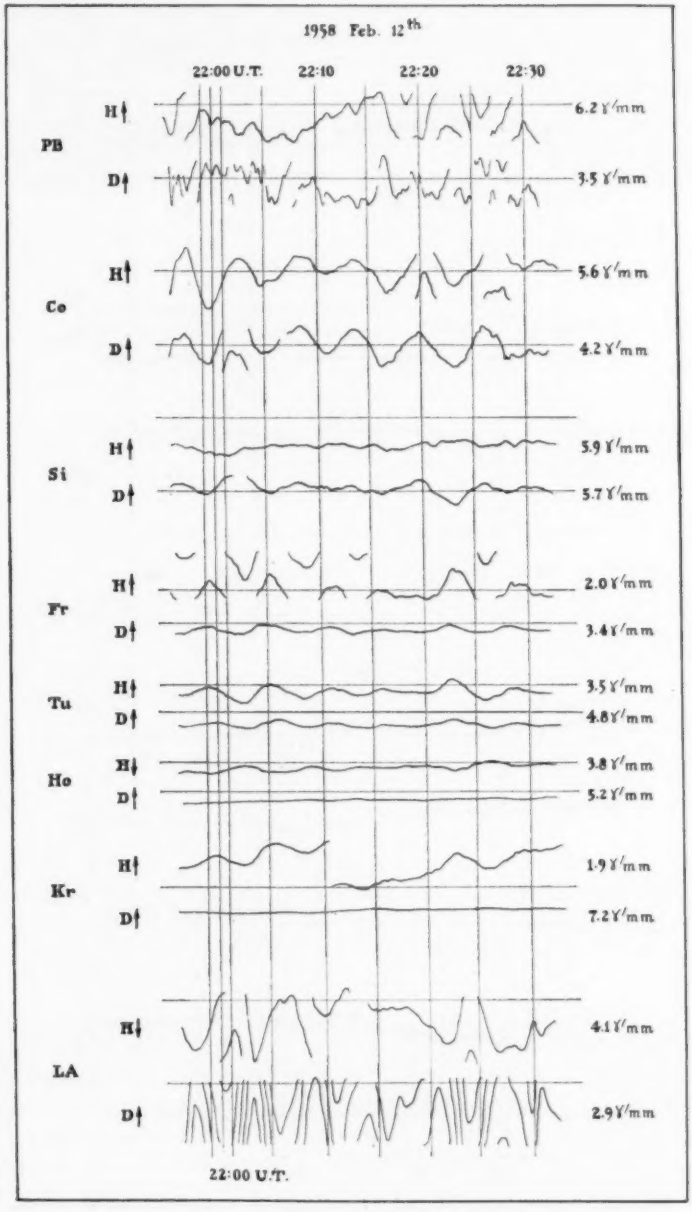

FIG. 13.—Example of *LPc*. Traces from rapid-run magnetograms at various stations on 1958 February 12.

before local noon. Besides this time association there is further evidence of the relation between *Pc*'s and *LPc*'s. Sometimes beating oscillations of *Pc*'s, which appear mainly in middle latitudes, occur simultaneously with *LPc*'s in polar regions. Moreover, the periods of both the beating *Pc*'s and the *LPc*'s are about the same, viz. from 3 to 7 m (Kato & Watanabe 1957, 1958). These close relations between *Pc*'s and *LPc*'s indicate that both pulsations have a common source, probably outer atmospheric oscillations.

6. Discussion of the results

(*a*) *Hydromagnetic oscillations in the outer atmosphere.*—Although equations for hydromagnetic oscillations of the outer atmosphere have been set up by Dungey (1954), they are too complex to be solved in the general case. However, if there is

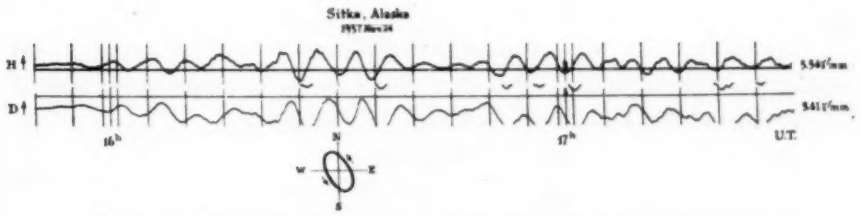

FIG. 14.—Example of *LPc* showing the polarization of the horizontal component. Traces from rapid-run magnetogram at Sitka on 1957 November 24.

no coupling between poloidal and toroidal oscillations, solutions may be obtained from the following two equations:

Poloidal

$$\left(\frac{\rho}{\mu_0 H_0^2}\frac{\partial^2}{\partial t^2} - R^{-2}\sin\theta\frac{\partial}{\partial\theta}(\sin\theta)^{-1}\frac{\partial}{\partial\theta} - \frac{\partial^2}{\partial R^2}\right)(R\sin\theta\,.\,E_\phi) = 0, \qquad (1)$$

Toroidal

$$\left\{\frac{\rho}{\mu_0}\frac{\partial^2}{\partial t^2} - (R\sin\theta)^{-2}[(\mathbf{H}_0\,.\,\nabla)(R\sin\theta)^2(\mathbf{H}_0\,.\,\nabla)]\right\}\left(\frac{u_\phi}{R\sin\theta}\right) = 0. \qquad (2)$$

Spherical polar coordinate (R, θ, ϕ) are used where R is the distance from the centre of the Earth, ρ the plasma density of the outer atmosphere, and μ_0 the permeability (mks units are used). The magnetic field $\mathbf{H}$ is considered to be the sum of a constant dipole field $\mathbf{H}_0$ and a small disturbance $\mathbf{h}$ introduced through the motion of the medium, where $|\mathbf{H}_0| \gg |\mathbf{h}|$.

The solutions of equations (1) and (2) involve the following components of the electric field $\mathbf{E}$, velocity $\mathbf{u}$ and disturbed magnetic field $\mathbf{h}$.

Poloidal

$$\mathbf{E}(0, 0, E_\phi), \quad \mathbf{u}(u_R, u_\theta, 0), \quad \mathbf{h}(h_R, h_\theta, 0) \qquad (3)$$

Toroidal

$$\mathbf{E}(E_R, E_\theta, 0), \quad \mathbf{u}(0, 0\,\mu_\phi), \quad \mathbf{h}(0, 0, h_\phi). \qquad (4)$$

The toroidal mode was studied by Dungey (1954), Kato & Watanabe (1956), and Obayashi & Jacobs (1957) as the possible origin of giant pulsations (*Pg*'s),

since the toroidal mode and *Pg*'s show similar characteristics. In particular the occurrence of *Pg*'s is restricted to places near the auroral zones and the main oscillating component is the *D*-component of the magnetic field. On the other hand, the synchronous nature over a wide area and the approximate meridional plane of polarization of *Pc*'s and *Pt*'s might be explained by the poloidal mode, as has been pointed out by Kato & Akasofu (1956) and Kato & Watanabe (1957, 1958). Following their analysis, and assuming that the field quantities depend on t through a factor $\exp(i\omega t)$, equation (1) can be written in the form

$$\left(\frac{\partial^2}{\partial R^2}+\frac{(1-\mu^2)}{R^2}\frac{\partial^2}{\partial \mu^2}\right)\psi = \frac{-\psi}{\eta^2} \tag{5}$$

where

$$R\sin\theta \,.\, E_\phi = \psi, \quad \cos\theta = \mu \tag{6}$$

and

$$\rho\omega^2/\mu_0 H_0^2 = 1/\eta^2. \tag{7}$$

Writing $\psi = f_1(x) \,.\, f_2(x)$ where $R = \eta x$, equation (5) can be solved by the method of separation of variables, f_1 and f_2 satisfying the equations

$$\frac{d^2 f_1}{dx^2}+\left(1-\frac{n(n+1)}{x^2}\right)f_1 = 0 \tag{8}$$

and

$$(1-\mu^2)\frac{d^2 f_2}{d\mu^2}+n(n+1)f_2 = 0. \tag{9}$$

For any integral value of n, the exact mode of the oscillations may be obtained from equations (8) and (9), if the variation of the Alfvén velocity $V_A = H_0(\mu_0/\rho)^{\frac{1}{2}} = \omega\eta$ in the outer atmosphere is known. However, without knowing the exact boundary conditions, it is possible to make a rough estimate of the period of the standing wave in the outer atmosphere which is confined between its inner and outer boundaries.

From the simple physical analogy of standing waves, the fundamental period and its harmonics are given by

$$T_n = \frac{T_1}{n} = \frac{2}{n}\int_{r_1}^{r_2}\frac{a}{V}dr \tag{10}$$

where T_n is the period of the harmonic of degree n and T_1 the fundamental period. r_1 and r_2 are the radii of the inner and outer boundaries of the outer atmosphere measured in units of the Earth's radius a. This relation implies eigen periods of the outer atmospheric oscillation equal to twice the travel time between the outer and inner boundaries. On the basis of our present knowledge, T_1 is about a few hundred seconds. This period is too large for *Pc*'s and *Pt*'s to be the direct expression of the fundamental wave.

Recently Dessler (1958, 1959) has shown that there are sharp gradients of the Alfvén velocity at the top and bottom of the outer atmosphere (as shown in the right half of Figure 18) where the waves are partially reflected back. Besides these sharp boundaries, equation (8) shows the existence of another barrier at the height

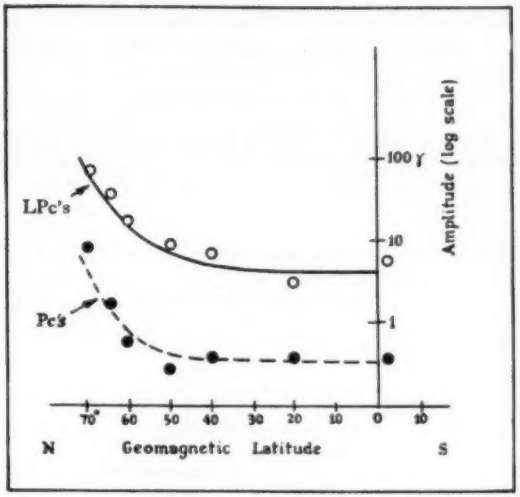

FIG. 15.—Amplitude distributions of *Pc* and *LPc* at 2215–2230 U.T. 1958 February 12.

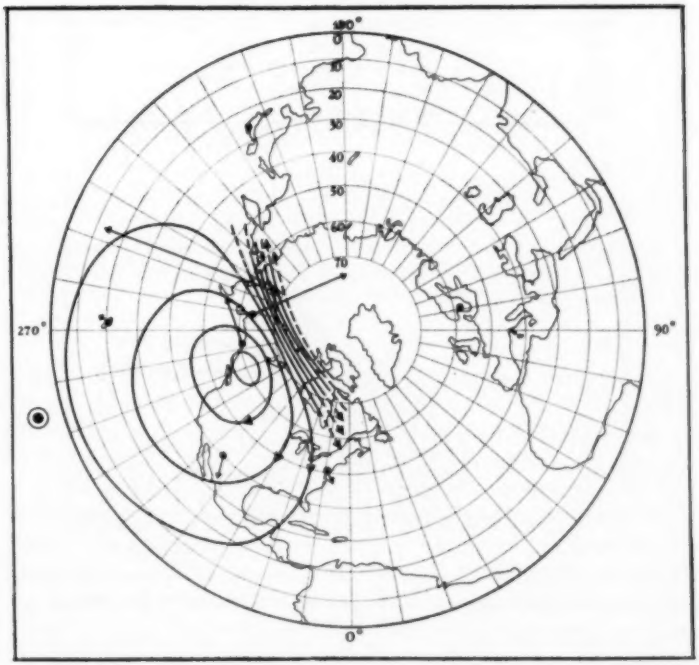

FIG. 16.—Equivalent overhead current system of *LPc* at 2215–2230 U.T. 1958 February 12. Electric current between successive lines is 5×10^4 A.

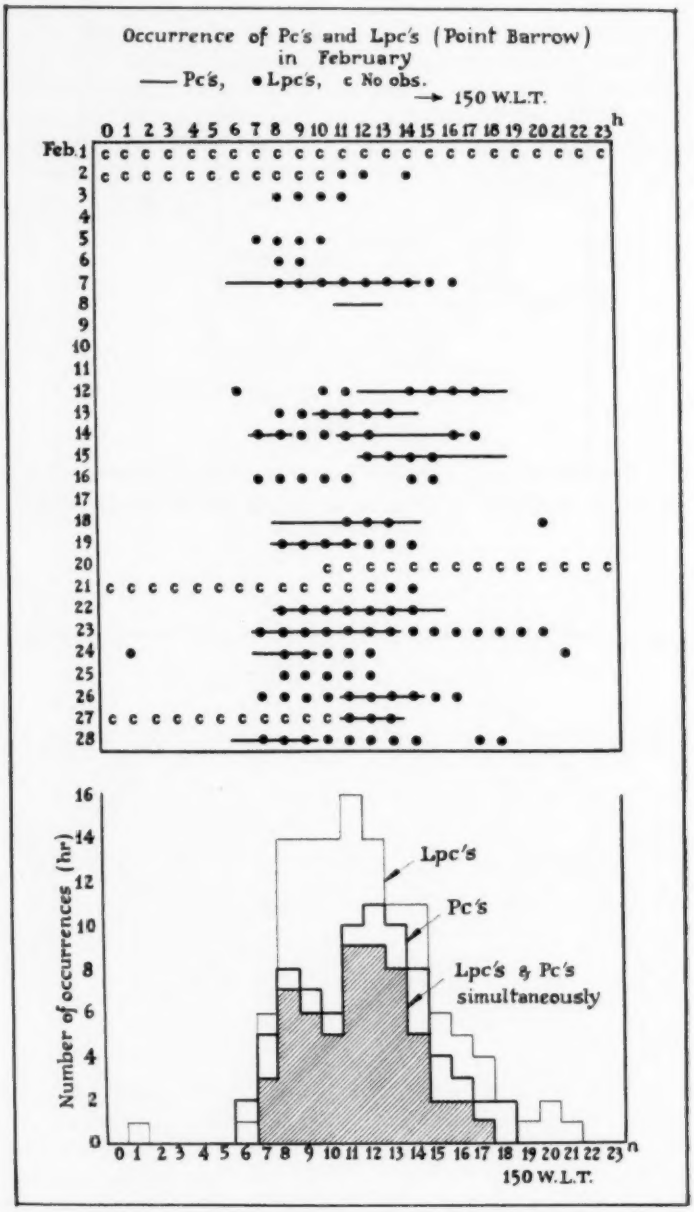

FIG. 17.—Hourly occurrence of *Pc*'s and *LPc*'s at Point Barrow in 1958 February.

of the Alfvén velocity maximum which becomes effective when the period of the waves is longer than about 10s although it may not become complete until the period exceeds 100s. This barrier for an Alfvén wave is similar to that caused by the ionosphere for an electromagnetic wave.

Although the exact behaviour of the propagation of Alfvén waves in the outer atmosphere cannot be established without further detailed knowledge of the outer atmosphere, plausible mechanisms for the generation of *Pc*'s, *LPc*'s and *Pt*'s are given below.

(*b*) *Model for Pc's and LPc's.*—In the outer atmospheric cavity standing waves whose periods are longer than about a minute cannot leak downwards sufficiently to be observed because the barrier is so high and thick. Thus only the higher harmonic waves T_n whose periods are less than a minute would be observed.

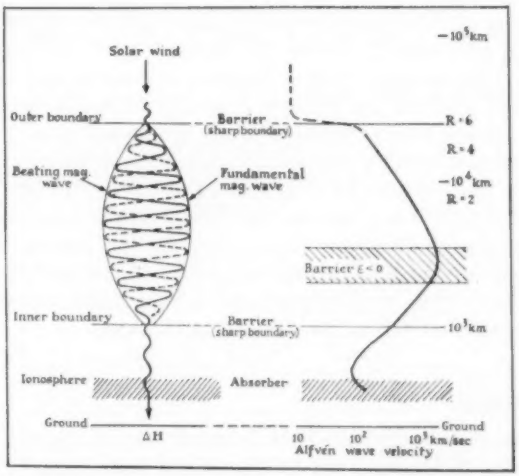

FIG. 18.—Schematic representation of *Pc* waves trapped in the outer atmosphere. The boundaries of this standing wave are formed by the sharp gradient of the Alfvén wave velocity shown on the right-hand side of the figure.

These higher harmonic waves interfere with each other and set up beating oscillations which are modulated by the fundamental period (Kato & Watanabe 1957, 1958). The beating of the higher harmonic waves is represented schematically on the left-hand side of Figure 18. The evidence that *Pc*'s sometimes show a beating oscillation with a period of about five minutes can be interpreted by the above model. *LPc*'s which appear mainly in the polar regions might be an expression of the leakage of the fundamental mode under the special circumstances that exist in the polar outer atmosphere, such as the remarkable difference in temperature between the auroral zone and moderate latitudes, as has been observed by Horowitz & LaGow (1958). The maximum occurrence of *Pc*'s around local noon can be understood since the perturbing force is located on the solar hemisphere where the corpuscular streams meet the outer atmospheric boundary. The centre of the current vortex in the equivalent overhead current system for the longer-period *Pc*'s at about latitude 50° and the latitudinal distribution of amplitude show that

the coefficients of the spherical harmonics predominate at $n = 3$, 5 and 7. The odd numbers come from symmetry with respect to the equator.

Since it is non-synchronous, it is not possible to consider the shorter-period *Pc* as originating as an outer atmospheric poloidal oscillation. It may, however, arise from hydromagnetic oscillations of the lower outer atmosphere or ionosphere below the barrier, since it shows local characteristics. The positive correlation between the occurrence of the shorter-period *Pc* and geomagnetic activity, and the approximate negative correlation of the occurrence of the longer-period *Pc* (Maple 1959), can easily be understood. Geomagnetic activity may help to develop the barrier, which would promote oscillations below, and at the same time inhibit the wave meeting the barrier from above.

(*c*) *Model for Pt's.*—The maximum occurrence of *Pt*'s at night and in the auroral zones leads to the conclusion that they are outer atmospheric oscillations which are excited by the same charged particles that cause aurora and bays. However, in spite of this close correlation, aurora and bays occur more frequently with increasing solar activity during the sun-spot cycle whereas the converse is true for *Pt*'s. This inverse relation between the occurrence of *Pt*'s and solar activity has been reported by Yanagihara (1959). It might be understood if the barrier were to develop to such an extent at the maximum of solar activity that the waves responsible for *Pt*'s were inhibited, in spite of the increased frequency of aurora and bays. It is reasonable to consider that the barrier may depend not only on geomagnetic activity (as is the case for *Pc*'s), but also on solar activity.

Although no typical *Pg*'s were observed during the International Geophysical Year, the similar inverse relation between solar activity and *Pg*'s, which is well known (Sucksdorff 1939), may be explained by the same reasoning; the barrier will exist for toroidal as well as for poloidal oscillations.

Acknowledgments

Data used in this study have been obtained from the geomagnetic stations of the United States of America, the I.G.Y. World Data Center A, the Coast and Geodetic Survey and Lovo station in Sweden, the Kakioka station in Japan, the Apia station operated by New Zealand and the Hermanus station in South Africa. The authors wish to acknowledge the above sources of data. The authors also express their sincere thanks to Mr T. Watanabe for his valuable private communications. The work was supported by the Geophysics Research Directorate, Air Force Cambridge Research Center, under Contract AF 19(604)–4068.

Geophysics Laboratory,
University of British Columbia,
Vancouver, B.C.:
1960 *May.*

References

Benioff, H., 1960. *J. Geophys. Res.*, **65**, 1413.
Dessler, A. J., 1958. *J. Geophys. Res.*, **63**, 507.
Dungey, J. W., 1954. *Ionos. Res. Lab.*, Penn. State Univ., Sci. Rep. No. 69.
Francis, W. E., Green, M. I. & Dessler, A. J., 1959. *J. Geophys. Res.*, **64**, 1643.

Holmberg, E. R. R., 1953. *Mon. Not. R. Astr. Soc. Geophys. Suppl.*, **6**, 467.
Horowitz, R. & LaGow, H. E., 1958. *J. Geophys. Res.*, **63**, 757.
Jacobs, J. A. & Sinno, K., 1959. Univ. Brit. Col., Geophys. Lab., Sci. Rep. No. 1.
Jacobs, J. A. & Sinno, K., 1960. *J. Geophys. Res.*, **65**, 107.
Kalashnikov, A. G., 1959. *I.A.G.A. Symposium on Rapid Geomagnetic Variations* (Utrecht).
Kato, Y. & Akasofu, S., 1956. Sci. Rep. Tohoku Univ., Ser. 5, 103.
Kato, Y. & Watanabe, T., 1956. Sci. Rep. Tohoku Univ., Ser. 5, 1.
Kato, Y. & Watanabe, T., 1957. Sci. Rep. Tohoku Univ., Ser. 5, 1.
Kato, Y. & Watanabe, T., 1958. *J. Geophys. Res.*, **63**, 741.
Maple, E., 1959. *J. Geophys. Res.*, **64**, 1395.
Obayashi, T. & Jacobs, J. A., 1958. *Geophys. J.*, **1**, 53.
Silsbee, H. C. & Vestine, E. H., 1942. *Terr. Mag.*, **47**, 195.
Sucksdorff, E., 1939. *Terr. Mag.*, **44**, 157.
Troitskaya, V. A., 1953. *Dokl. Akad. Nauk. SSSR*, **91**, 241.
Troitskaya, V. A., 1959a. *I.A.G.A. Symposium on Rapid Geomagnetic Variations* (Utrecht).
Troitskaya, V. A., 1959b. *I.A.G.A. Symposium on Rapid Geomagnetic Variations* (Utrecht).
Watanabe, T., 1959. *J. Geomag. Geoelec.*, **10**, 195.
Yanagihara, K., 1959. *J. Geomag. Geoelec.*, **10**, 172.

Note on Cusps in Seismic Travel-times

K. E. Bullen

(Received 1960 June 20)

Summary

When there is triplication in travel-time curves, it is often assumed that the cusps in the curves are necessarily associated with large wave amplitudes. Models which give a good representation of various types of seismic velocity variation are here set up to show that there are important cases in which this assumption does not apply. The analysis, which is facilitated by use of the variable $\alpha = 2d \log r/d \log \eta$, shows fairly directly that $d\Delta/dp$, where Δ and p are the angular length and parameter of ray, is sometimes discontinuous, sometimes continuous, at a cusp.

1. Preliminaries

In this note, an examination of the character of cusps in seismic travel-time curves is carried to greater detail than previously (Bullen 1945, 1959). It has often, but erroneously, been taken for granted that a cusp in the graph of the travel-time t against the angular distance Δ is necessarily associated with abnormally large wave amplitudes. A purpose of the present note is to help clear up the confusion which appears to exist on this question.

Let v be the (P or S) seismic velocity at distance r from the centre of an Earth model (as usual, taken to be spherically symmetrical). The question at issue can be sharply focused by representing relevant features of velocity distributions in terms of η and α, where

$$\eta = r/v, \tag{1}$$

$$\alpha = 2d\log r/d\log \eta. \tag{2}$$

The utility of the variable α has been previously demonstrated (1945, 1960), especially in respect of the quality of the approximation given by taking α constant over ranges of values of r.

Cusps may arise in $t-\Delta$ graphs when v or its gradient $(-dv/dr)$ increases discontinuously with increase of depth, or when the gradient increases continuously but rapidly. Each of these cases will be considered.

By (1), a positive jump in v corresponds to a negative jump in η. By (2), a positive jump in $-dv/dr$ corresponds to a negative jump in α.

We shall consider families of rays terminating at both ends at a level-surface $r = r_0$. Other level-surfaces, $r = r_1$ and $r = r_2$, where $r_2 < r_1 < r_0$, will also be referred to. The subscripts 0, 1 and 2 will indicate values of functions of r at $r = r_0, r_1, r_2$, respectively.

2. First model

We consider first a model containing an outer layer L, for which $r_1 \leqslant r \leqslant r_0$ and in which α takes the constant value α_0, overlying a layer N, for which $r \leqslant r_1$, and in which $\alpha = \kappa\alpha_0$, where κ is constant. The velocity v is taken to be continuous at the boundary $r = r_1$, while the velocity gradient is taken to jump discontinuously from L to N; thus η is continuous at the boundary, and $\kappa < 1$.

For rays entirely in L, we have (1959, section 7.3)

$$\Delta = \alpha_0 \cos^{-1}(p/\eta_0), \tag{3}$$

$$t = \alpha_0(\eta_0^2 - q^2)^{\frac{1}{2}}, \tag{4}$$

$$d\Delta/dp = -\alpha_0(\eta_0^2 - p^2)^{-\frac{1}{2}}, \tag{5}$$

where p is the usual ray-parameter.

For rays penetrating N, it can be deduced (fuller detail is being published in a further paper on ray theory) that

$$\Delta = \alpha_0\{\cos^{-1}(p/\eta_0) - (1-\kappa)\cos^{-1}(p/\eta_1)\}, \tag{6}$$

$$t = \alpha_0\{(\eta_0^2 - p^2)^{\frac{1}{2}} - (1-\kappa)(\eta_1^2 - p^2)^{\frac{1}{2}}\}, \tag{7}$$

$$d\Delta/dp = \alpha_0\{-(\eta_0^2 - p^2)^{-\frac{1}{2}} + (1-\kappa)(\eta_1^2 - p^2)^{-\frac{1}{2}}\}. \tag{8}$$

Consider variations as p decreases continuously from the value η_0, for which $\Delta = 0$. At $p = \eta_0$, $d\Delta/dp$ is by (5) equal to $-\infty$; $d\Delta/dp$ then increases continuously to the moderate value $-\alpha_0(\eta_0^2 - p^2)^{-\frac{1}{2}}$ at $p = \eta_1$, where, by (8), it jumps discontinuously to $+\infty$ (since $\kappa < 1$). As p further decreases, (8) shows that $d\Delta/dp$ decreases continuously from $+\infty$, passing through a zero at $p = \eta'$, where

$$\eta_1^2 - \eta'^2 = (1-\kappa)^2(\eta_0^2 - \eta'^2). \tag{9}$$

Inspection of (3), (4), (6) and (7) shows that each of Δ and t is continuous at both η_1 and η'.

From these details, it is easy to construct Figures 1, 2 and 3 in which the points A, A', A'' correspond to one another, etc. Figure 3 shows the well-known triplication of the time-curve for this class of case.

Figures 1 and 2, however, reveal an important feature not made explicit in the writer's previous work (1945). Whereas C' corresponds to an ordinary minimum of Δ (against p), at which $d\Delta/dp$ is continuous, B' corresponds to a node-point maximum at which $d\Delta/dp$ is discontinuous and does not in general vanish. Thus there is a significant difference in the character of the cusps at B and C which is not discernible from Figure 3 alone.

The difference is of practical importance, since p is proportional to $\cos e$, where e is the angle of emergence of a ray, so that a condition for large wave amplitudes at a given value of Δ is $d\Delta/dp = 0$. This condition is realized at C but not at B. Thus although there are cusps at both B and C, large amplitudes are to be expected at the distance corresponding to C, but *not* to B.

3. Second model

In the second model, we take circumstances as in the first model, except that there is now a discontinuous jump in v at the level r_1. Let η_a and η_b, where $\eta_b < \eta_a$, be the values of η just above and just below this level.

The time-curve still has the appearance of Figure 3, but the branch BC now corresponds to rays which lie entirely in L and are reflected upward at the boundary $r = r_1$.

For $\eta_a \leqslant p \leqslant \eta_0$ (the branch AB; unreflected rays in L), (3), (4) and (5) continue to apply.

For $\eta_b \leqslant p \leqslant \eta_a$ (the branch BC; reflected rays), we have

$$\Delta = \alpha_0\{\cos^{-1}(p/\eta_0) - \cos^{-1}(p/\eta_a)\}, \tag{10}$$

$$t = \alpha_0\{(\eta_0^2 - p^2)^{\frac{1}{2}} - (\eta_a^2 - p^2)^{\frac{1}{2}}\}, \tag{11}$$

$$d\Delta/dp = \alpha_0\{-(\eta_0^2 - p^2)^{-\frac{1}{2}} + (\eta_a^2 - p^2)^{-\frac{1}{2}}\}. \tag{12}$$

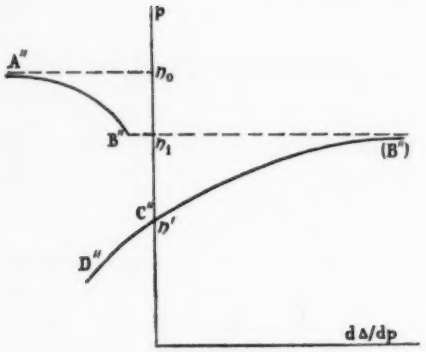

FIG. 1.

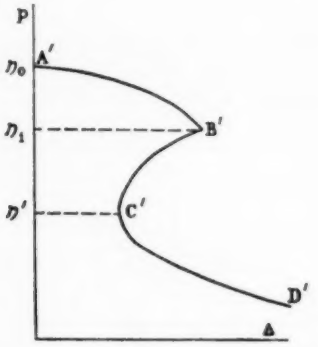

FIG. 2.

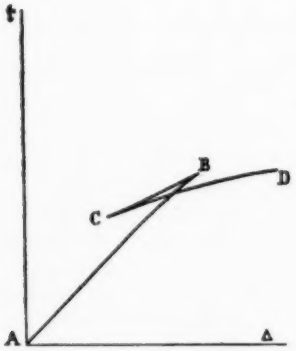

FIG. 3.

For $p \leqslant \eta_b$ (the branch CD; rays entering N),

$$\Delta = \alpha_0\{\cos^{-1}(p/\eta_0) - \cos^{-1}(p/\eta_a) + \kappa\cos^{-1}(p/\eta_b)\}, \tag{13}$$

$$t = \alpha_0\{(\eta_0^2 - p^2)^{\frac{1}{2}} - (\eta_a^2 - p^2)^{\frac{1}{2}} + \kappa(\eta_b^2 - p^2)^{\frac{1}{2}}\}, \tag{14}$$

$$d\Delta/dp = \alpha_0\{-(\eta_0^2 - p^2)^{-\frac{1}{2}} + (\eta_a^2 - p^2)^{-\frac{1}{2}} - \kappa(\eta_b^2 - p^2)^{-\frac{1}{2}}\}. \tag{15}$$

These equations show that Δ and t are again continuous throughout the whole range of values of p, but that $d\Delta/dp$ is discontinuous, and in general not zero, at both B and C.

Hence in this case, large wave amplitudes are to be expected at *neither* of the distances corresponding to B and C.

4. Third model

In the first two models, there were discontinuous changes in η or α between L and N. We now consider a third model, containing L as before, but between L and N containing a layer M, for which $r_2 \leqslant r \leqslant r_1$ and in which α decreases continuously from a_0 to $\kappa\alpha_0$. (We continue to take α constant and equal to α_0, $\kappa\alpha_0$ in L, N, respectively, with $\kappa < 1$; and we take η continuous throughout L, M and N; N now occupies the region $r \leqslant r_2$.)

For mathematical convenience, we take

$$d\alpha/d\eta = c\eta \tag{16}$$

in M, where c is a positive constant, so that

$$2\alpha_0(1-\kappa) = c(\eta_1^2-\eta_2^2). \tag{17}$$

It can be deduced (from equations in the writer's text (1959, Section 7.23)) that, in general,

$$\frac{d\Delta}{dp} = -\frac{\alpha_0}{\sqrt{(\eta_0^2-p^2)}} + \int_p^{\eta_0} \frac{d\alpha/d\eta}{\sqrt{(\eta^2-p^2)}}\,d\eta. \tag{18}$$

For rays entirely in L, (18) yields (5), as usual. For rays with lowest points in M, (18) yields

$$\begin{aligned}\frac{d\Delta}{dp} &= -\frac{\alpha_0}{\sqrt{(\eta_0^2-p^2)}} + \int_p^{\eta_1} \frac{d\alpha/d\eta}{\sqrt{(\eta^2-p^2)}}\,d\eta \\ &= -\alpha_0(\eta_0^2-p^2)^{-\frac{1}{2}} + c(\eta_1^2-p^2)^{\frac{1}{2}},\end{aligned} \tag{19}$$

by (16). And for rays which enter N,

$$d\Delta/dp = -\alpha_0(\eta_0^2-p^2)^{-\frac{1}{2}} + c(\eta_1^2-p^2)^{\frac{1}{2}} - c(\eta_2^2-p^2)^{\frac{1}{2}}. \tag{20}$$

By (5), (19) and (20), $d\Delta/dp$ is now continuous for the whole range of values of p concerned. For rays entirely in L, $d\Delta/dp$ is negative (as usual). For rays entering M, it can be deduced from (19) that, as p decreases, $d\Delta/dp$ passes continuously through a single zero (corresponding to B'' in Figure 4) in the range $\eta_2 < p < \eta_1$, and so becomes positive, provided

$$c > \alpha_0\{(\eta_1^2-\eta_2^2)(\eta_0^2-\eta_2^2)\}^{-\frac{1}{2}},$$

i.e., by (16), provided

$$\kappa < 1 - \tfrac{1}{2}(\eta_1^2-\eta_2^2)^{\frac{1}{2}}(\eta_0^2-\eta_2^2)^{-\frac{1}{2}}. \tag{21}$$

For rays penetrating N, as p further decreases, $d\Delta/dp$ may change back from positive to negative, passing through a second zero (the point C'' of Figure 4). This can be inferred from the fact that, for $p = 0$, (20) gives

$$d\Delta/dp = -\alpha_0\eta_0^{-1} + c(\eta_1-\eta_2); \tag{22}$$

and, by (16), the right side of (22) is negative if

$$\kappa > 1 - (\eta_1+\eta_2)/2\eta_0. \tag{23}$$

There is no difficulty in finding values of η_1/η_0 and η_2/η_0 which satisfy both the conditions (21) and (23) with $\kappa < 1$, and which give sensible models. Thus the curve shown in Figure 4 gives a further type of possible behaviour of $d\Delta/dp$. The corresponding $p-\Delta$ curve is shown in Figure 5, while the $t-\Delta$ curve has the same general appearance as Figure 3, with triplication again.

The interesting feature of the present model is that $d\Delta/dp$ is now zero for both B and C, so that large amplitudes may occur at the distances corresponding to *both* cusps.

5. Discussion

The models presented show that, when there is triplication in the time-curve as in Figure 3, three main cases arise, in which there may be abnormal wave amplitudes at distances corresponding (*a*) to neither B nor C, (*b*) to C but not B, (*c*) to both B and C.

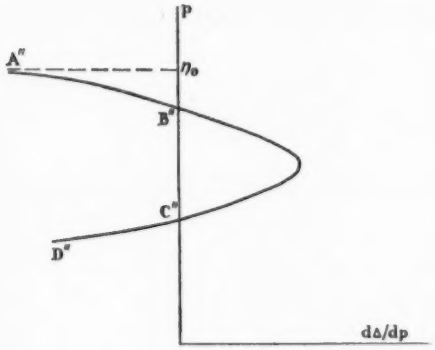

FIG. 4.

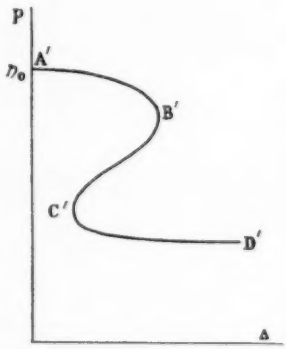

FIG. 5.

The discrimination between (*a*) and (*b*) rests on whether v is continuous or not. Even a small jump in v at the appropriate level can substantially reduce abnormally large amplitudes that might otherwise occur.

The discrimination between (*b*) and (*c*) rests on the fine distinction between a sudden and a rapid but continuous change in the gradient $-dv/dr$.

The analysis shows that sudden changes in the *second* or higher derivatives of v with respect to r, as well as sudden changes in the first derivative or in v itself, can have important influences on amplitudes. Thus further illustration is provided of the danger in trying to infer even broad features of velocity variations from amplitude data.

A central result is that, in the important case of a so-called "second-order" discontinuity in v, i.e. a sudden increase in $-dv/dr$ or decrease in α, large amplitudes are not in general associated with the cusp B. On the other hand, large amplitudes may be associated with B if the discontinuity is what might be called a "third-order" one.

The analysis for the case in which v suffers a sudden diminution with increase of depth is being set down elsewhere; this case also lends itself readily to discussion with the use of η and α. It is easy to show that the cusp which arises

in this case (see e.g. Bullen 1959, p. 117, Figure 28) is in general associated with large amplitudes, corresponding for example to the well-known observations of *PKP* waves near 142°.

Department of Applied Mathematics,
University of Sydney,
Sydney,
Australia:
1960 *June* 10.

References

Bullen, K. E., 1945. *Mon. Not. R. Astr. Soc. Geophys. Suppl.*, **5**, 91.
Bullen, K. E., 1959. *Introduction to the Theory of Seismology* (Cambridge: University Press), 2nd ed., reprinted, with revisions.
Bullen, K. E., 1960. *Geophys. J.*, **3**, 258.

Research Note

Note on the Paper of A. H. Cook, "The External Gravity Field of a Rotating Spheroid to the order of e^3"

Walter D. Lambert

(Received 1960 March 14)

Summary

A. H. Cook published in the September 1959 number of this Journal an article entitled "The External Gravity Field of a Rotating Spheroid to the order of e^3". Cook's formulas for the potential of such a spheroid stop with the term in $P_6(\sin\phi)$, which is given, as indicated, by the title, to an accuracy of e^3. This note states, without proof, formulas for the coefficients of $P_{2n}(\sin\phi)$ with no limit on n and no limit to the formal numerical accuracy of such coefficients.

Some of Cook's other formulas may be simplified by a slight change in notation.

Dr Cook's paper appeared in the September 1959 number of this Journal, pp. 199–214. It should be noted that the spheroid in question is an exact ellipsoid of revolution, assumed to be an exact surface of equilibrium under the combined effects of its own gravitational attraction and the centrifugal effects of uniform rotation about its minor axis.

Cook gives, formula (5.2), page 211, formulas for the J's, the coefficients of the expansion of the gravitational potential of the ellipsoid in terms of the zonal harmonics of the geocentric latitude multiplied by appropriate powers of the reciprocal of the radius vector. Cook's formulas are accurate to the third order of small quantities, such as the flattening, and include the zonal harmonic of degree six. The purpose of this note is to show that perfectly general formulas, accurate to any desired order of smallness, may be given for terms of any degree. Also, some of Cook's other formulas can be slightly simplified by using a slightly different parameter to express the centrifugal effect. Only the results are stated here. The proofs are given in Technical Paper (716)–2–261 of the Mapping and Charting Research Laboratory of The Ohio State University Research Foundation, Columbus, Ohio.

For various reasons, it seems inconvenient to adhere entirely to Cook's notation. Instead, the following symbols will be used:

	This paper	Cook
Semi-major axis of ellipsoid	a	a
Semi-minor axis of ellipsoid	b	b
First eccentricity of ellipsoid	$e = \sin\alpha$	none
Second eccentricity of ellipsoid	$\epsilon = \tan\alpha$	none
Flattening of ellipsoid	$f = 2\sin^2\frac{\alpha}{2}$	e
Mass of ellipsoid	M	M
Newtonian constant of gravitation	k	f
Radius vector of point in space	r	r
Geocentric latitude of point in space	θ	θ
Angular velocity of rotation of ellipsoid	ω	ω
Zonal harmonic of degree $2n$	$P_{2n}(\sin\theta)$	$P_{2n}(\sin\theta)$
Coefficient of $\left(\frac{a}{r}\right)^{2n}P_{2n}(\sin\theta)$ in the expansion of the potential	A_{2n}	J_{2n}
Mass of the spheroid	M	M

Other symbols will be introduced as needed.

The potential of the ellipsoid under the assumed conditions can be expressed in closed form in terms of curvilinear coordinates. This has been done more than once. But curvilinear coordinates are much less convenient in practice than the ordinary spherical coordinates (r, θ). Because of symmetry no third coordinate (corresponding to longitude) is needed. The direct transformation of the formulas for curvilinear coordinates into the corresponding formulas for spherical coordinates is laborious and leads to no general results. This difficulty can be avoided, as here, by the use of a highly artificial scheme of densities: A homogeneous fluid ellipsoid in equilibrium with a superficial coating of high negative density. We know that a given gravitational field can be produced by infinitely many distributions of density and, since this artificial scheme of densities can be shown to give the same formula for gravity on the surface of the ellipsoid as the formula derived from curvilinear coordinates, which is independent of any special scheme of density, the results for the artificial density scheme are valid also for exterior space.

The formulas in terms of curvilinear coordinates involve the use of Legendre functions of the second kind with an imaginary variable $i\cot\alpha$. These are needed, incidentally, in the present discussion. We assume

$$q_1(\alpha) = -Q_1(i\cot\alpha) = 1 - \alpha\cot\alpha = 1 - \frac{\tan^{-1}\epsilon}{\epsilon},$$

$$q_2(\alpha) = -iQ_2(i\cot\alpha) = \frac{1}{2}\left[(3\cot^2\alpha + 1)\alpha - 3\cot\alpha\right] \tag{1}$$

$$= \frac{1}{2}\left[\left(\frac{3+\epsilon^2}{\epsilon^2}\right)\tan^{-1}\epsilon - \frac{3}{\epsilon}\right].$$

We have also

$$q'_2(\alpha) = \frac{dq_2(\alpha)}{d\alpha} = 3\operatorname{cosec}^2\alpha q_1(\alpha) - 1. \tag{2}$$

For small values of α or ϵ these forms are inconvenient for practical computation and expressions as power series are preferable. The series are often expressible as hypergeometric series, a fact that makes it easy to pass from a series in ϵ to a series in e. In the customary notation

$$\begin{aligned} q_2(\alpha) &= \frac{2}{15}\epsilon^3 F\left(\frac{3}{2}, 2, \frac{7}{2}, -\epsilon^2\right) \\ &= \frac{2}{15}\epsilon^3\left[1 - \frac{6}{7}\epsilon^2 + \frac{5}{7}\epsilon^4 - \frac{20}{33}\epsilon^6 + \ldots\right] \\ &= \frac{2}{15}e^3\left[1 + \frac{9}{14}e^2 + \frac{25}{56}e^4 + \frac{175}{528}e^6 + \ldots\right]. \end{aligned} \tag{3}$$

In what follows it is convenient to use a modification of q_2, namely, $\psi = 3q_2/\epsilon$, or in series form

$$\begin{aligned} \psi &= \frac{2}{5}\epsilon^2 - \frac{12}{35}\epsilon^4 + \frac{2}{7}\epsilon^6 - \frac{8}{33}\epsilon^8 + \ldots \\ &= \frac{2}{5}e^2 + \frac{2}{35}e^4 + 0 \cdot e^6 - \frac{16}{1155}e^8 \ldots \\ &= \frac{4}{5}f - \frac{6}{35}f^2 - \frac{8}{35}f^3 - \frac{38}{231}f^4 \ldots . \end{aligned} \tag{4}$$

We shall also need the quantity ψ_1 and its reciprocal;

$$\psi_1 = \psi \Big/ \left(\frac{2}{5}e^2\right).$$

$$\begin{aligned} \psi_1 &= 1 + \frac{1}{7}e^2 + 0 \cdot e^4 - \frac{8}{231}e^6 \ldots \\ &= 1 + \frac{2}{7}f - \frac{1}{7}f^2 - \frac{64}{231}f^3 \ldots . \end{aligned} \tag{5}$$

$$\begin{aligned} \frac{1}{\psi_1} &= 1 - \frac{1}{7}e^2 + \frac{1}{49}e^4 + \frac{359}{11319}e^6 \ldots \\ &= 1 - \frac{2}{7}f + \frac{11}{49}f^2 + \frac{1948}{11319}f^3 \ldots . \end{aligned} \tag{6}$$

Imagine an unyielding sphere of radius a and uniform density ρ_1. Gravity on its surface will be

$$G = \frac{4}{3}\pi k \rho_1 a. \tag{7}$$

Let this sphere rotate with the same angular velocity as the Earth. The angular acceleration at the equator of rotation will be $\omega^2 a$. Let us form the ratio of this to gravity G and call it m_1:

$$m_1 = \frac{\omega^2 a}{G} = \frac{3\omega^2}{4\pi k \rho_1}.$$

Now instead of a sphere of unyielding material let us suppose that we have a fluid ellipsoid of the same density ρ_1 throughout and with an equatorial radius equal to a. Its mass, because of the flattening, will be slightly less than that of the sphere of radius a. The condition for equilibrium of this fluid ellipsoid is

$$\psi = m_1 = \frac{3\omega^2}{4\pi k\rho_1}. \tag{8}$$

If ρ_1 were the density of our actual Earth, this quantity m_1 would be equal to the quantity that Cook calls m. See middle of page 204 after equation (3.8a).

But if we take ρ_1 as the density of the actual Earth, the flattening comes out approximately equal to $\frac{5}{4}m_1$. This is too large. Instead let us take the flattening what we know it to be, say 1/297 for the International Ellipsoid. This means that ρ_1 comes out as greater than 7 g/cm^3, which exceeds the mean density of the Earth. To bring the mean density down, let us apply a surface coating of sufficiently high negative density, a coating such as was used long ago by Pizzetti. However absurd this set-up may be in a physical sense, the mathematical conclusions derived from its use are sound enough.

The potential V_1 of the homogeneous ellipsoid of density ρ_1, and eccentricity e for an exterior point whose coordinates are (r, θ) is given by

$$V_1 = \frac{4\pi ka^2b}{r}\rho_1\left(\frac{m_1}{\psi}\right)\left[\frac{1}{1\cdot3} - \frac{1}{3\cdot5}\left(\frac{ae}{r}\right)^2 P_2 + \frac{1}{5\cdot7}\left(\frac{ae}{r}\right)^4 P_4 - \right.$$
$$\left. - \frac{1}{7\cdot9}\left(\frac{ae}{r}\right)^6 P_6 + \ldots + \frac{(-1)^n}{(2n+1)(2n+3)}\left(\frac{ae}{r}\right)^{2n} P_{2n} + \ldots\right]. \tag{9}$$

The argument $\sin\theta$ is understood with the P's, which represent, as usual, zonal harmonics.

We now use the fact that the potential of a homoeoid is uniform over the surface. Let ρda be the surface density of the coating, whose mass is to be subtracted from that of the too massive fluid ellipsoid to bring the total mass down to that of the Earth. We understand ρ to be very large and da to be very small, with their product approaching the necessary finite limit, the total mass being

$$M = \frac{4}{3}\pi a^2 b\rho_m \tag{10}$$

where ρ_m is the mean density of the Earth. The limiting value of ρda turns out to be

$$\rho da = \frac{a}{3}\rho_m\left(\frac{m_1}{\psi} - 1\right). \tag{11}$$

This gives for V_2, the potential of the coating

$$V_2 = \frac{4}{3}\frac{\pi ka^2b}{r}\rho_m\left(\frac{m_1}{\psi} - 1\right)\left[1 - \frac{1}{3}\left(\frac{ae}{r}\right)^2 P_2 + \frac{1}{5}\left(\frac{ae}{r}\right)^4 P_4 - \frac{1}{7}\left(\frac{ae}{r}\right)^6 P_6 + \right.$$
$$\left. + \ldots + \frac{(-1)^n}{2n+1}\left(\frac{ae}{r}\right)^{2n} P_{2n} + \ldots\right]. \tag{12}$$

Substitute for ψ its equal $\frac{3}{2}e^2\psi_1$. The resultant potential $V = V_1 - V_2$ may be written

$$V = V_1 - V_2 = \frac{kM}{r}\left[1 - \frac{1}{3}\left(e^2 - \frac{m_1}{\psi_1}\right)\left(\frac{a}{r}\right)^2 P_2 + \frac{1}{5}e^2\left(e^2 - \frac{10}{7}\frac{m_1}{\psi_1}\right)\left(\frac{a}{r}\right)^4 P_4 - \right.$$

$$- \frac{1}{7}e^4\left(e^2 - \frac{5}{3}\frac{m_1}{\psi_1}\right)\left(\frac{a}{r}\right)^6 P_6 + \ldots + \qquad (13)$$

$$\left. + \frac{(-1)^n}{2n+1}e^{2n-2}\left(e^2 - \frac{5n}{2n+3}\frac{m_1}{\psi_1}\right)\left(\frac{a}{r}\right)^{2n} P_{2n} + \ldots\right].$$

By using expression (6) for $1/\psi_1$ it is seen that equation (13) checks perfectly with Cook's equation (5.2), page 211, where the various coefficients J_{2n} (here called A_{2n}) are expressed to quantities of the third order of smallness. Formula (13), however, enables any coefficient, even those beyond A_6, to be computed to any desired degrees of formal accuracy. For the present, however, this advantage is theoretical and esthetic rather than practical. Cook remarks, in effect, that it seems more logical and more convenient to take the coefficient $(a/r)^{2n}P_{2n}$ as it stands rather than to tie it up to a numerical coefficient, the reciprocal of the highest power of $\sin\theta$ in $P_n(\sin\theta)$. This is what is done in the *JD* notation, where

$$A_2 = \frac{2}{3}J \text{ and } A_4 = \frac{8}{35}D.$$

A similar opinion as to the most convenient notation has been expressed by Brouwer (1959).

The quantity

$$\left[e^2 - \frac{5n}{2n+3}\left(\frac{m_1}{\psi_1}\right)\right]$$

is positive up to $n = 5$, but for $n = 5$ it is extremely small and for $n = 6$ and beyond it is negative.

The advantage of using ψ_1 rather than ψ is that ψ_1 is very nearly equal to unity, so that m_1, (m_1/ψ_1) and m (to be defined later) differ from one another by quantities of the second order of smallness and may be equated to one another in approximate comparisons of different expressions for the same quantity.

Cook's m, which is the m_1 here used, differs slightly from what may be called the traditional m, the ratio of the centrifugal acceleration at the equator to gravity at the equator. Denote equatorial gravity by g_e. Then

$$m = \frac{\omega^2 a}{g_e}. \qquad (14)$$

For an exact relation between m and m_1, as here used, we define a new function η based on expressions (1) by the equations

$$\eta = 1 - \frac{3}{\epsilon^2}q_1 = 1 - \frac{3}{\epsilon^2}\left(1 - \frac{\tan^{-1}\epsilon}{\epsilon}\right),$$

or in terms of the hypergeometric function

$$\eta = \frac{3}{5}\epsilon^2 F\left(1, \frac{5}{2}, \frac{7}{2}, -\epsilon^2\right)$$
$$= 3\left[\frac{\epsilon^2}{5} - \frac{\epsilon^4}{7} + \frac{\epsilon^6}{9} - \frac{\epsilon^8}{11} + \ldots\right] \tag{15}$$
$$= \frac{3}{5}\left[\epsilon^2 + \frac{2}{7}\epsilon^4 + \frac{8}{63}\epsilon^6 + \frac{16}{231}\epsilon^8 + \ldots\right].$$

For the present we need the quotient η/ψ rather than η alone

$$\frac{\eta}{\psi} = 1 + \frac{1}{6}\epsilon\frac{q'_2}{q_2}.$$

By q'_2 is meant the derivative of q_2 with respect to α. By division we find

$$\frac{\eta}{\psi} = \frac{3}{2}\left[1 + \frac{1}{7}\epsilon^2 - \frac{16}{441}\epsilon^4 + \frac{208}{11\,319}\epsilon^6 \ldots\right]$$
$$= \frac{3}{2}\left[1 + \frac{1}{7}\epsilon^2 + \frac{47}{441}\epsilon^4 + \frac{3011}{33\,957}\epsilon^6 \ldots\right] \tag{16}$$
$$= \frac{3}{2}\left[1 + \frac{2}{7}f + \frac{125}{441}f^2 + \frac{1068}{3773}f^3 \ldots\right].$$

The relation between m_1 and m, as here defined, is

$$m_1 = \frac{m}{1 + m\frac{\eta}{\psi}} \tag{17}$$

$$m = \frac{m_1}{1 - m_1\frac{\eta}{\psi}}.$$

To small quantities of the third order we have

$$m_1 = m - \frac{3}{2}m^2 - \frac{3}{7}m^2 f + \frac{9}{4}m^3. \tag{18}$$

Apply this to Cook's formula (3.9), page 204, changing the m's to m_1's to conform to the notation of this paper. The coefficient of $\sin^2\phi$ in terms of m_1 and f is

$$\frac{5}{2}m_1 - f + \frac{15}{4}m_1^2 - \frac{17}{14}fm_1 - \frac{1}{98}f^2 m_1 - \frac{3}{4}fm_1^2 + \frac{45}{8}m_1^3.$$

Replace m_1 by m. There results

$$\frac{5}{2}m - f - \frac{17}{14}mf - \frac{1}{98}mf^2. \tag{19}$$

Three terms have cancelled out and the remaining third-order term has an unusually small coefficient. The coefficient of $\sin^2 2\phi$ is changed from

$$\frac{1}{8}f^2-\frac{5}{8}m_1 f+\frac{17}{56}m_1 f^2-\frac{15}{16}m_1^2 f$$

to

$$\frac{1}{8}f^2-\frac{5}{8}mf+\frac{17}{56}mf^2, \tag{20}$$

a cancellation of one third-order term. The coefficient of $\sin^2\phi\sin^2 2\phi$, being already of the third order, is not simplified by the change.

The quantity η/ψ can be made to appear in Cook's equation (3.8a), page 204. That equation is equivalent to

$$\frac{kM}{ab}=g_e\left(1+m\frac{\eta}{\psi}\right). \tag{21}$$

P.O. Box 687,
Canaan, Connecticut, U.S.A.:
1960 *March.*

References

Brouwer, D., 1959. *Astron. J.*, **64**, 396.
Cook, A. H., 1959. *Geophys. J.*, **2**, 199.

Letter to the Editors

The Palaeomagnetic Poles for the Lower Jurassic of Europe

K. M. Creer,* E. Irving† and S. K. Runcorn*

(Received 1960 March 31)

From his palaeomagnetic study of some Lower Jurassic rocks of N.W. Europe, Girdler (1959) concluded that the direction of the geomagnetic field was significantly different from the present dipole field, corresponding to a pole lying in the region of the Caspian Basin, a result which is quite different from that inferred from the polar wandering diagram for Europe given by Creer, Irving and Runcorn (1957) and different from that obtained by Hargraves and Fischer (1959) from some Lower and Middle Jurassic beds of Central Europe. But we consider that there is an alternative interpretation of his results.

The directions of magnetization of many of his formations, the Bridport sands, Yeovil sands, normally magnetized specimens of the Cotswold sands, yellow sands and grey sands of the Blea Wyke Beds, stereograms of which are shown in Figures 2, 3, 5b, 6a and 6b respectively of his paper, are grouped around the present dipole field—a result which shows either that the geomagnetic field in Lower Jurassic times was similar in direction to the present dipole field, or that, if it was not, the original magnetization decayed and was replaced by one acquired in recent times. Girdler presents no evidence but on page 355 of his paper he presumes the latter. His conclusion, therefore, so far as his English work is concerned is based only on the directions of magnetization of the Midford sands and the reversely magnetized specimens of the Cotswold sands (Figs. 4a and 5a respectively of his paper), which being different from the present dipole field are thought by him to be primary. In fact these directions are scattered sufficiently close to a plane passing through the present dipole field, as is shown in the polar equal area projections below, to cause one to suspect the presence of two magnetizations, (a) the primary or original one and (b) a secondary or later one along the present dipole field. Girdler does not mention this possibility, although it has been demonstrated in sediments many times before, e.g. by Kawai and Kume (1953), by Creer (1955, 1957) and Runcorn (1956). Such a secondary component is stable in the sense that repeat measurements after six months or more show no change in its direction or intensity. A well-known test for stability (Graham's (1949) fold test) is applied by Girdler to the Midford sands, in which he says that the directions of magnetization are less scattered after correction is made to the geological dip of the beds

* Physics Department, King's College, Newcastle upon Tyne, England.
† Geophysics Department, Australian National University, Canberra, Australia.

than before (see Figs. 4b and 4a respectively of his paper), although streaking is still present.

Figure 1 combines the data on Girdler's Figures 4a and 4b; the dots are directions of magnetization of specimens with respect to the present horizontal, but

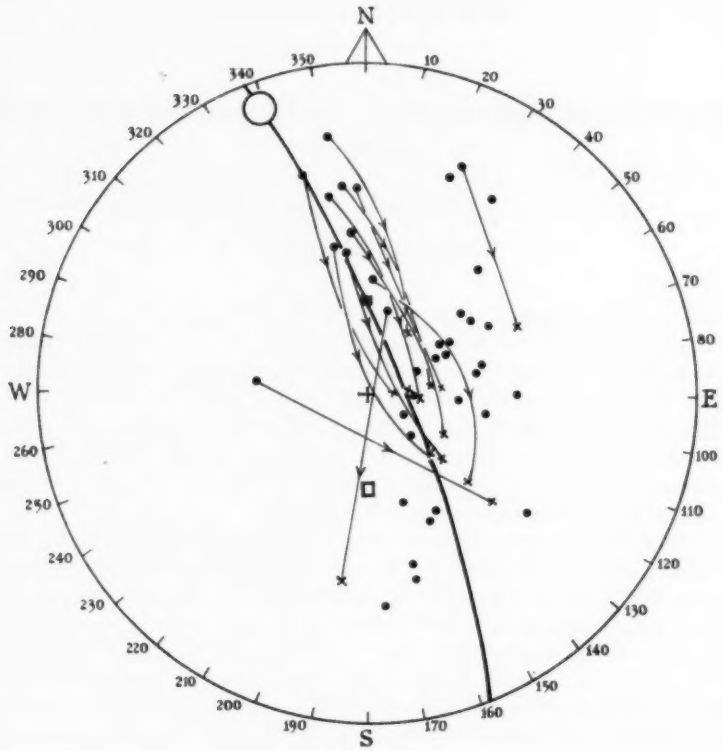

FIG. 1.

those from tilted beds are joined by lines to the directions of magnetization, represented by crosses, which are corrected for geological dip. These two latter sets of directions lie along a great circle passing through the present dipole field, represented by a full square. Those directions in the N.W. quadrant of the diagram, which have not been corrected for geological dip, are likely to be the vector resultant directions of a secondary magnetization along the present dipole field superposed on a magnetization along the Jurassic geomagnetic field, which is not very different in direction from the present one. This magnetization was apparently acquired before the rocks were tilted to their present dip, a geological tilt which would cause this primary magnetization to move to a position with respect to present horizontal, indicated by the large open circle on the figure. Thus we do not consider that Girdler's argument for the stability of these rocks carries any weight and, of course, no arguments for the stability of the directions of magnetization in flat lying beds in the Midford sands or the "reversely magnetized" specimens of the Cotswold

sands shown in Figure 2 are available. They of course may, too, be suspected of secondary magnetization, but if so, the primary magnetization must be assumed to be one opposed to the present dipole field, represented by the open square in

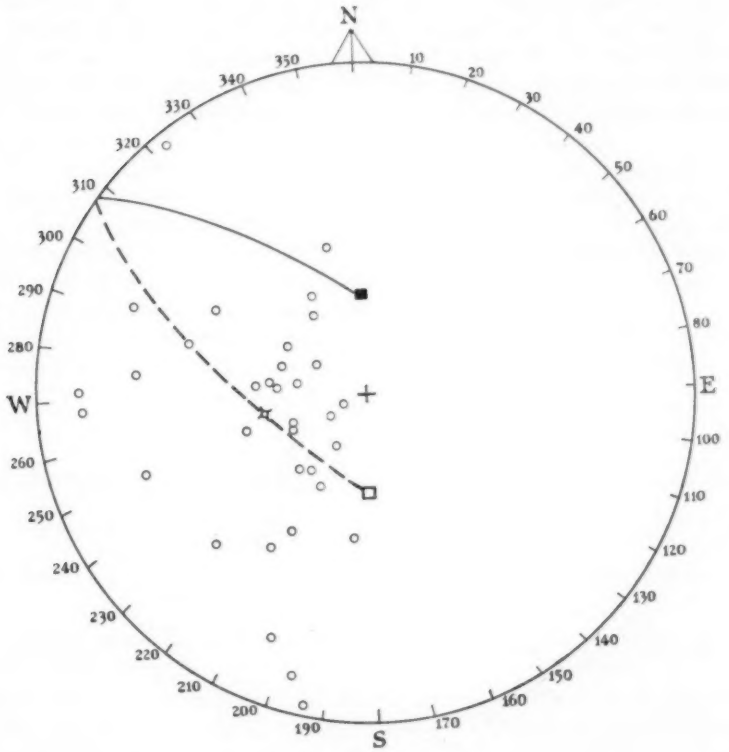

FIG. 2.

Figures 1 and 2. It is however clear that these points are not well fitted by any one great circle, but as there are an infinity of such joining the supposed primary and secondary magnetizations of these rocks, this may not be surprising. Alternatively, the divergences from this plane may be due, as Creer (1957) has shown, to a temporary component of magnetization present in the specimens acquired during the experiments.

Girdler supports his conclusion concerning the direction of the geomagnetic field in Jurassic times in England by measurements on some tuffs of Hettangian age from the northern Pyrenees. Again Graham's fold test is applied and it is stated, although it is by no means obvious, that the directions of magnetization are less scattered after corrections have been made for geological dip (Figure 8b) than before (Figure 8a). The use of a statistical method appropriate to a symmetrical distribution is hardly appropriate in this case. Further, Girdler's statement that "when geological corrections are applied the directions of magnetization become less scattered" is even more surprising as he states that through lack of adequate field mapping the assumed geological dip is subject to an error of $\pm 15^{\circ}$ (p. 360).

Finally, it may be noted that the directions of magnetization with respect to the present horizontal are distributed close to a plane including the present dipole field (see Figure 3); this again implies the presence of a secondary component of magnetization.

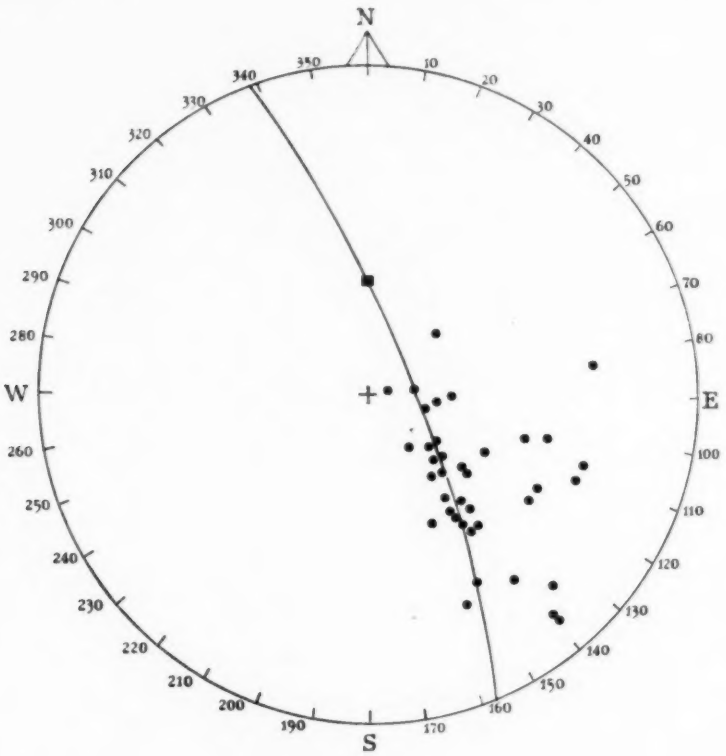

FIG. 3.

We consider that Girdler's observations do not enable any significant statement to be made concerning the position of the geomagnetic pole relative to Western Europe during the Lower Jurassic.

References

Creer, K. M., 1955. Thesis, University of Cambridge.
Creer, K. M., 1957. *Phil. Trans. Roy. Soc. A.*, **250**, 130–143.
Creer, K. M., Irving, E. & Runcorn, S. K., 1957. *Phil. Trans. Roy. Soc. A.*, **250**, 144.
Girdler, R. W., 1959. *Geophys. J.*, **2**, 353–363.
Graham, J. W., 1949. *J. Geophys. Res.*, **54**, 131–167.
Hargraves, R. B. & Fischer, A. G., 1959. *Geophys. J.*, **2**, 34–41.
Kawai, N. & Kume, S., 1953. *Geomag. and Geoelec.*, **5**, 66–70.
Runcorn, S. K., 1956. *Bull. Geol. Soc. Amer.*, **67**, 301–316.

Comment by R. W. Girdler.

The author is aware of a possible secondary component of magnetization being present in the Upper Lias Sands; this is discussed on page 355 of his paper and Figure 7 on page 358 was drawn to emphasize the varying degrees of stability.

The objection concerning the Midford Sands arises because it so happens that applying the geological correction required for some of the samples involves moving the remanent vectors along great circles which pass close to the Earth's present dipole field. The alternative explanation of the results given in the above letter is unlikely for the following reasons:

(*a*) The samples not requiring geological correction do not lie close to a great circle passing through the Earth's present dipole field as can been seen from Figure 1 of the above letter. The sands are remarkably similar (see the geological references cited at the end of the paper) and come from a small area in Somerset; it would be surprising if only those requiring geological correction should lie on the proposed great circle when the majority of the others do not.

(*b*) The following table shows the results of calculating the mean directions of magnetization of the specimens requiring geological correction separately:

	θ	ϕ	α	K	N	S
(*a*) Samples not requiring correction	97·5	69·1	9·7	8·8	30	14
(*b*) Geologically corrected samples	118·1	70·6	11·5	15·3	12	6
(*c*) Mean of all samples	103·5	69·8	7·4	10·2	42	20

(The symbols have the same meaning as for the table given on page 358 of the author's paper.)

The mean directions together with their circles of confidence at the 95 per cent level are illustrated in Figure 1. These statistics are calculated from the geologically corrected results which do not show obvious streaking along great circles through the present dipole field. The agreement for specimens requiring geological corrections and those not requiring geological corrections is very good and would hardly be expected if a secondary component of magnetization is important.

(*c*) The mean direction of all the samples is approximately 180° different from that of the reversely magnetized Cotswold Sands which are of nearly the same age (Girdler 1959). Previously (e.g. Blackett (1956), Irving & Green (1957) and others), this has been considered evidence of stability. It is probably significant that the writers of the letter note that the reversely magnetized Cotswold Sands "are not well fitted by any one great circle".

It is concluded that there is no good evidence, unlike the excellent example of Creer (1957), that a secondary component of magnetization parallel to the present dipole field is important in the Midford and Cotswold Sands.

Throughout this work much thought has been given to stability and it is unfortunate that the sediments are too weakly magnetized to enable laboratory experiments to be performed. The Upper Lias Sands of the west of England were deposited continuously as one unit in a time interval of probably less than 6×10^6 years and this is comparable, if not less than the time covered in sampling by other workers for other periods. As previously pointed out, some of the Upper

Lias Sands do show a secondary component of magnetization along the direction of the present dipole field. Figure 7 has been redrawn (Figure 2) with the reversely magnetized Cotswold Sands plotted as a normal direction. The great circle through the present dipole field and the mean directions of magnetization is shown as a dotted line. In the absence of any other data the directions of n.r.m. of the Cotswold and Midford Sands (180° opposed) are taken to be close to the field direction for the Jurassic period.

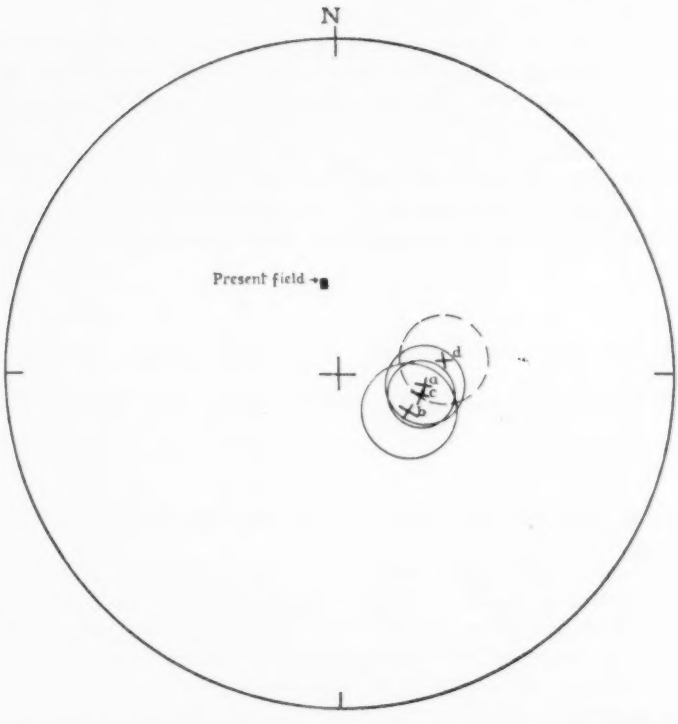

FIG. 1.—Mean directions of natural remanent magnetization of Midford and Cotswold Sands together with circles of confidence at the 95 per cent level. (*a*) For samples not requiring geological correction, (*b*) for geologically corrected samples, and (*c*) for all samples. The mean direction for the Cotswold Sands (*d*) is shown with the circle of confidence as a dashed line.

The work was an attempt to fill a gap in our knowledge of palaeomagnetism, very few results having been obtained for the Jurassic period. Most interesting is the presence of an easterly declination (slightly larger than for the Triassic) and the fairly steep inclination of 67°. The writers of the letter make no comment on the fact that the latter is very close to that found by Nairn (1957), discussed on p. 359, and also on the fact that the rocks of Hargraves & Fischer come from a thrust area and are unusually tightly clustered. Finally, it is perhaps not surprising that the result does not agree with the smoothed polar wander curve of

Creer, Irving & Runcorn for this assumes no continental movements or local movements of the Earth's crust and as more and more results become available it is possible that their polar wander curve will become much more complex.

R. W. GIRDLER

Durham Colleges,
Science Laboratories,
South Road,
Durham City:
1960 *June* 20.

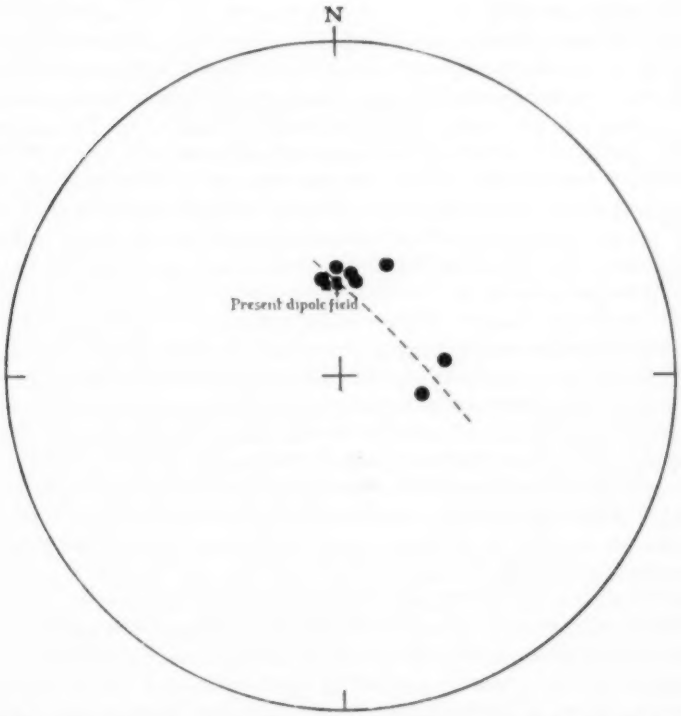

FIG. 2.—Mean directions of natural remanent magnetization of all the Upper Lias Sands with great circle passing through the present dipole field.

References

Blackett, P. M. S., 1956. *Lectures on Rock Magnetism* (Israel: Weizmann Press).
Creer, K. M., 1957. *Phil. Trans. Roy. Soc. A*, **250,** 130.
Girdler, R. W., 1959. *Nature*, **184,** 540.
Irving, E. & Green, R., 1957. *Mon. Not. R. Astr. Soc. Geophys. Suppl.*, **7,** 348.
Nairn, A. E. M., 1957. *Adv. in Phys.*, **6,** 162.

Geophysical Discussion of the Royal Astronomical Society

A discussion of papers received during the session was held in the rooms of the Royal Astronomical Society on 1960 April 22 at 16h 15m under the Chairmanship of *Dr R. Stoneley, F.R.S.*

Dr K. F. Bowden, of the Tidal Institute, Liverpool, presented a paper written by himself, *L. A. Fairbairn* and *P. Hughes*, on **The Distribution of Shearing Stresses in a Tidal Current** (1959). The shearing stress in a uniform liquid flowing steadily along an open channel, increased linearly from the surface to the bottom, regardless of turbulence, and the distribution of velocity with depth could be determined theoretically. When the flow varied with time, and effects due to the Earth's rotation were added, as in the case of tidal flow, no direct inference could be drawn about the distribution of shearing stress with depth. The investigation discussed was aimed at determining the shearing stress as a function of depth from measurements of the vertical distribution of current throughout the tidal cycle and from estimates of the bottom friction. The equations of the system were given. Current measurements were made in Red Wharf Bay, Anglesey, North Wales, from an anchored vessel, using a Doodson recording current meter augmented by a Charnock meter for some near-bottom measurements. The velocity profiles were determined and the bottom stress was calculated. The stress determination gave a nearly linear profile from surface to bottom at the times of maximum flood and maximum ebb, but departed strongly at other stages of the tidal cycle. The eddy viscosity tended to be higher at mid-depths than at the boundaries and to reach a maximum when the current was greatest, about three hours before and after high water.

In the discussion, the *Chairman* asked what was the effect on the stress determinations of viscous drag due to wind on the sea's surface. The speaker answered that, with a 10-knot wind, the stress on the surface was 0·6 dyn/cm^2 compared with a figure between 3 and 4 dyn/cm^2 at the bottom and had been neglected. It would have been an improvement to take this into account but would have required measuring and recording the wind speeds, and they had not the instruments for this. *Professor Sheppard* asked if the physical causes were clear as to why the eddy viscosity was different between the flood and ebb of the tide. *Dr Bowden* said the case was not clearly understood; there was no density gradient to account for it, but the current velocity was slightly different in the two cases.

Dr K. M. Creer, of King's College, Newcastle, followed and delivered the paper written by himself, *E. Irving* and *A. Nairn* on **Palaeomagnetism of the Great Whin Sill** (1959). This described the results of a study of the remanent magnetism in rock samples collected at thirty-two sites in the Whin Sill of Northumberland and Durham. The authors also reported that the mean directions of magnetization had an oval distribution, discussed the possibility that this scatter reflected the geomagnetic secular variation during the time of interjection,

and proposed a method for calculating the errors associated with the palaeomagnetic pole positions. It was concluded that a direction of 187°·8 declination and −4°·9 inclination represented the vector mean of the magnetizations they had observed. There was not time for discussion of this paper.

The third paper was by *Mr J. E. Jackson*, of Cambridge University, on **Observations with the Cambridge Pendulum Apparatus in North, Central and South America in 1958** (1959). In introducing this report the author reviewed the needs for geodetic study which prompted these observations. About 100 000 stations between which the gravity differences should be known to a 1 mgal accuracy were required for accurate knowledge of the shape of the Earth, these should be fairly uniformly distributed over the Earth's surface, and at several stations the absolute value of gravity should be measured. The Cambridge Pendulum Apparatus was used in making the observations reported. This consisted of four invar pendulums swung in pairs. Eleven stations were occupied both on the outward and on the return journeys from England to South America: Teddington, Madison, Mexico City, Panama, Caracas, Quito, Lima, La Paz, Santiago, Buenos Aires and Rio de Janeiro. The computed gravity differences were given. Several slides were shown of the gravity stations and their surroundings. In the discussion which followed *Dr A. H. Cook* remarked there were now five stations where absolute measurements of g had been made.

Dr J. C. Weston of the Department of Scientific and Industrial Research spoke on his paper, **Underground Explosions** (1960). The low frequency of the energy radiated from underground explosions was proportional to the square of the frequency of the seismic wave (f^2) and to the square of the total energy (W^2). The f^2 law was derived from relationships between pulse shapes and the radiated spectrum. The W^2 law came from a consideration of body waves. Underwater explosions had provided evidence for these laws, but in underground explosions only the W^2 law had been verified. Some comments were made about the frequency distribution in underground and underwater explosions, and about the theoretical source level and critical radiation in underground explosions. There was no discussion.

Sir Harold Jeffreys was the last speaker and delivered a paper by *Professor K. E. Bullen* of Sydney University on **The Derivation of Seismic Velocities at Depth from Travel-Time Curves** (1960). In deriving the distribution of velocity with depth from travel-times, the usual method is to find $dt/d\Delta$, and then an integral depending on $dt/d\Delta$ had to be worked out numerically to give a relation between Δ and the maximum depth reached by the ray. In practice the work was rather laborious. What made it worse was that one might want to examine the effect of changing t over some range of Δ, and the only way of finding it was to do all the work again. It was known that there was an exact solution of v of the form $\alpha-\beta r^2$, but Bullen pointed out some time ago that there was another, if v were of the form Ar^{-k}, when the times were proportional to $\sin\frac{1}{2}(k+1)\Delta$. The paper depended on using this as a first approximation. With Bullen's treatment a first approximation did facilitate later steps. He applied it to the Earth's main core and got results agreeing closely with those found by direct integration. *Jeffreys* commented that it was rather odd that it should be so because d^2c/dr^2 is positive for the first approximation and the actual values were usually negative, as for $v=\alpha-\beta r^2$, but the method did manage it. Effectively it introduced $d\log c/d\log r$ and when this was found c came by one integration of a fairly small quantity.

The Chairman thanked the speakers and adjourned the discussion at 18h 10m.

References

Bowden, K. F., Fairbairn, L. A. & Hughes, D., 1959. *Geophys. J.*, **2**, 288.
Bullen, K. E., 1960. *Geophys. J.*, **3**, 258.
Creer, K. M., Irving, E. & Nairn, A. E. M., 1959. *Geophys. J.*, **2**, 306.
Jackson, J. E., 1959. *Geophys. J.*, **2**, 337.
Weston, D. E., 1960. *Geophys. J.*, **3**, 191.

Book Reviews

Palaeomagnetism and Stratigraphic Correlation

A. N. Khramov

(published by the Government Science publishers of petroleum and mineral fuel literature, Leningrad 1958, 204 pp. In Russian.)

This book, its author says, was written "because of the unbearable absence in Russia of a book explaining the present state of knowledge and methods of palaeomagnetism", and "is directed at a wide circle of geologists and geophysicists and also at the specialist who is beginning palaeomagnetic research with an eye to its use both in stratigraphical problems and in tracing the geological history of the Earth's magnetic pole".

It is divided into three chapters. The first contains a general account of palaeomagnetism and its implications for geology and geophysics based chiefly on work prior to 1955 in countries other than Russia. There are many small inaccuracies in reporting and also some curious referencing, for instance, Table 7, page 48, refers to Hospers (1955) for studies of the lava flows of Mt Etna which were made in 1926 by Chavallier, but it is likely that Mr Khramov has preferred to give reference to reviews in journals available in Russian translation when the originals are not available. The second chapter deals with palaeomagnetic work in Turkmenia where beds from Jurassic to Pleistocene have been studied, and the third deals with work on Ordovician to Lower Triassic rocks from the Russian Platform. The second chapter should interest oil geologists and the second and third chapters are necessary reading for research workers in palaeomagnetism.

The Russian work confirms the two most important features of palaeomagnetic results from other countries, namely the occurrence of serial reversals of polarity superimposed on the steady drift of the directions from period to period. Mr Khramov, following most "western" workers, interprets the former as due to reversals of the main geomagnetic field and the latter as due to polar wandering. The discrepancy between the pole results obtained from different continents he regards as strong evidence of continental drift and bemoans the unnecessary hostility to this idea amongst Soviet geologists.

The work in Turkmenia arose from the need for more accurate stratigraphic correlation of rock formations whose equivalents in Caucasia yield oil. A close study of Upper Tertiary and Quaternary beds has been made with less detailed work on Jurassic, Cretaceous and Lower Tertiary formations. An alternating succession of "normal" and "reversed" zones has been established from surface sections, and this is correlated with similar effects in bore-core material. Several promising methods of distinguishing between different zones of the same polarity are proposed and applied with some success. Results from transition beds between "normal" and "reversed" zones suggest that reversal of the Earth's field is not due to decay of the Earth's dipole followed by build up in the opposite direction,

but rather to its toppling over through 180°. Regarding the pole positions obtained from the Turkmenian work it is of interest that the north pole for the Plio-Pleistocene has the co-ordinates 75 N, 122 W. This revives the opinion once held that a polar displacement towards North America was necessary to explain the assymetry of the Pleistocene glaciation. Similar effects should, but have not turned up in work elsewhere, but this could be due to inadequate correlations and the limited data.

The work in European Russia is notable chiefly for studies of the Permian classical sections in the eastern Urals. Except for the highest levels of the Permian (the Tartarian which could in part be Lower Triassic) the directions are all "reversed" as for Permian beds elsewhere in the world. The pole agrees very well with that obtained from the western European Permian. The level of the return to "normal" polarity in the Tartarian promises to be a useful world-wide datum.

A translation into English of this book will be published in 1960 or early 1961 by the Australian National University.

E.I.

Introduction to Geophysical Prospecting

M. B. Dobrin

(2nd edition, 1960, 446 pp., McGraw-Hill, 74s.)

This is the second edition of the book originally published in 1952. It is a second edition in more than name: new sections have been added at the expense of some of those in the first edition and the text with its very useful references has been thoroughly revised to bring it up to date. The number of revisions illustrates the appreciable extent to which prospecting techniques have been modified in the past decade. The basic methods are unchanged but there have been considerable developments in both the instruments and the interpretation techniques. Particularly in seismic work, these have coincidentally led to a better appreciation of the effect of the recording process on the data quality.

Seismic methods occupy a predominant position in the industry at the present day and the sequence of chapters in this edition has been revised to emphasize this, with additional space being devoted to both reflection and refraction techniques. The new material here includes magnetic tape recording, corrected record sections, geophone patterns and recent interpretation methods. One particularly interesting addition is a chapter on the geological interpretation of reflection records with its discussion of geological/geophysical coordination. The author is to be congratulated on avoiding the woolly talk which usually surrounds this topic and on illustrating in practical terms why this coordination is required.

Developments in gravity and magnetic surveys have been less spectacular than those in seismic surveys but the sections in interpretation have been extended and the latest instrumental developments included. The chapters on radioactive and electrical methods have also been enlarged although in the case of electrical methods perhaps not sufficiently to satisfy the mining geophysicist. This extra material has been incorporated at the expense of three chapters of the first edition: of these,

the only serious loss is that dealing with well-logging methods although its omission is justifiable in view of the tendency of well-logging to become an independent geophysical field.

The short chapter on earthquake seismology and the structure of the Earth has been retained; in spite of the author's apologia for its presence, it seems somewhat out of place in this book. Whilst commercial geophysics owes a great debt to earthquake seismology, one would hope that any geophysics student could be left to acquire this background information elsewhere. The least satisfactory part of the book is perhaps that dealing with seismic instruments. Although it includes recent developments and has been largely rewritten, there are a number of minor errors and rather misleading statements.

In spite of these minor criticisms, this book, like its first edition, is very comprehensive, well-produced and very readable. It can be firmly recommended to its intended readership of students and of those practising geophysicists who require a quick reference to fields outside their own speciality.

A.T.D.

Geophysical Journal

RECOMMENDATIONS TO AUTHORS

1. Authors are advised to follow the general suggestions for the preparation of scientific papers given in *Notes on the preparation of papers to be communicated to the Royal Society* and in *The printing of mathematics* by T. W. Chaundy, P. R. Barrett and C. Batey (Oxford University Press, 1954). In particular the abbreviations for the names of periodicals used in the *Geophysical Journal* are those given in *Notes on the preparation of papers . . .* and the symbols, signs and abbreviations are those recommended for British scientific publications by the Symbols Committee of the Royal Society.

2. Papers should be typewritten with double spacing and on one side of the paper only. Two copies, one of them the top copy, should be submitted. All papers must be accompanied by a summary; summaries are not required for *Letters to the Editors*.

3. Tables are printed without rules. They should be numbered serially with Arabic numerals. Table headings should be brief. Units should be placed at the head of the column. Tables should be typed on separate sheets and their positions in the text indicated on the copy.

4. Illustrations, especially photographs, should be kept to a minimum, and the same information should not in general be given in both tables and illustrations. Line drawings should be in dense black ink on smooth white board or transparent tracing film. Original drawings must not be lettered; lettering should be indicated on copies or photoprints which must be supplied in addition to the originals. Wherever possible, lettering should be kept outside the diagram so that it may be set in type. Diagrams should be drawn at twice to three times the size at which they will be printed. The maximum dimensions for diagrams, when reduced and with their lettering and captions, are 8 in by 5 in. A wide variety of flat tints of dots, lines and shadings can be applied to line drawings by the blockmaker. Photographs for reproduction should be unmounted glossy prints and should be accompanied by lettered prints.

5. References should be quoted in the form recommended by the Royal Society but authors may also quote titles of papers if they wish. References in the text are made in the form (Smith 1940).

6. Authors whose work involves much mathematics should follow carefully the recommendations in *The Printing of Mathematics*.

7. The Editors will be glad to advise authors on any special points of difficulty arising in the preparation of papers for the *Journal*.

Geophysical Journal

RECOMMENDATIONS TO AUTHORS

1. Authors are advised to follow the general suggestions for the preparation of scientific papers given in *Notes on the preparation of papers to be communicated to the Royal Society* and in *The printing of mathematics* by T. W. Chaundy, P. R. Barrett and C. Batey (Oxford University Press, 1954). In particular the abbreviations for the names of periodicals used in the *Geophysical Journal* are those given in *Notes on the preparation of papers* . . . and the symbols, signs and abbreviations are those recommended for British scientific publications by the Symbols Committee of the Royal Society.

2. Papers should be typewritten with double spacing and on one side of the paper only. Two copies, one of them the top copy, should be submitted. All papers must be accompanied by a summary; summaries are not required for *Letters to the Editors*.

3. Tables are printed without rules. They should be numbered serially with Arabic numerals. Table headings should be brief. Units should be placed at the head of the column. Tables should be typed on separate sheets and their positions in the text indicated on the copy.

4. Illustrations, especially photographs, should be kept to a minimum, and the same information should not in general be given in both tables and illustrations. Line drawings should be in dense black ink on smooth white board or transparent tracing film. Original drawings must not be lettered; lettering should be indicated on copies or photoprints which must be supplied in addition to the originals. Wherever possible, lettering should be kept outside the diagram so that it may be set in type. Diagrams should be drawn at twice to three times the size at which they will be printed. The maximum dimensions for diagrams, when reduced and with their lettering and captions, are 8 in by 5 in. A wide variety of flat tints of dots, lines and shadings can be applied to line drawings by the blockmaker. Photographs for reproduction should be unmounted glossy prints and should be accompanied by lettered prints.

5. References should be quoted in the form recommended by the Royal Society but authors may also quote titles of papers if they wish. References in the text are made in the form (Smith 1940).

6. Authors whose work involves much mathematics should follow carefully the recommendations in *The Printing of Mathematics*.

7. The Editors will be glad to advise authors on any special points of difficulty arising in the preparation of papers for the *Journal*.

Contents

PAGE

F. F. Evison, C. E. Ingham, R. H. Orr & J. H. Le Fort, Thickness of the Earth's crust in Antarctica and the surrounding oceans 289

A. R. Ritsema, Focal mechanisms of some earthquakes of the year 1950 307

J. H. Piddington, A theory of polar geomagnetic storms 314

J. A. Jacobs & K. Sinno, Worldwide characteristics of geomagnetic micropulsations 333

K. E. Bullen, Note on cusps in seismic travel-times 354

Research Note

W. D. Lambert, Note on the paper of A. H. Cook, "The external gravity field of a rotating spheroid to the order of e^3". 360

Letter to the Editors

K. M. Creer, E. Irving & S. K. Runcorn, The palaeomagnetic poles for the Lower Jurassic of Europe 367

Report of Meeting

Geophysical Discussion of the Royal Astronomical Society, 1960 April 22 374

Book Reviews 377

Printed in Great Britain by J. W. Arrowsmith Ltd., Bristol